MORPHODYNAMICS OF GRAVEL BEACHES AND THEIR RESPONSE TO NOURISHMENT

by

Sofi Farazande

B.S., Civil Engineering, Boğaziçi University, 2020

Submitted to the Institute for Graduate Studies in
Science and Engineering in partial fulfillment of
the requirements for the degree of
Master of Science

Graduate Program in Coastal and Hydraulics Engineering
Boğaziçi University

2022

ACKNOWLEDGEMENTS

First off, I would like to express my deepest gratitude to my thesis supervisor Prof. Emre Otay for his invaluable guidance and support throughout this study. Each time I had a question, he introduced new theoretical details, showed another perspective, and so helped me find answers. I also thank him for involving me in the beach nourishment project through which I improved my practical and theoretical background in coastal engineering.

I would like to thank all members of Boğaziçi University Coastal Engineering Laboratory for the cooperation and solidarity environment they provided during the beach nourishment project. I specially thank Pelin Uzun and Berke Bıçak for their precious suggestions regarding modeling and their friendship.

I would like to express my appreciations to Assoc. Prof. Cihan Bayındır for his valuable comments on this thesis and encouragement for an academic career.

I am endlessly grateful to my family for their unconditional love and support throughout my life. Thanks to their presence and faith in me, I had the power to never give up even in the hardest times.

Finally, I would like to express my gratitude to my friends who were always by my side no matter what happened. I especially thank Güney Işık Tombak, my beloved one, for his never-ending encouragement, support, and love.

ABSTRACT

MORPHODYNAMICS OF GRAVEL BEACHES AND THEIR RESPONSE TO NOURISHMENT

Modeling the long term beach morphology after nourishment provides a better understanding of the nature of the beach. In this thesis, the morphodynamics of a gravel beach at Kalemyel Bay after two nourishments in March 2020 and March 2021 are modeled. The model of each year focuses on four cross-sections and their profile evolution in one year after the nourishment. SWAN software is used to model the wave climate which has the most important factor for the profile evolution. 8 wave conditions that have the highest impact on the profile evolutions have been selected and used in the morphology model. The morphologic changes due to cross-shore sediment transport are simulated in XBeach-G. Longshore sediment transport is modeled with the diffusion equation. The results obtained from the longshore model are superposed on the XBeach-G outputs of the cross-sections. The results of the XBeach-G of the profiles after the nourishment in March 2020 remain less evolved compared to the site measurements. This may imply that an unconsidered storm occurred in Summer 2020 at Kalemyel Bay. The results of the XBeach-G for the nourishment in March 2021 are in line with the long-term estimations of the Boğaziçi University Coastal Engineering Laboratory. However, for simulations of both years, longshore transport is overestimated especially on the west side of the beach. The irregular beach fill along the shore affects the longshore transport results. Still, there is a dominance of the cross-shore transport over the longshore transport. The average beach width loss due to cross-shore transport after second nourishment, where the average width gain was 5.90 m, is 3.65 m, while for longshore transport this amount is 1.64 m. It is deduced that the nourishment can be designed such that the fill is thicker in the middle of the beach than the sides since the material will move to the ends of the domain in time.

ÖZET

ÇAKIL KUMSALLARIN MORFODİNAMİĞİ VE BESLEMEYE TEPKİSİ

Kumsal beslemesinin uzun vade için morfoloji modellemesi, kumsalın doğasının daha iyi anlaşılmasını sağlar. Bu tezde, Kalemyel Koyu'ndaki çakıl bir kumsalın Mart 2020 ve Mart 2021'de iki besleme sonrası morfodinamiği modellenmiştir. Her yılın modeli, beslemeden sonraki bir yıl için dört enkesit ve bunların profil gelişimi için çalıştırılmıştır. Profil gelişimi için en önemli etken olan dalga iklimini modellemek için SWAN kullanılmıştır. Profil gelişimleri üzerinde en yüksek etkiye sahip olan 8 dalga koşulu seçilmiş ve morfoloji modelinde girdi olarak kullanılmıştır. Kıyıya dik sediman taşınımından kaynaklanan morfolojik değişiklikler XBeach-G ile simüle edilmiştir. Kıyıya yanal sediman taşınımı difüzyon denklemi ile modellenmiştir. Yanal taşınım modelinden elde edilen sonuçlar, enkesitlerin XBeach-G çıktıları üzerine bindirilmiştir. Mart 2020'deki beslemeden sonrası için olan XBeach-G sonuçlarındaki profillerin saha ölçümlerine kıyasla daha az gelişmiş olduğu görülmüştür. Bu durum, 2020 yazında Kalemyel Koyu'nda beklenmedik bir fırtınanın meydana geldiğinin göstergesi olabilir. Mart 2021'deki besleme için XBeach-G sonuçları, Boğaziçi Üniversitesi Kıyı Mühendisliği Laboratuvarı'nın uzun vade tahminleri ile uyumludur. Bununla birlikte, her iki yılın simülasyonları için, özellikle sahilin batı tarafında yanal sediman taşınımı olduğundan fazla tahmin edilmiştir. Kumsal boyunca düzensiz kumsal beslemesi, yanal taşınım sonuçlarını etkilemiştir. Yine de, kıyıya dik taşınımı, kıyıya yanal taşınıma baskındır. Kumsal genişliğinin ortalama 5,90 m arttığı ikinci beslemeden sonra kıyıya dik taşınımdan kaynaklanan ortalama kumsal genişliği kaybı 3,65 m iken, bu miktar yanal taşınım için 1,64 m'dir. Tasarım, kumsalın ortasındaki besleme malzemesinin kalınlığı kenarlardan daha yüksek olacak şekilde yapılabilir, çünkü malzeme zamanla sahanın uçlarına doğru hareket eder.

TABLE OF CONTENTS

LIST OF FIGURES

LIST OF TABLES

LIST OF SYMBOLS

B	Berm height
D_{50}	Medium diameter of particle size distribution
G	Longshore diffusivity constant
g	Gravitational acceleration
H_b	Breaking wave height
H_{iA1}	Incident wave height at 6 m depth of cross-section A1
H_{iA2}	Incident wave height at 6 m depth of cross-section A2
H_{iB}	Incident wave height at 6 m depth of cross-section B
H_{iC}	Incident wave height at 6 m depth of cross-section B
H_{iD}	Incident wave height at 6 m depth of cross-section B
H_s	Significant wave height
h_*	Depth of closure
i	Space step
j	Time step
K	Longshore transport coefficient
k	Hydraulic conductivity
L	Length of the domain
N	Number of data points
n	Data points
N_x	Number of nodes in the shoreline direction
p	Porosity of sediment
S	System matrix for the implicit finite difference method
s	Specific gravity of sediment
T	Wave period
t	Time
t_1	Time counter starting from the nourishment in March 2020
t_2	Time counter starting from the nourishment in March 2021
x	Shore-parallel direction for the longshore diffusivity model

y	Shore-normal position for the longshore diffusivity model
y_0	Normal distance berween the pre-nourishment and post-nourishment shorelines
y_{act}	Actual values at data points
y_{pred}	Predicted values at data points
κ	Spilling breaker

LIST OF ACRONYMS/ABBREVIATIONS

1D	One Dimensional
2D	Two Dimensional
3D	Three Dimensional
BC	Boundary Condition
BUCEL	Boğaziçi University Coastal Engineering Laboratory
CERC	Coastal Engineering Research Center
CTD	Conductivity, Temperature, and Depth
DSAS	Digital Shoreline Analysis System
E	East
ENE	East-Northeast
ESE	East-Southeast
JONSWAP	Joint North Sea Wave Project
LU	Lower-Upper
MAE	Mean Absolute Error
N	North
NE	Northeast
NMAE	Normalized Mean Absolute Error
NNE	North-Northeast
NNW	North-Northwest
NRMSE	Normalized Root Mean Square Error
NW	Northwest
RMSE	Root Mean Square Error
RTK GPS	Real Time Kinematic Global Positioning System
S	South
SE	Southeast
SMC	Coastal Modeling System
SSE	South-Southeast
SSW	South-Southwest

SW	Southwest
SWAN	Simulating Waves Nearshore
TUDKA-99	Turkish National Vertical Control Network
W	West
WNW	West-Northwest
WSW	West-Southwest

1. INTRODUCTION

Beach nourishment to recover coastal erosion has become a frequent practice that provides more available space for beach use. This has both social and economic significance by affecting touristic activity [1]. This thesis aims to model the morphodynamic evolution of a semi-protected gravel beach at Kalemyel Bay, in the North-East of Fethiye Bay (Figure 1.1), which has been subject to two beach nourishments with a one-year interval, one in March 2020 and the other in March 2021. The nourishment designs and the corresponding site investigations are conducted by Boğaziçi University Coastal Engineering Laboratory (BUCEL). In the scope of the research, reports of the previous years are analyzed, field measurements are conducted, sediment samples are collected, sieve analysis is performed, and the wave model is obtained for the bay (by use of SWAN). The beach has a length of approximately 300 m and a slight curvature. According to measurements done in November 2019, the median diameter of the beach is 0.0058 m. These properties allow us to consider the region as a pocket gravel beach. In addition, there is a submerged berm formed of concrete blocks (which is also called sill) in order to prevent excessive sediment loss through the sea. The sill lies approximately over the -2.5 m depth contour, so its distance from the shoreline varies according to its longshore position. The dimensions of each sill are measured as $100\text{cm} \times 100\text{cm} \times 150 - 200\text{cm}$ [2] and shown in the Figure 1.2. The shoreline is parallel to the horizontal direction in Figure 1.2. In light of this information, the closure depth and the possible sustainable increase of the present dry gravel beach are computed. The timeline of the project can be seen in Figure 1.3 and Table 1.1. Our goal is to estimate the long-term morphology of the beach after nourishment in April 2021, by calculating the depth of closure, cross-shore and longshore sediment transport rates, and modeling the evolution of the beach profile.

Morphodynamics in pocket gravel beaches depends on the local wave and sediment dynamics, coastal configuration, and lithological influence. Therefore, these beaches need to be treated as unique systems [3]. With this motivation, a comprehen-

sive model should be developed to be able to predict the long-term beach response. A site-specific model will contain many parameters in order to be accurate. Once such a model is developed, it may provide a more authentic model applicable to other gravel beaches as well. Hereby, more efficient beach nourishment designs can be made for similar gravel pocket beaches in the future. In addition, we know that one result of the climate crisis, which is the most important problem of our time, is sea-level rise. The Bruun Rule states that sea-level rise causes shoreline recession. Soft coastal structures such as beach nourishment may help maintain coastal stability and resilience to climate change.

Figure 1.1. Project location map in Fethiye Bay (Google Earth, 2022).

Morphodynamics of the beach is explained by cross-shore and longshore sediment transport formulations. Based on Bagnold's energetic concept [4], Bailard and Inman developed a sediment transport rate equation for surf zones on a plane sloping beach [5, 6]. Another model developed from Bagnold's concept is the BG model, which has also applications in predicting the gravel nourishment evolution [7]. 3D Eulerian-Lagrangian model of [8] sets forth the significance of shear lift force and turbulent flow fluctuation for sediment saltation regime. For shallow water bed evolution, coupled equations such as Saint Venant-Exner have also been used. Its combination with the

advection-diffusion equation revealed that the adaptation length is mainly controlled by the particle advection velocity, particle diffusivity, and entrainment/deposition rates [9]. The highly nonlinear Boussinesq equation and Shields parameter provide also the transport rate calculation, and are also applicable to model coarse-grained beaches [10, 11].

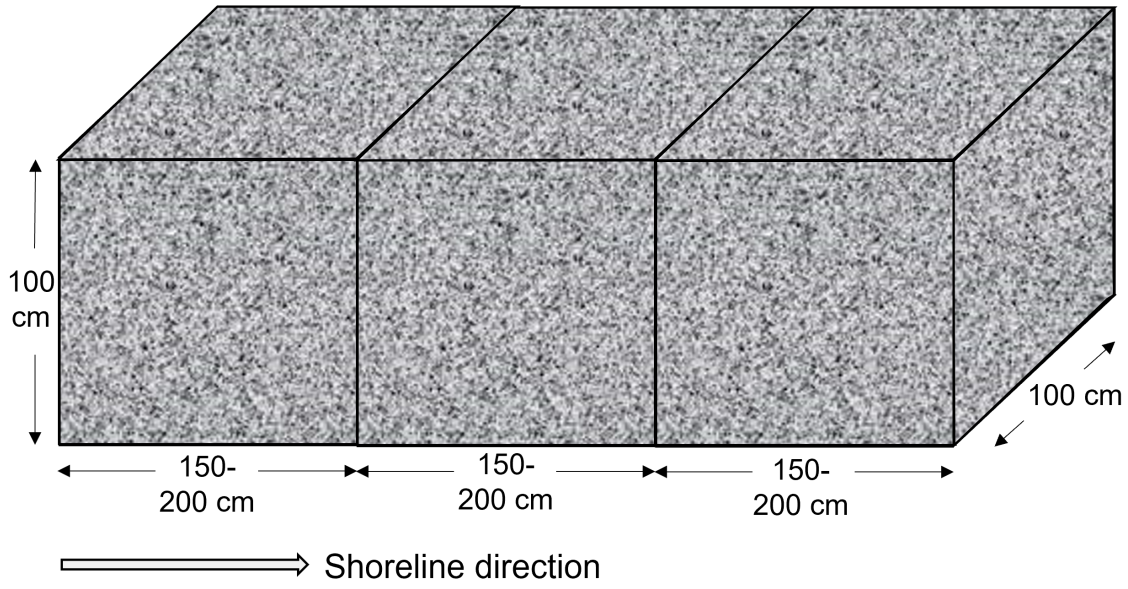

Figure 1.2. Representative concrete blocks forming the sill.

In addition to theoretical models, site surveys and tracking methods are also used to reveal particular roles of transport parameters. Video monitoring is used to study storm response [12] and to assess the nourishment performance of gravel embayed beaches [13], while tracer experiments are conducted to investigate the role of pebble and cobbles in transport [14, 15]. RFID technologies are also used to determine the role of particle shape, the mechanism of pebble transport in the swash zone and to define the geology of the active sediment layer [1, 16–18].

In order to apply this knowledge to a specific beach nourishment project, the required inputs should be collected. Hence, a site investigation is the first step. Field measurement and sampling are usually conducted by equipment such as current meter, pressure transducer, GPS technologies, and/or modeling software [19–22].

The next step is to select a proper model for the morphodynamics of the beach so that the profile evolution after the application of nourishment design can be predicted. There are numerous software available to model sediment transport and beach morphology. SMC is a software that can be used to calculate the net littoral drift with its waves, current, water level, sediment transport, and morphology modules [23]. Delft3D is a comprehensive open software with hydrodynamics, morphology, wave, and water quality modules. The wave module of Delft3D is based on the SWAN software [19]. DSAS gives the rate of change statistics of shoreline change from historical shoreline positions and is used for shoreline analysis in morphology studies [13]. XBeach is a 2D numerical model based on the non-linear shallow water equations [24]. XBeach-G model is an extended version of XBeach-G to simulate the storm impact on gravel beaches. Different from XBeach, XBeach-G is a 1D model and considers only cross-shore sediment transport. However, in the case of storms coming with an oblique angle to the shore, the combination of XBeach-G with the longshore transport formulation may yield more accurate results [25]. Besides, to provide a complete design methodology for embayed beaches in dynamic equilibrium, the Dynamic Equilibrium Planform should be studied [23]. Regarding the accuracy of XBeach-G model for gravel beaches, it is selected for this thesis for the simulation of cross-shore profile changes. Moreover, the coupling of XBeach-G with a longshore model can be a choice in case of need to include the longshore transport to the model. Using two 1D (or quasi-2D) model may also help better distinguishing physical processes acting in each direction and their ratios. Compared to 3D models, 1D or 2D models are easier to calibrate and to test for the error source as well. The 3D models' structures are so sophisticated that in case of any problem, their internal codes cannot be intervened. Furthermore, it would be hard to comment on the processes which result in the final morphology separately in such complex models. For this reason, it is preferred to create simulations with simpler models in this study.

To best assess the success of a nourishment, the project should be continuously monitored with multiple surveys. According to comprehensive post-nourishment surveys, [26] stated that the most significant parameters for the equilibrium beach profile

formation after nourishment are the steepness and probability of occurrence of the wave perpendicular to the coast, the profile starting slope, the energy reduction coefficient, and the width of the meadow. It is also known that the rounder is the shape of sediment, the more contribution to offshore transport and thus to the loss of nourishment [27]. Moreover, the minerals that constitute the sediment particles may play a deterministic role in the fate of the beach fill since the probability of sediment cracking or the formation of particles depends on the chemical properties of the particles [28].

In light of the previous studies, we aim to determine the most important model parameters and develop a site-specific model to estimate the long-term evolution of the nourishment site. The remainder of this thesis is organized as follows: the Methodology chapter gives a review of the data obtained from BUCEL and explains the software and equations used for the profile evolution analysis. In the next chapter, the results are discussed. In the end, conclusion and recommendation for more sustainable nourishment projects and modeling their evolution are included.

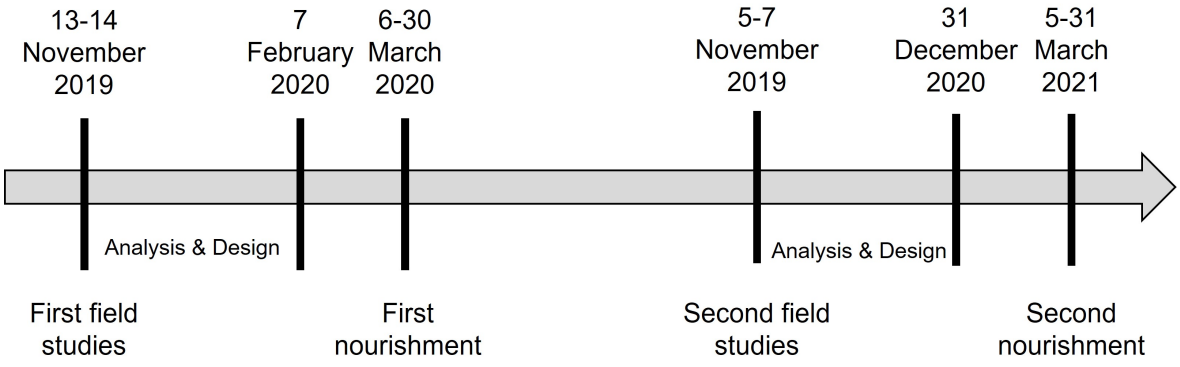

Figure 1.3. Timeline of the project conducted by BUCEL.

Table 1.1. Timeline of the Beach Nourishment Project.

Dates	**Activity**
13-14 November 2019 Measurements	First topographic, hydrographic, shoreline, water quality, and sea-level change measurement and sediment sampling by BUCEL. RTK GPS is used for stop-and-go measurements along the shoreline, 0.5m, and 1m depths, with lateral intervals of 20m. RTK GPS Rover unit and Sonar are mounted on the boat for hydrographic measurements, so the bathymetry map is obtained. The water level is recorded by a tide gauge every 15 minutes. Water salinity, temperature, and density are measured with a CTD device. Sediment samples are taken at the shoreline, in the middle of the beach, at -1m and -2m depths.
15 November 2019 – 7 February 2020 (Analysis & Design)	Sediments are subjected to sieve analysis and D50 values of each depth of each cross-section are determined. From the collected topographic and hydrographic data, a bathymetric map was drawn with the help of the PDS2000 program. The location, depth, distance from the shore, and dimensions of the concrete sill are involved in the map. The waves in the bay are modeled by SWAN and the swell data for the boundary condition are taken from Copernicus. Swells come from the South-West, while the local winds mostly cause waves from North-West. Bruun's Equation (1954) and two-parameter potential equations were used to find the equilibrium profiles in coastal sections. Hallermeier (1981) definition is used to calculate the depth of closure. The design parameters are selected accordingly.
6-30 March 2020 Measurements	Along 280 m, it was fed with fine-medium gravel (D50 = 7.3 mm) similar to the present one and 1667 m3 gravel for the long-term extension of the beach to the sea by an average of 2 m.
5-7 November 2020 Measurements	Shoreline, above-beach, -0.5, and -1 meter lines were measured by mobile GPS. The coastal profiles between the pavement and the sill at the bottom were measured using level, mira, and meter. The water level is recorded by a tide gauge every 15 minutes. For sediment analysis, a total of 16 samples were taken along the four sections along the Main Beach, at four points in each section, in the middle of the beach (+1 m), waterline (0 m), -1 m, and -2 m depths. Salinity, temperature, and density data were measured at 8 different points in the Kalemyel Bay, with a CTD device.
9 November 2020 - 31 December 2020 (Analysis & Design)	Sediments are subjected to sieve analysis and D50 values of each depth of each cross-section are determined. From the collected topographic and hydrographic data, a bathymetric map was drawn with the help of the PDS2000 program. The location, depth, distance from the shore, and dimensions of the sill are involved in the map. Wave data and depth of closure are taken from the previous BUCEL report (February 2020). The design parameters are selected accordingly.
5-31 March 2021 Measurements	For the long-term +2 m beach expansion, 1667 m3 of fine-medium size (D50 = 7.3 mm) gravel was used for nourishment. Right after the nourishment, the shore expanded by an average of 5.9 m from its original state, yielding an additional dry beach of 280 m in length and 1666 m2. (It is expected that by November 2021, the shoreline moves towards its position in November 2020 and reaches a partial equilibrium where the total gain in the dry beach is 2m and the area is 561 m2 in the long term.)

2. METHODOLOGY

Before starting the wave climate and sediment transport models, the two years studies of BUCEL on the research site are accumulated and analyzed. There had been two site measurements in November 2019 and November 2020. Accordingly, two nourishment designs are delivered. The two nourishment are applied in March 2020 and March 2021 respectively. There are also estimated equilibrium beach profiles that the sections are expected to reach in the long term. This chapter gives an overview of the data obtained from BUCEL, then explains the wave climate and beach morphology models that are used.

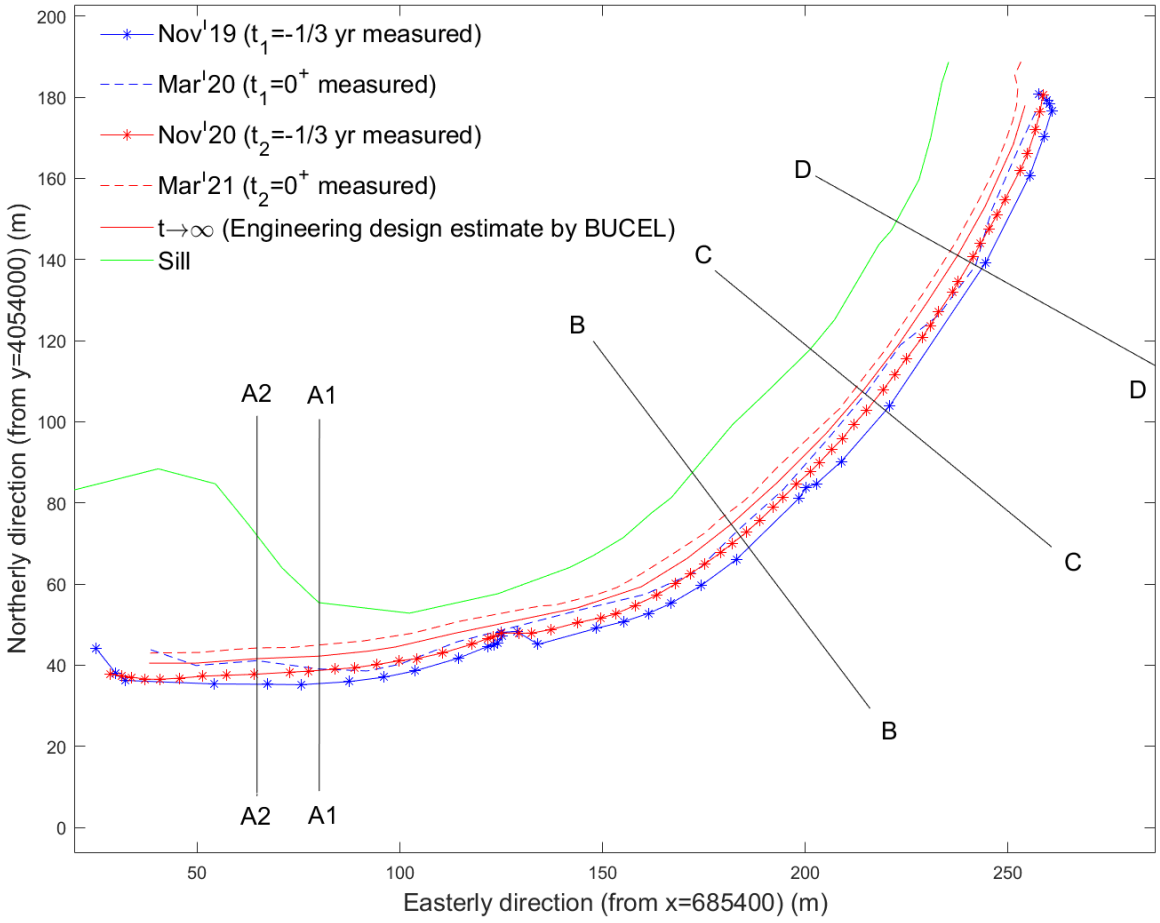

Figure 2.1. Changes in the beach in plan view.

2.1. Data Analysis

Changes in cross-sectional profiles and the location of the shorelines in plan view with easterly and northerly directions due to two nourishment projects are plotted in Figure 2.1. The dotted blue line corresponds to the first measurement conducted by BUCEL in November 2019. In the studied period, this is when the shoreline is the farthest back. In the four analyzed sections, the vertical datum for Figure 2.2, Figure 2.3, Figure 2.4, Figure 2.5, and Figure 2.6 is selected as the TUDKA-99 level and the horizontal datum is selected as November 2019 shoreline.

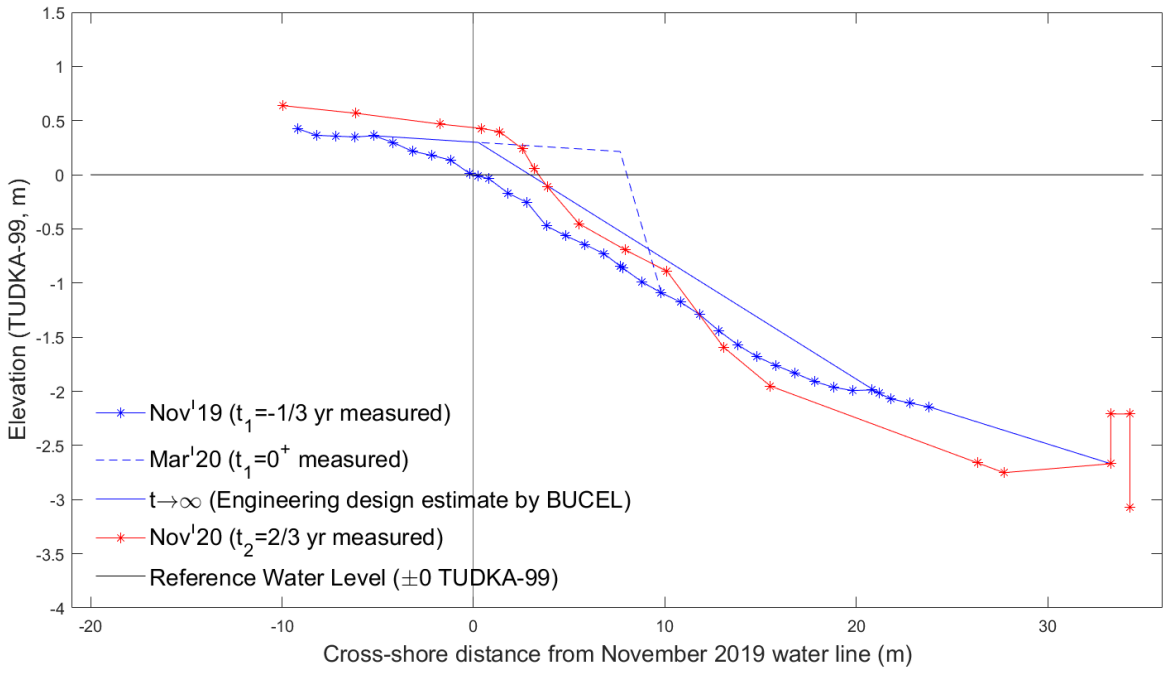

Figure 2.2. Changes in the beach cross-section A1 in cross-sectional view.

During the two years that BUCEL conducted the nourishment project, different cross-sections were studied in detail. They have studied five profiles in detail the first year and four profiles the second year. The last three transect lines (named cross-sections B, C, and D) are the same for both year's studies. One of the cross-sections studied in the first year is not studied in detail the following year because it overlaps with the pier. Due to a survey inconsistency, in the first year and the

second year slightly different transect lines are selected as the initial profile of the cross-section A. In this thesis, these transects are called cross-section A1 and cross-section A2 for the transect line studied in November 2019 and November 2020, respectively. Therefore, the evolution of these two cross-sections cannot be compared from one year to another. Only the model results of the profile evolution of cross-section A1 after the first nourishment can be compared with the following year's measurements of the same cross-section.

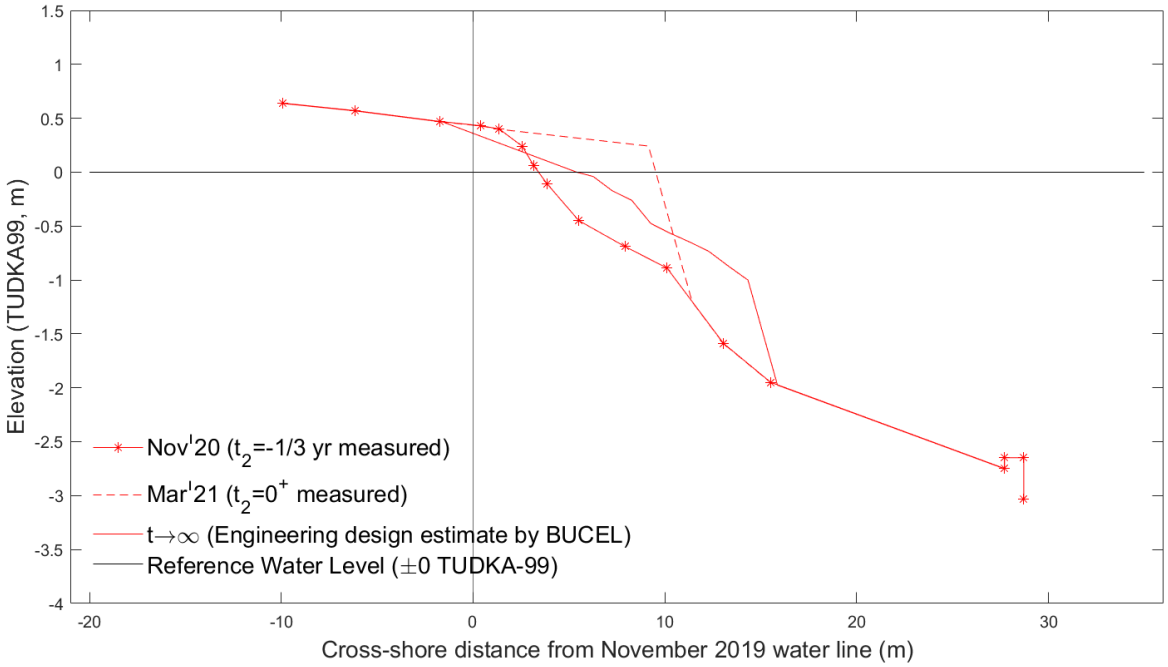

Figure 2.3. Changes in the beach cross-section A2 in cross-sectional view.

Regarding the slopes of the profiles shown with the blue dotted lines in Figure 2.2, Figure 2.4, Figure 2.5, and Figure 2.6, the original profile slopes were approximately 1:10 for cross-sections A1, 1:8 for B and C, and 1:10 for C and D. The application of the first nourishment design, which is shown with the blue dashed lines in Figure 2.2, Figure 2.4, Figure 2.5, and Figure 2.6, proposed by BUCEL provided a beach expansion of 8.18 m to cross-section A1, 8.51 m to cross-section B, 8.83 m to cross-section C and 8.70 m to cross-section D right after the nourishment. We can observe an average of 8.55 m expansion on the coast in March 2020. Naturally, the profile moved backward

in time, towards its position in November 2019. The design was made in such a manner that there would be a net 3 m gain in the cross-shore direction in the long term. Nourishment design slopes were 1:80 for cross-section A1 and 1:30 for cross-sections B, C, and D, which are the first mild slopes shown with blue dashed lines in Figure 2.2, Figure 2.4, Figure 2.5, and Figure 2.6, respectively. The bank slope for each cross-section was 1:1.6 (slope of the second part of the blue dashed lines in Figure 2.2, Figure 2.4, Figure 2.5, and Figure 2.6), which is the angle of repose of the selected fill material.

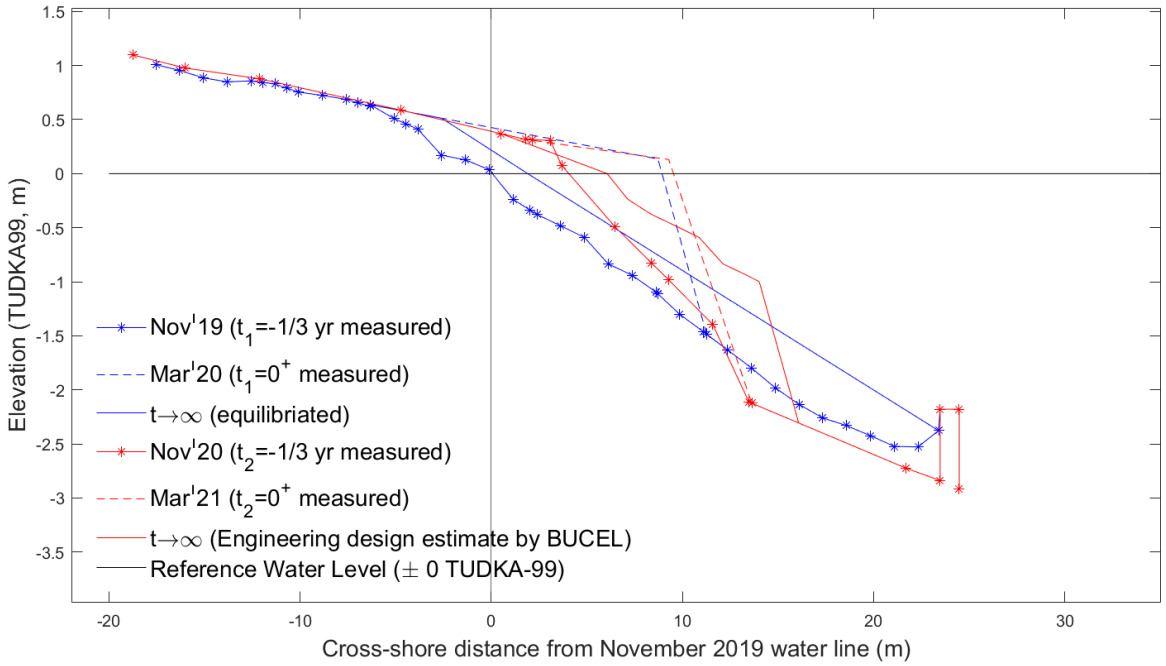

Figure 2.4. Changes in the beach cross-section B in cross-sectional view.

When BUCEL conducted the measurement in November 2020, only 7-8 months had passed since nourishment and the profile adjustment estimated for the long-term had not been completed yet. Though, there had been a significant evolution through the long-term estimations shown with blue straight lines in Figure 2.2, Figure 2.4, Figure 2.5, and Figure 2.6. In the measurements shown with red dotted lines in Figure 2.2, Figure 2.3, Figure 2.4, Figure 2.5, and Figure 2.6, the net dry beach gains from the original shoreline were 3.51 m in cross-section A1, 4.06 m in cross-section B, 4.20 m in

cross-section C, and 3.77 m in cross-section D. Expectedly, the measured slopes were also milder than the bank slope. The slopes at that time were approximately 1:10 for cross-sections A1 and A2 (Figure 2.2 and Figure 2.3), 1:7 for cross-section B (Figure 2.4), 1:7.5 for cross-section C (Figure 2.5), and 1:8 for cross-section D (Figure 2.6). Regarding these values and the general trend of evolution in 6 months, it can be noted that the first design was successful.

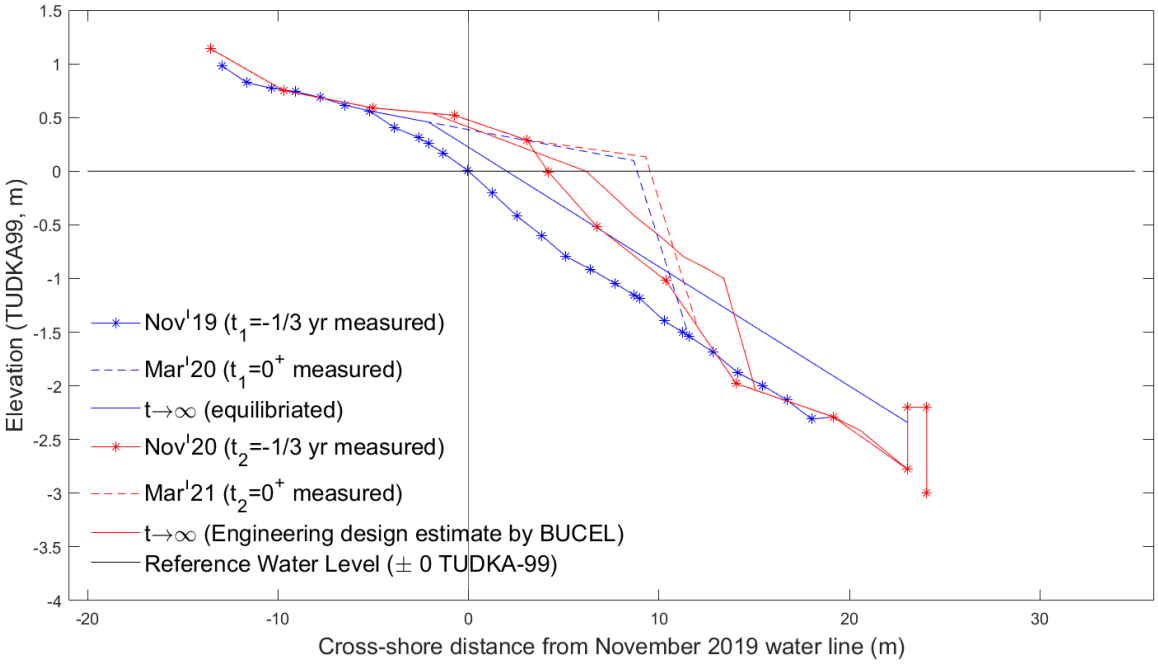

Figure 2.5. Changes in the beach cross-section C in cross-sectional view.

The second nourishment design aimed to add a 2 m length to the coast in the cross-sectional direction in the long term. The net dry beach length added to cross-sections immediately after the nourishment is calculated as the distance between the red dotted line and red dashed line at shoreline in Figure 2.3, Figure 2.4, Figure 2.5, and Figure 2.6. For cross-section A2 this value is 6.12 m (Figure 2.3), cross-section B it is 5.47 m (Figure 2.4), cross-section C it is 5.34 m (Figure 2.5), and cross-section D it is 5.64 m (Figure 2.6). The design beach slopes are 1:50 for cross-section A2, 1:40 for cross-section B and C, and 1:30 for cross-section D, which are the first mild slopes shown with blue dashed lines in Figure 2.3, Figure 2.4, Figure 2.5, and Figure 2.6, respectively.

Therefore, there is an average of 6 m expansion in the cross-shore direction. The bank slope is again 1:1.6 everywhere (slope of the second part of the blue dashed lines in Figure 2.3, Figure 2.4, Figure 2.5, and Figure 2.6). In the long-term, the nearshore beach slopes are estimated to be approximately 1:30 in cross-sections A2 (Figure 2.3) and B (Figure 2.4), 1:20 in cross-section C (Figure 2.5), and 1:26 in cross-section D (Figure 2.6).

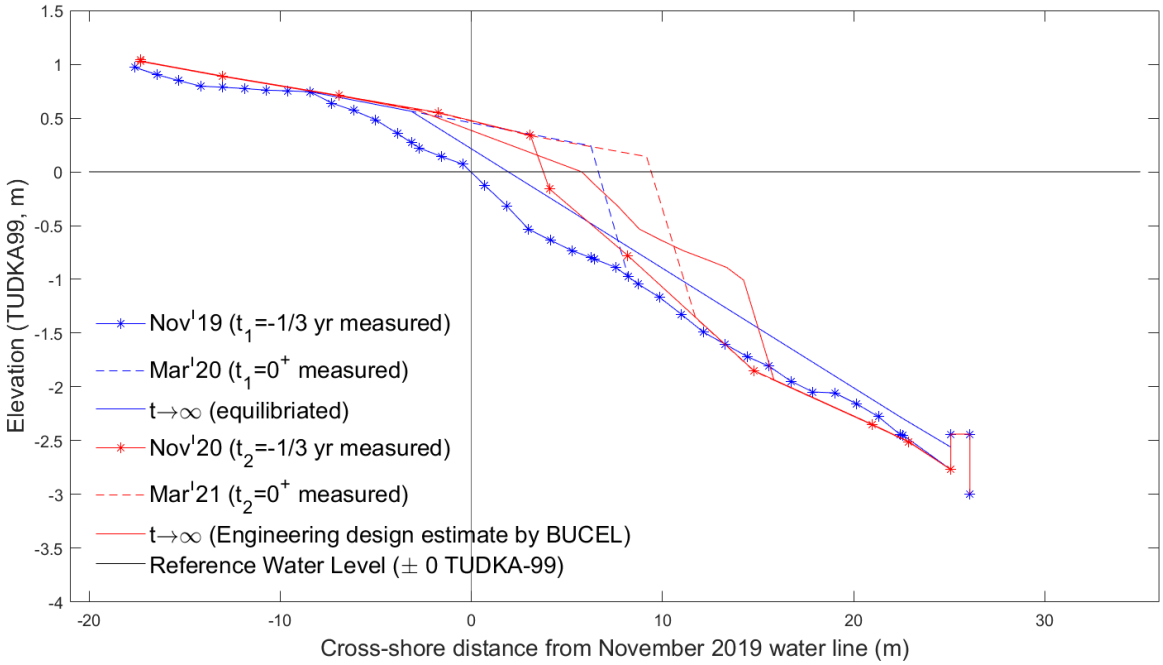

Figure 2.6. Changes in the beach cross-section D in cross-sectional view.

Waves have the most significant impact on coastal sediment transport phenomena. To predict the long-term morphology of the nourished beach, firstly the wave climate of the bay is investigated. Next, using the detailed wave output of SWAN, the XBeach-G model is run to estimate the profile evolution due to the cross-shore sediment transport. Nevertheless, the cross-shore results were not sufficient to explain the measured changes in the beach morphology. Therefore, the shoreline change due to the longshore transport is added to the model by use of the CERC equation for longshore diffusivity. At this point, the most important assumption made is that gravel particles are not dislodged markedly except in storm conditions. For this reason, the models simulate only the storm durations occurred in one year, instead of the whole year. The

accuracy of this assumption is tested and decided to be in an acceptable range for a long-term estimation.

2.2. Wave Climate

SWAN is a third-generation wave model developed at the Delft University of Technology to compute random, short-crested wind-generated waves in coastal regions. The main inputs are bathymetry, wind, and wave conditions at the boundaries. The outputs of the model are wavelength, wave height, and wave period. It is possible to create static or dynamic models by use of SWAN by giving a time series of wind and/or wave conditions as input. In this thesis, stationary runs of SWAN are used for multiple wind conditions.

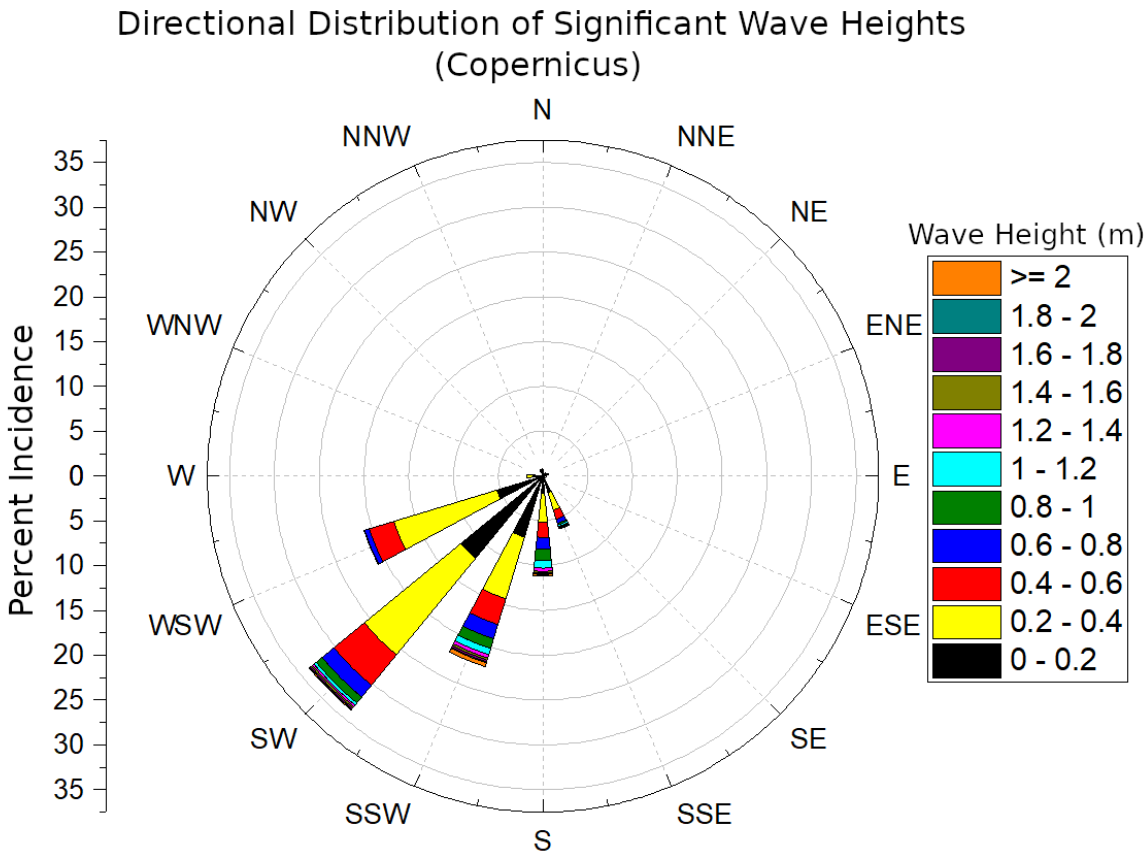

Figure 2.7. Incoming direction and wave height (in m) distribution of hourly significant wave in Fethiye Bay [2].

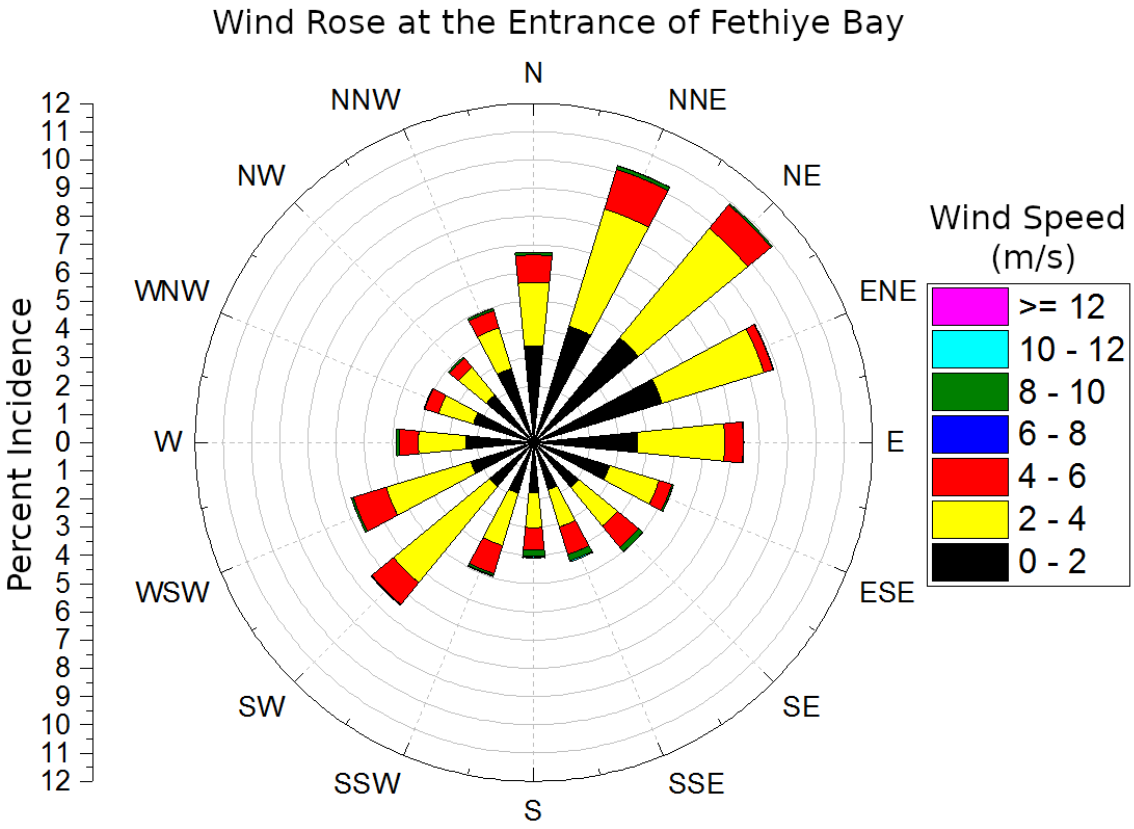

Figure 2.8. Incoming direction and magnitude (in m/s) distribution of incoming wind in Fethiye Inner Bay [2].

BUCEL analyzed the wave climate of the Fethiye Bay on large scale creating a coarse grid in the SWAN software [2]. For this purpose, they used wave time series data taken from Copernicus from the nearest data region to the study site. Copernicus provides data only at some specific locations. BUCEL used the data of a point at the entrance of the Fethiye bay. The Figure 2.7 shows the incoming direction and wave height distribution of hourly significant wave in Fethiye Bay. The numerical data of the swell conditions at the boundaries and wave velocities for the same direction is given in Table 2.1, and the wave rose is given in Table 2.2. They analyzed the data determining yearly averaged hourly significant wave heights, periods, and corresponding directions and performed their analysis using the most critical wave height and direction as the swell boundary condition for SWAN. For the wind input, they used the local wind

data of Fethiye Inner Bay taken from Genc et al. 2019 [29] who used the ECMWF wind data between the years 2000 and 2018. The data taken from Genc et al. 2019 is schematized by BUCEL as in the Figure 2.8. The numerical data of the wind rose is given in Table 2.3. The location of the wave and wind rose data is shown in Figure 2.9.

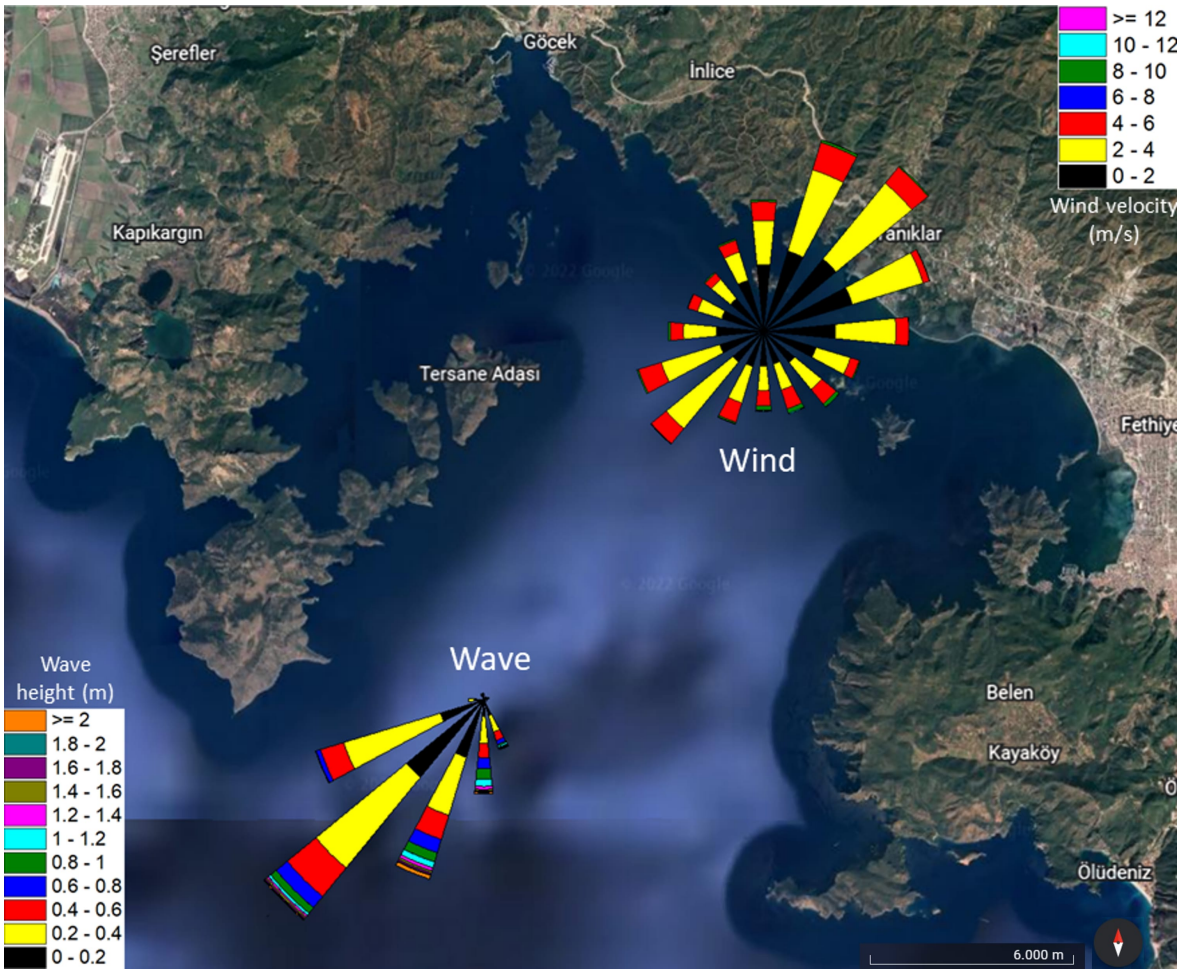

Figure 2.9. Direction and magnitude distribution of wind and wave at Fethiye Bay [2].

Using the outputs of the BUCEL analysis, a more detailed wave climate model of the Kalemyel Bay with a finer mesh is generated using SWAN. The wave climate of the Kalemyel Bay is simulated by the SWAN model. For the mesh, a grid area of 685198 m $\times$ 4053701 m with a bathymetry resolution of 7.5 m $\times$ 9 m. The computational grid with orientation of 38^o counterclockwise with the positive x-axis, has a resolution 3 m $\times$ 3 m. The bathymetry data which is taken from Navionics (2022) is shown in

Figure 2.10 and is used as an input for SWAN. Additionally, wave and wind data are used as same as [2].

Wave conditions that cause changes in beach morphology in the investigation site are caused by winds given in Table 3.1, Table 3.2, and Table 3.3. These are winds of 10 m/s from North-West which occurs 0.32 hour in a year, 10 m/s from North-North-West which occurs 0.32 hour in a year, 10 m/s from West which occurs 0.63 hour in a year, 10 m/s from North which occurs 0.32 hour in a year, 10 m/s from North-North-West which occurs 0.95 hour in a year, 10 m/s from West-South-West which occurs 0.32 hour in a year, 7 m/s from North-West which occurs 5.37 hours in a year, and 7 m/s from West-North-West which occurs 3.16 hours in a year [2]. Hence, it is decided to run only these situations to estimate long-term profiles. The results are first validated with the data taken between 5-7 November 2020, nearly 7 months after the first nourishment. Then, the same wave climate results are used as inputs to model the morphodynamics after the last nourishment which took place between 5-31 March 2021.

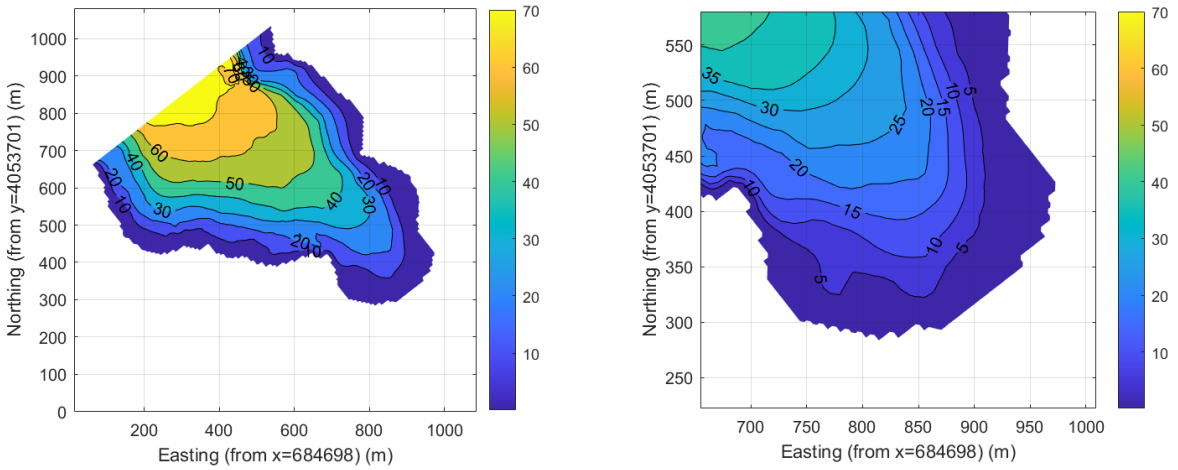

Figure 2.10. Bathymetry data of Kalemyel Bay (Navionics 2022).

As it can be seen in the Figure 2.9, the swells at the entrance of the bay mostly come from the southwest. However, the protected location of the bay prevents the swells coming from the open sea from affecting the beach to a great extent. For this

reason, it has been observed that wind waves created by local winds, especially in Fethiye Bay, play a more active role in the formation of waves affecting the facility.

Table 2.1. Swell conditions at the boundaries and wave velocities from the same directions (from BUCEL 2020 analysis).

Swell direction	Average significant wave height (m)	Average swell period s(s)	Significant swell period (s)	Average wind velocity (m/s)
SW	0.49	5.42	4.30	2.81
WSW	0.33	4.52	4.70	2.82
SSW	0.75	5.37	4.70	2.89
S	0.82	5.03	5.20	3.06

Table 2.2. Wave rose data for Fethiye Bay from Copernicus (taken from BUCEL data analysis).

	1 h/year		**12 h/year**		**1 h/weak**	
Direction	H_s **(m)**	T_m **(s)**	H_s **(m)**	T_m **(s)**	H_s **(m)**	T_m **(s)**
S	3.2	7	1.9	6.3	1.1	5.6
SSW	3	7.1	1.6	6.3	0.86	5.5
SW	2.3	7.1	1.6	6.3	0.86	5.5
WSW	2.4	7.1	1.4	6.3	0.81	5.6
W	1.1	6.5	1.3	5.9	0.74	5.2

Table 2.3. Wind rose data for Fethiye Bay [29].

Direction	Max wind speed (m/s)	Total hours	0-2 (m/s)	2-4 (m/s)	4-7 (m/s)	7-10 (m/s)	10-13 (m/s)	$\geq$ 30 (m/s)	Direction ratio (%)
N	10.92	11.238	5.688	3.738	1.638	168	6	0	6.75
NNE	12.83	17.058	7.170	7.224	2.436	210	18	0	10.24
NE	10.23	18.234	8.004	8.322	1.788	114	6	0	10.95
ENE	10.96	14.790	7.914	6.294	552	24	6	0	8.88
E	8.06	12.402	6.150	5.130	1.0988	24	0	0	7.45
ESE	10.47	8.634	4.686	3.054	780	102	12	0	5.18
SE	11.24	8.352	3.468	2.922	1.632	306	24	0	5.01
SSE	12.63	7.362	2.910	2.304	1.698	384	66	0	4.42
S	15.24	6.828	2.964	2.070	1.332	354	90	18	4.10
SSW	14.54	8.256	3.138	3.228	1.716	138	30	6	4.96
SW	10.78	12.420	3.384	7.332	1.650	48	6	0	7.46
WSW	10.10	11.262	3.894	7.332	1.650	48	6	0	7.46
W	10.66	8.130	4.032	2.796	1.116	174	12	0	4.88
WNW	8.11	6.780	3.732	2.154	834	60	0	0	4.07
NW	10.28	6.552	3.636	2.106	702	102	6	0	4.96
NNW	11.01	8.262	4.560	2.508	1.050	138	6	0	4.96
Cum. Dur. (h)		166.560	75.330	66.402	22.038	2.472	294	24	-

2.3. Beach Morphology

Using the incident wave to the beach, long-term profile evolution for the selected cross-sections is analyzed. The main phenomenon that causes a change in the profile shape is sediment transport. In this chapter, the method to analyze changes due to cross-shore and longshore sediment transport are explained. The results obtained from the models are superposed to obtain the total morphological change. By superposing these two transport modes, we assume that these two processes are linear. The longshore diffusivity equation (Equation 2.1) is a linear equation. Even though the cross-shore sediment transport has a nonlinear nature [4–6], it is assumed to be nearly nonlinear in this thesis and it is tested through experiments explained in Section 3.2. in detail. Hence, these two processes are modeled separately, and the results are added to each other linearly. XBeach-G is used for the cross-shore transport, and the diffu-

sivity equation is used for the longshore transport model since there are examples in the literature where their results give accurate results for gravel beaches [25].

2.3.1. Cross-shore sediment transport

XBeach-G is a subset of the main XBeach project that simulates storm impacts on gravel beaches. While XBeach is a two-dimensional model, XBeach-G is a one-dimensional model considering only the cross-shore sediment transport. The large part of change in the profiles in the long-term is expected to be due to cross-shore sediment transport. Hence, XBeach-G can be used to estimate the profile evolution related to cross-shore transport after nourishment.

The model is run for each cross-section twice (except from cross-section A1 of the first year's study and cross-section A2 of the following year which are not exactly the same sections); one time for simulating the profile evolution after the first nourishment in March 2020, and one time for simulating the profile evolution after the second nourishment in March 2021. The simulation of the profile after the first nourishment is compared to measurements during the field investigation in November 2020.

On a common desktop computer, the simulation to computation time ratio of XBeach-G simulations is approximately 1:1–2:1 [30]. Therefore, only periods with high wave impact are simulated with the assumption that coarse sediments response poorly to calm or moderate wave climate. To test this assumption, several test cases are run in XBeach-G with an initial profile subjected to different significant wave heights. The selected initial profile is the measured post-nourishment in 5-7 November 2020 of cross-section C (which can be seen in Figure 2.5). During the simulation, the significant wave height input is increased over 30 minutes time periods starting from 0.2 m up to 0.6 m. It is shown that on a profile that reached the equilibrium to a large extent, the effect of the waves with significant wave heights lower than 0.6 m is not remarkable.

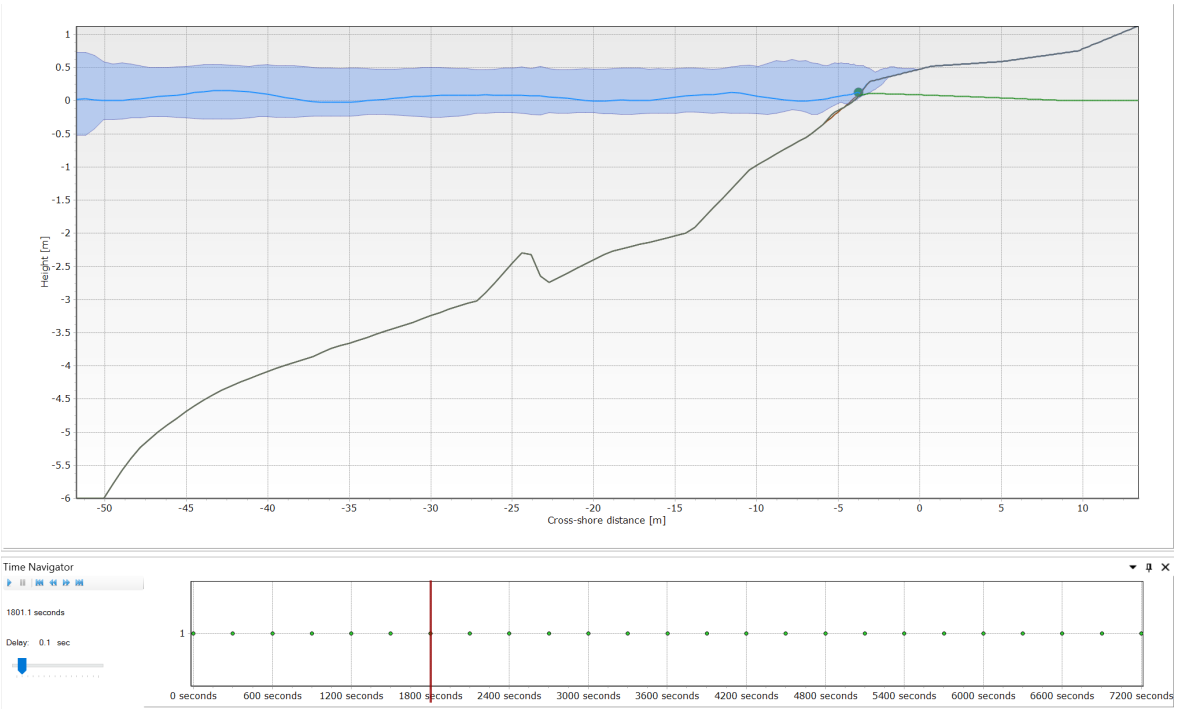

Figure 2.11. Test case: Cross-section C measured in Nov'20 subject to $H_s = 0.2$ m for 30 minutes, initial profile shown with the gray line and the evolved profile is shown with brown line.

For all test cases and model runs, morphological parameters are selected according to site investigations and data analysis. For results shown in Figure 2.11, Figure 2.12, and Figure 2.13; the medium diameter is $D_{50} = 0.0049$ m, hydraulic conductivity is $k = 0.1369$ m/s (obtained from Hazen's empirical equation for coarse-grain soils [31]), and the JONSWAP spectrum is used for the wave module. For the morphology calculation, Van Rijn formula is selected on the model with an angle of repose of 33^o. The gray lines in the referred figures show the initial profiles and the brown lines show the evolved profile. Below the profiles, there is a time navigator that allows the user to see the profile at a selected output time. The outputs are printed at time intervals specified by the user. Initial profiles are shown with gray line and evolved profiles are shown with brown line. The blue colored area is the range of water level changing due to waves and tides and the blue line is the water surface elevation. Green line shows the groundwater level. The small green circle stand for the instantaneous shoreline or run-up.

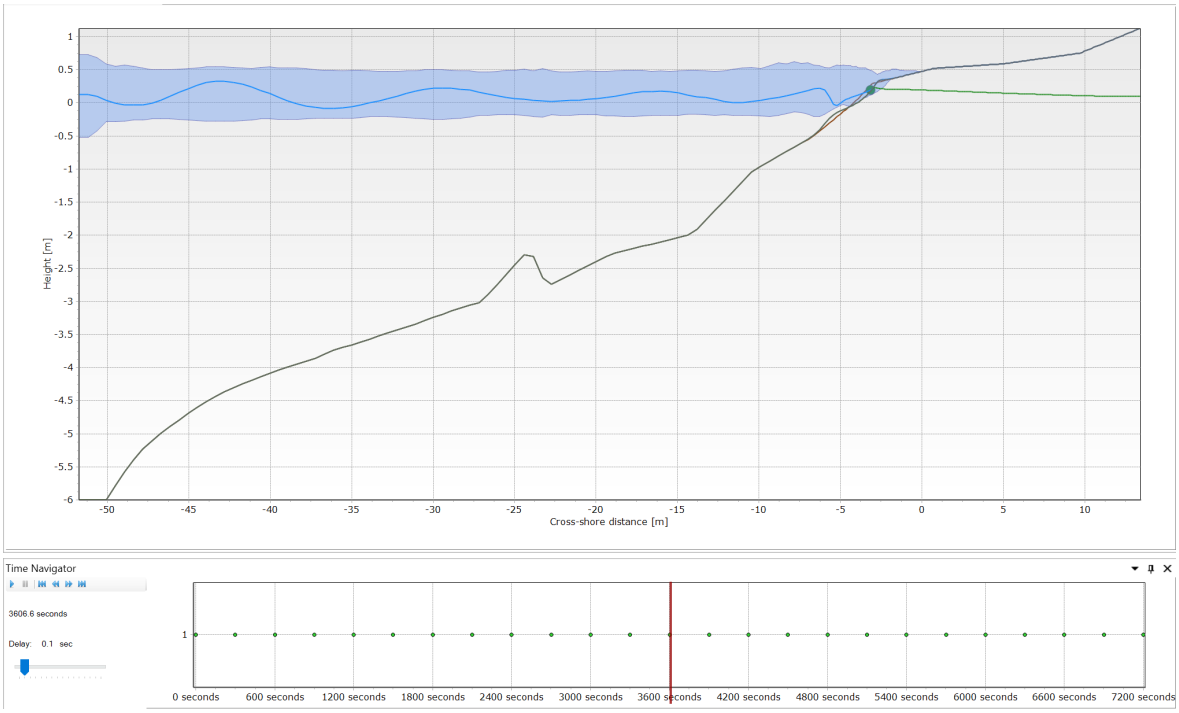

Figure 2.12. Test case: Cross-section C measured in Nov'20 subject to $H_s = 0.4$ m for 30 minutes after being subject to $H_s = 0.2$ m for 30 minutes, initial profile shown with the gray line and the evolved profile is shown with brown line.

Regarding the results obtained by the test cases, the consequences of only several wave conditions are decided to be studied. Wave conditions that cause changes in beach morphology in the investigation site are caused by winds of 10 m/s from North-West which occurs 0.32 hour in a year, 10 m/s from North-North-West which occurs 0.32 hour in a year, 10 m/s from West which occurs 0.63 hour in a year, 10 m/s from North which occurs 0.32 hour in a year, 10 m/s from North-North-West which occurs 0.95 hour in a year, 10 m/s from West-South-West which occurs 0.32 hour in a year, 7 m/s from North-West which occurs 5.37 hours in a year, and 7 m/s from West-North-West which occurs 3.16 hours in a year [2]. Hence, it is decided to run only these situations to estimate long-term profiles.

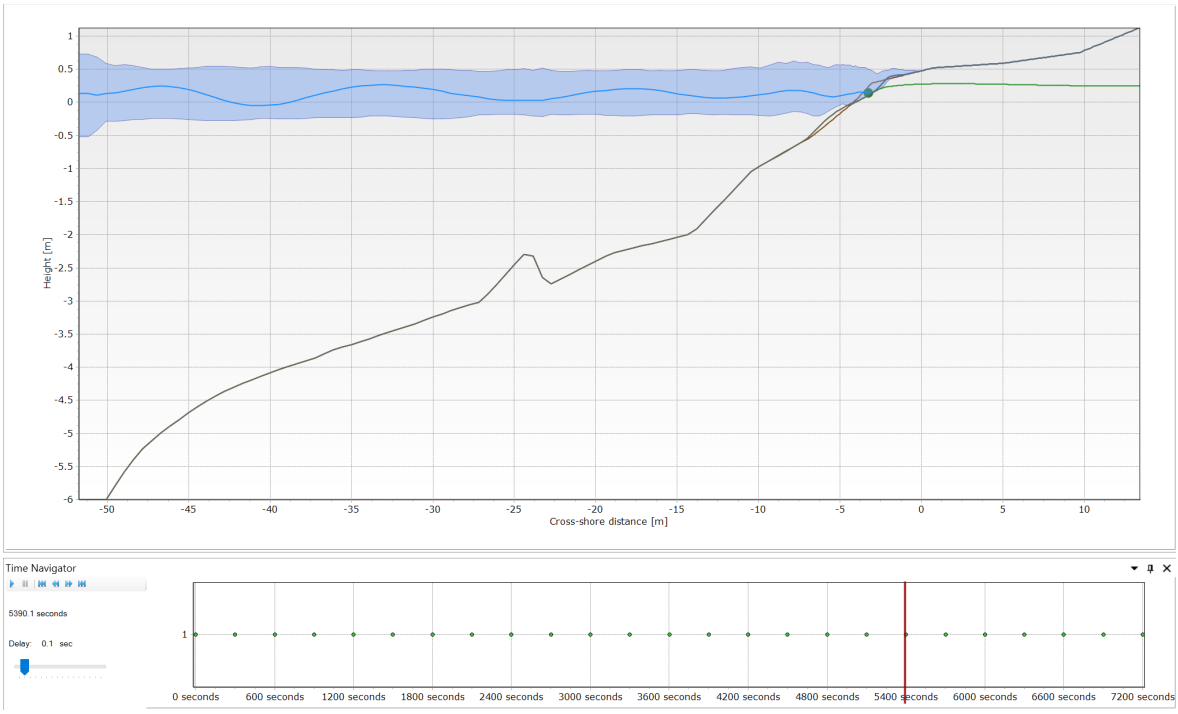

Figure 2.13. Test case: Cross-section C measured in Nov'20 subject to $H_s = 0.6$ m for 30 minutes after being subject to $H_s = 0.2$ m and $H_s = 0.4$ m for 30 minutes each, initial profile shown with the gray line and the evolved profile is shown with brown line.

2.3.2. Longshore Sediment Transport

Even though the major part of profile change is estimated to be caused by cross-shore transport, only cross-shore analysis of sediment motion is not sufficient in the project site since longshore current gradients are essential at non-straight shorelines such as embayed or pocket beaches [32]. There are many formulas suggested at different times by different scientists for the longshore sediment transport rate. In this study, the most commonly used CERC equation for diffusivity is used to predict the shoreline recession due to longshore sediment transport. This is also known as the Pelnard-Considere equation for the one-line model [33]. This equation has the form of the 1D transient diffusion equation

$$\frac{\partial y}{\partial t} = G\frac{\partial^2 y}{\partial x^2}, \tag{2.1}$$

where y is the shoreline position, x is the longshore direction, and G is the longshore diffusivity and can be taken as constant in many applications. In the derivation of Equation (2.1), G is assumed to be constant to have this form of linear diffusivity equation. However, it can be assumed variable in time by setting it equal to different values in different time steps. The open formula for G is

$$G = \frac{K H_b^{5/2} \sqrt{g/\kappa}}{8(s-1)(1-p)(h_* + B)}, \tag{2.2}$$

where K is the longshore transport coefficient, H_b is the breaking wave height, g is the gravitational acceleration, κ is the spilling breaker, s is the specific gravity of the sediment, p is the porosity of the sediment, h_* is the depth of closure, and B is the berm height. In a case of different wave heights, G can also have different values throughout the simulation. However, for the sake of simplicity, a constant G value is selected for each simulation in this thesis. Shoreline changes after beach fill of arbitrary shapes can be modeled by the numerical solution of this equation. Regarding the shape of the beach, the boundary conditions are selected as Dirichlet type of boundary condition. Given that the shoreline position at the position x and time t is expressed as $y(x,t)$, the boundary condition has the following form

$$y(0,t) = y(0,0), \tag{2.3}$$

$$y(L,t) = y(L,0), \tag{2.4}$$

where L is the length of the domain. This boundary condition suggests that the endpoints of the shoreline do not change in time. This selection is made since the endpoints of the shoreline are rocks that are considered to be immobile for the duration that the simulation is run.

The initial condition for the problem is selected as the perpendicular distance of the shoreline after nourishment to the shoreline before nourishment at each x position.

To be able to use this one-line model, the problem domain should be slightly modified in order to satisfy the criteria of the one-line theory. One-line model is

applicable for straight shorelines where the depth contours are parallel to the shoreline. However, in the study site of this project, the beach is a pocket beach and the depth contours are accordingly curved. For this reason, the initial shoreline is assumed to be straight, multiple points on the shoreline before and after nourishment are selected and the perpendicular distance between them is calculated and given as the initial condition. The shoreline direction shown with s in the Figure 2.14 is x in the equations, and the normal direction n is the shoreline position y. Hence, x in the equations is the tangential distance along the shore, and y is the normal distance from the shoreline. The figure representatively shows the shoreline position after nourishment.

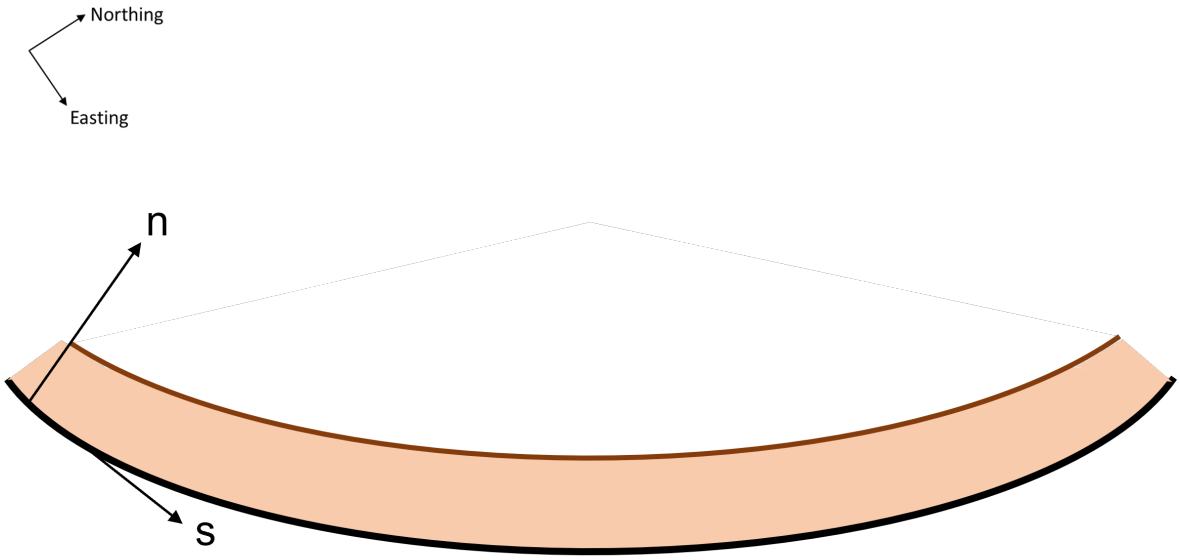

Figure 2.14. Representative of local coordinates used for the one-line model.

One of the most efficient and simple ways of approximating a 1D second-order partial differential equation is by adopting the finite difference method. For modeling the present problem numerically, the implicit finite difference scheme is used, which is described in the Figure 2.15. The governing equation is discretized as below

$$\frac{y_i^{j+1} - y_i^j}{\Delta t} = G\frac{y_{i-1}^{j+1} - 2y_i^{j+1} + y_{i+2}^{j+1}}{\Delta x^2}, \tag{2.5}$$

which for the unknown time step can be written as

$$y_i^{j+1} = y_i^j + \frac{G\Delta t}{\Delta x^2}\left(y_{i-1}^{j+1} - 2y_i^{j+1} + y_{i+2}^{j+1}\right), \tag{2.6}$$

where i denotes the space index and j the time index. In the implicit scheme, the right-hand side also includes the next time step. This means that for the next time step, one known value and three unknown ones are used. With this method it is not possible to find each nodal value of the next time step separately, however, solving the whole system will allow finding all nodal values of the next step at once. For this aim, the equation can be written in the matrix form, passing all the terms related to the unknown time step to the right-hand side. Meanwhile, for the ease of notation, we can define $r = \frac{G\Delta t}{\Delta x^2}$. So, the equation is written as

$$-ry_{i-1}^{j+1} + (1+2r)y_i^{j+1} - ry_{i+1}^{j+1} = y_i^j. \tag{2.7}$$

Or in the matrix form, the equation can be written as

$$\begin{bmatrix} ... & ... & ... & ... & ... & ... & 0 \\ \vdots & 0 & 0 & ... & ... & ... & ... \\ ... & -r & 1+2r & -r & 0 & ... & ... \\ ... & 0 & -r & 1+2r & -r & 0 & ... \\ ... & ... & 0 & -r & 1+2r & -r & ... \\ ... & ... & ... & 0 & 0 & \vdots & ... \\ 0 & ... & ... & ... & ... & ... & ... \end{bmatrix} \begin{bmatrix} \vdots \\ \vdots \\ y_{i-1}^{j+1} \\ y_i^{j+1} \\ y_{i+1}^{j+1} \\ \vdots \\ \vdots \end{bmatrix} = \begin{bmatrix} \vdots \\ \vdots \\ y_{i-1}^{j} \\ y_i^{j} \\ y_{i+1}^{j} \\ \vdots \\ \vdots \end{bmatrix}. \tag{2.8}$$

Naming the tridiagonal matrix as S (standing for the system matrix), the system of equation can be written as

$$Sy^{j+1} = y^j. \tag{2.9}$$

Before solving the matrix equation for each time step, boundary conditions and initial conditions must be applied to the first and last line of the matrix. To apply Dirichlet boundary conditions given in Equation (2.4), it is sufficient to make the following

modification in the system matrix

$$S(1,1) = 1, \tag{2.10}$$

$$S(1,2) = 0, \tag{2.11}$$

$$S(N_x, N_x - 1) = 0, \tag{2.12}$$

$$S(N_x, N_x) = 1, \tag{2.13}$$

where N_x is the number of nodes in the shoreline direction. In this way, the last value of y will always repeat itself by giving the initial value (given that the initial condition at this end is consistent with the boundary condition). It should be noted that except for the defined boundary values and tridiagonal terms, all other terms of S are null. The initial condition can be simply applied as follows

$$y(x,0) = y_0, \tag{2.14}$$

where y_0 stands for the normal distance between the pre-nourishment and post-nourishment shorelines for each case.

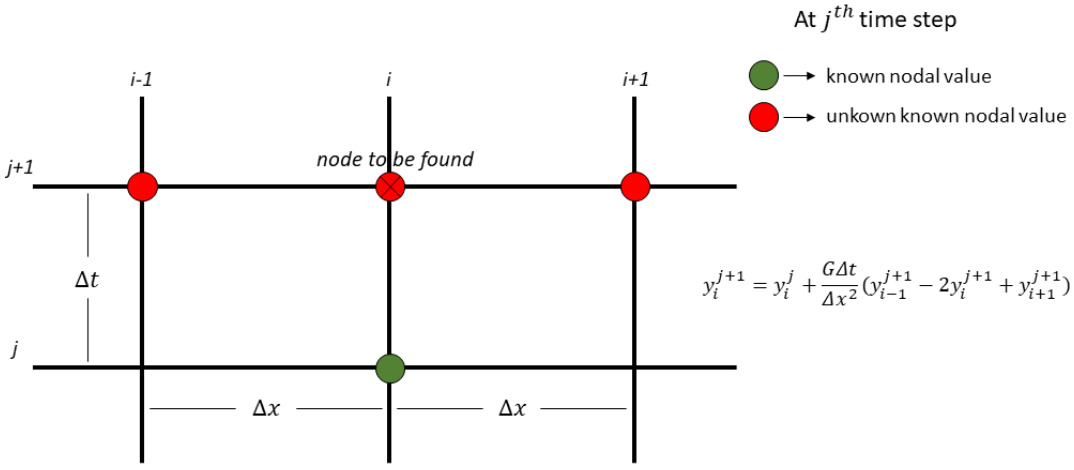

Figure 2.15. Implicit Finite Difference Scheme for 1D diffusion equation.

The algorithm for the implicit finite difference scheme is solved in MATLAB. Despite MATLAB's ability to solve big size matrices, repeating this process in a big number of iterations (here, for each time step) is time-consuming. To speed up the

matrix operation, the LU decomposition technique is used. LU decomposition consists of two steps. After having decomposed the matrix S to the corresponding lower L and upper U diagonal matrix, such that $S = LU$, Equation (2.9) can be easily solved as follows

$$Sy^{j+1} = y^j \quad \rightarrow \quad LUy^{j+1} = y^j. \tag{2.15}$$

Defining $w = Uy^{j+1}$, the matrix equation becomes

$$Lw = y^j. \tag{2.16}$$

The right-hand side of the Equation (2.16) is the multiplication of a lower triangular matrix and a column vector, which can be easily solved by finding each element one by one and substituting it into the other one starting from the top. Once the equation is solved for w,

$$Uy^{j+1} = w \tag{2.17}$$

can be solved for y^{j+1}, which is the solution that we seek at each time step. Again, the right-hand side of the Equation (2.17) consists of the multiplication of an upper triangular matrix and a column vector. Hence, each element of y^{j+1} can be easily found one by one, starting from the bottom.

3. RESULTS AND DISCUSSION

This chapter includes the wave climate results obtained by SWAN for the conditions stated in Chapter 2, and beach morphology results after two consecutive nourishment obtained by XBeach-G for cross-shore sediment transport and the diffusivity model for longshore sediment transport. The ratios of cross-shore and longshore transport rates are compared for each profile for two consecutive years by comparing the model results with the measurements of November 2020.

3.1. Nearshore Wave Climate Results

The wave climate of the Kalemyel Bay is modeled for the wind conditions stated in the Section 2.2. All the 8 wind conditions are simulated separately in static models. For boundary conditions, the wave height and peak period values of the coarse grid simulations of BUCEL [2] at the entrance of the study domain with the same wind conditions are used. They simulated for the whole Fethiye Bay of 24.8 km × 17.2 km dimensions, with a bathymetry grid of 100 m × 100m, computational grid of 50 m × 50 m.

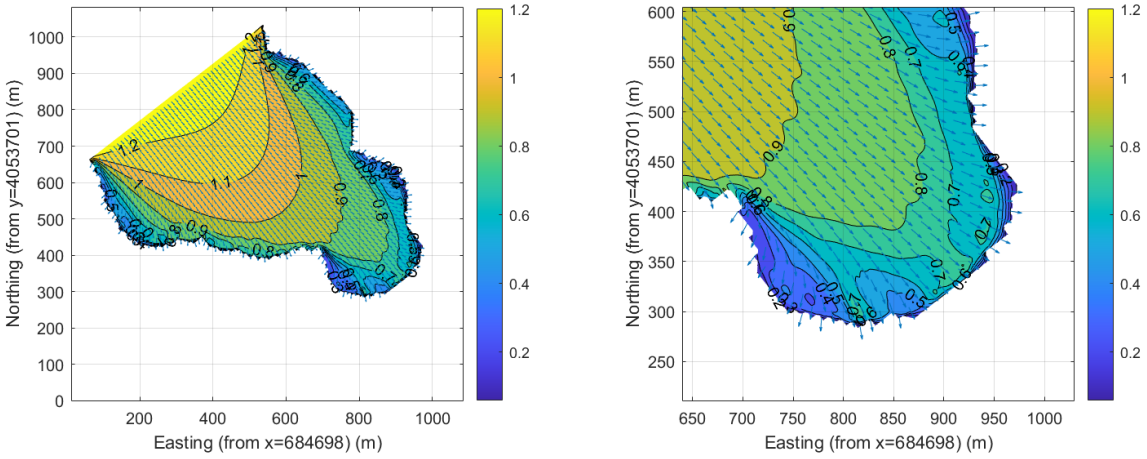

Figure 3.1. SWAN results for significant wave heights in Kalemyel Bay, Wind: 10 m/s NW, Wave BC: $H_s = 1.16$ m, $T = 4.52$ s.

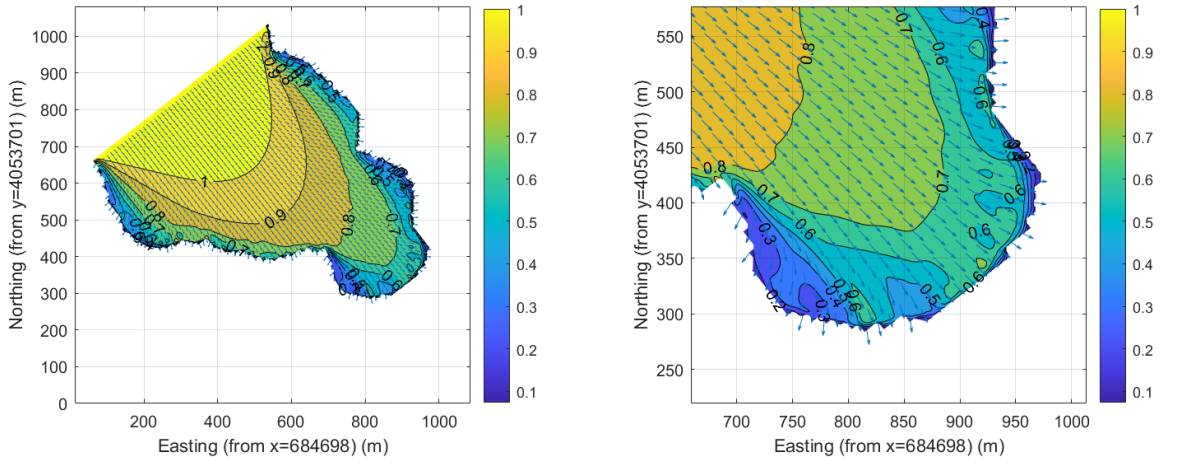

Figure 3.2. SWAN results for significant wave heights in Kalemyel Bay, Wind: 10 m/s NNW, Wave BC: $H_s = 1.05$ m, $T = 4.52$ s.

Kalemyel Bay can be categorized as an embayed beach due to its specific location in Fethiye Bay and its protection from the waves. The most extreme wave conditions which cause changes in the morphology of the gravel beach are simulated by SWAN. In Figure 3.1, Figure 3.2, Figure 3.3, Figure 3.4, Figure 3.5, Figure 3.6, Figure 3.7, and Figure 3.8 significant wave height and wave directions are shown for each of these conditions.

The wave height contours on the area where the beach is located is zoomed for a better resolution. The wave heights read from these figures are used as inputs for XBeach-G.

In all of the cases, the wave height contours decrease as they move on from the entrance of the Kalemyel Bay through the inner parts. The main reason for this decrease is the diffraction that the waves are subjected to at the entrance of the bay. Considering the whole of Fethiye Bay, the waves that arrive at Kalemyel Bay are already diffracted passing through the corners until arriving at the mouth of the bay. That is why the incoming direction of waves is the same for all cases at that boundary, which is the Northwest direction. The wave height boundary condition is read from the coarse grid analysis of BUCEL at that location for the corresponding wind inputs.

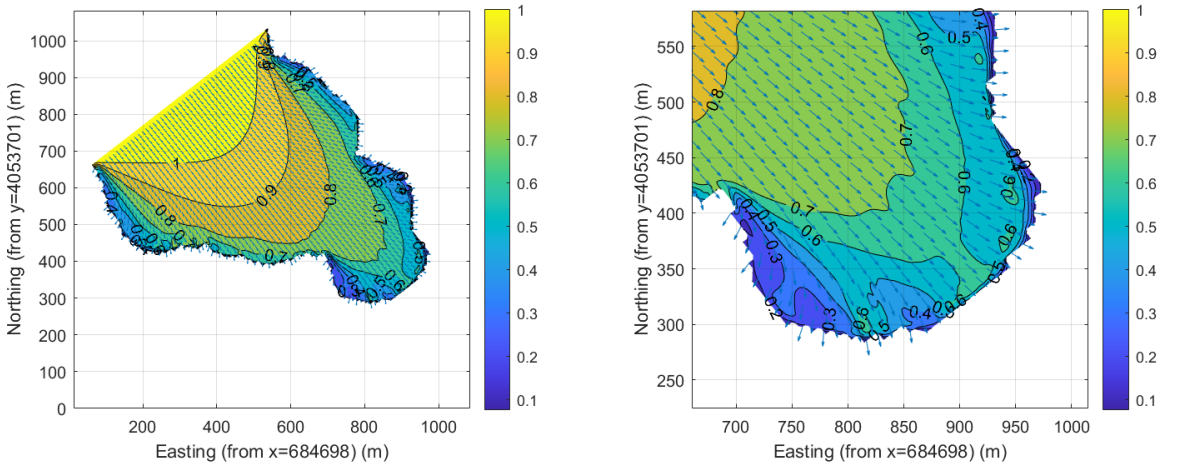

Figure 3.3. SWAN results for significant wave heights in Kalemyel Bay, Wind: 10 m/s W, Wave BC: $H_s = 1$ m, $T = 4.52$ s.

The direction of the waves near the entrance of the bay is affected by the wind direction. However, through the inner parts, the directions become more and more perpendicular to the shoreline due to refraction. Shoaling phenomena are not observable from these SWAN outputs because it happens very close to the shore, where the waves start to feel the bottom.

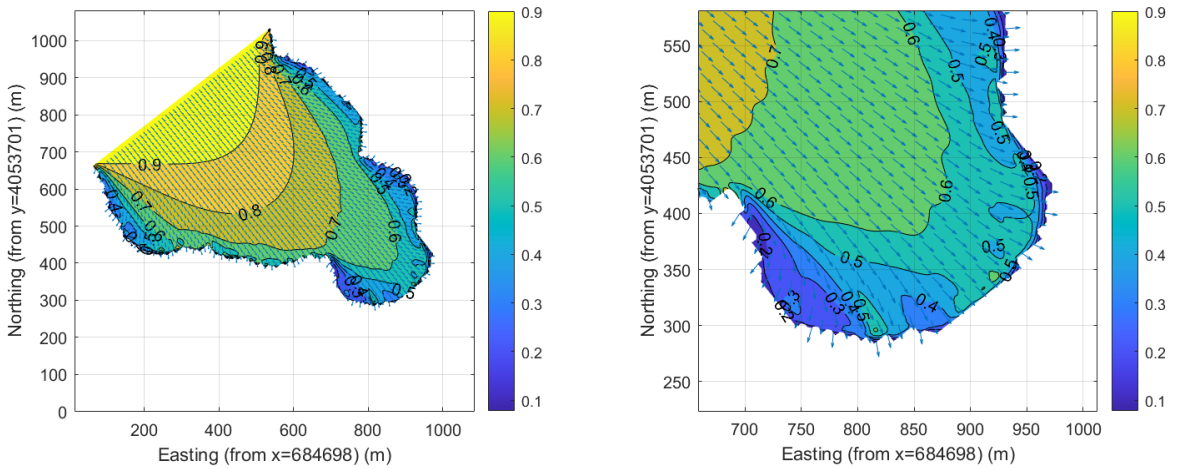

Figure 3.4. SWAN results for significant wave heights in Kalemyel Bay, Wind: 10 m/s N, Wave BC: $H_s = 0.9$ m, $T = 4.52$ s.

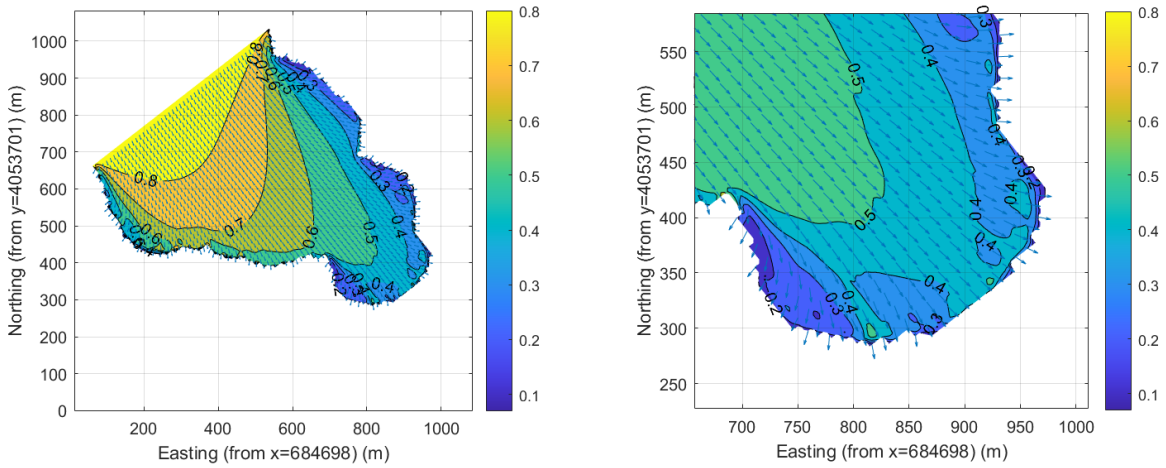

Figure 3.5. SWAN results for significant wave heights in Kalemyel Bay, Wind: 10 m/s NNE, Wave BC: $H_s = 0.8$ m, $T = 4.52$ s.

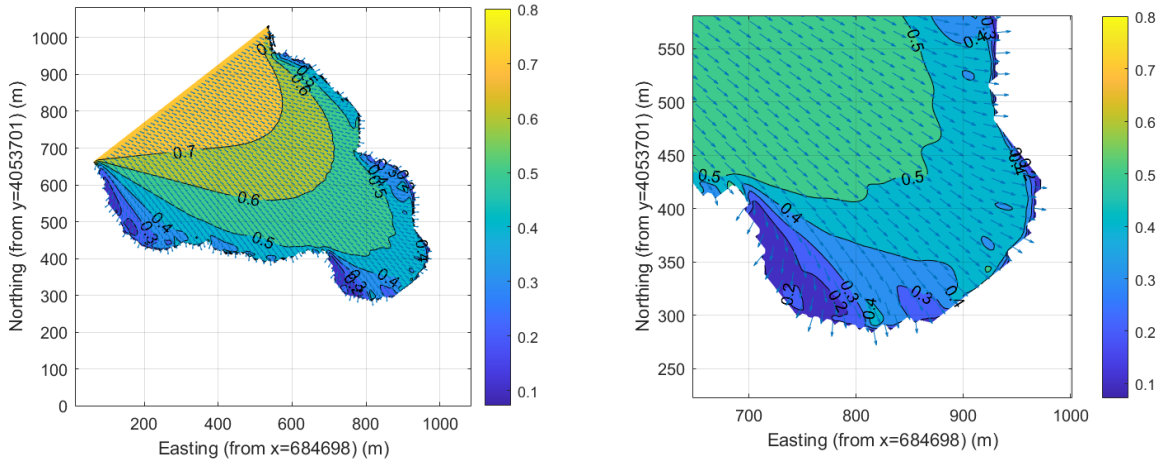

Figure 3.6. SWAN results for significant wave heights in Kalemyel Bay, Wind: 10 m/s WSW, Wave BC: $H_s = 0.75$ m, $T = 4.52$ s.

Wave height values near the boundaries are consistent with the wave heights given as boundary conditions of the model. Then, they decrease because of diffraction and refraction effects on the wave height. Each case cause different wave conditions at each cross-section. The highest waves that reach the beach on the average occur with the wind of 10 m/s coming from Northwest, and the lowest ones occur with the wind of 7 m/s coming from Northwest and West-Northwest. The irregularities in the wave height contours near the shore are due to irregular depth contours that can also be seen in Figure 2.10.

The wave heights are read from these figures and are used as inputs for the morphology models. The profiles given to XBeach-G are from the 6 m depth up to the dry beach area. Therefore, the wave conditions at 6 m depth should be entered to XBeach-G. These values are read from these figures for each cross-section by superposing them with the bathymetry map obtained from Navionics (2022). The wind with velocity of 10 m/s which comes from NW causes a significant wave height of 0.65 m at cross-section A1 and A2, 0.75 m at the cross-section B, 0.75 at the cross-section C, and 0.47 at the cross-section D, which can be seen in Figure 3.1. The wind with velocity of 10 m/s which comes from NNW causes a significant wave height of 0.60 m at cross-section A1 and A2, 0.65 m at the cross-section B, 0.65 at the cross-section C, and 0.65 at the cross-section D, which can be seen in Figure 3.2. The wind with velocity of 10 m/s which comes from W causes a significant wave height of 0.55 m at cross-section A1 and A2, 0.65 m at the cross-section B, 0.65 at the cross-section C, and 0.65 at the cross-section D, which can be seen in Figure 3.3. The wind with velocity of 10 m/s which comes from N causes a significant wave height of 0.55 m at cross-section A1 and A2, 0.65 m at the cross-section B, 0.65 at the cross-section C, and 0.60 at the cross-section D, which can be seen in Figure 3.4. The wind with velocity of 10 m/s which comes from NNE causes a significant wave height of 0.42 m at cross-section A1 and A2, 0.45 m at the cross-section B, 0.43 at the cross-section C, and 0.40 at the cross-section D, which can be seen in Figure 3.5. The wind with velocity of 10 m/s which comes from WSW causes a significant wave height of 0.35 m at cross-section A1 and A2, 0.47 m at the cross-section B, 0.43 at the cross-section C, and 0.43 at the cross-section D, which can be seen in Figure 3.6. The wind with velocity of 7 m/s which comes from NW causes a significant wave height of 0.32 m at cross-section A1 and A2, 0.40 m at the cross-section B, 0.37 at the cross-section C, and 0.37 at the cross-section D, which can be seen in Figure 3.7. The wind with velocity of 10 m/s which comes from WNW causes a significant wave height of 0.32 m at cross-section A1 and A2, 0.38 m at the cross-section B, 0.38 at the cross-section C, and 0.35 at the cross-section D, which can be seen in Figure 3.8. These values can be read also in the Table 3.1, Table 3.2, and Table 3.3.

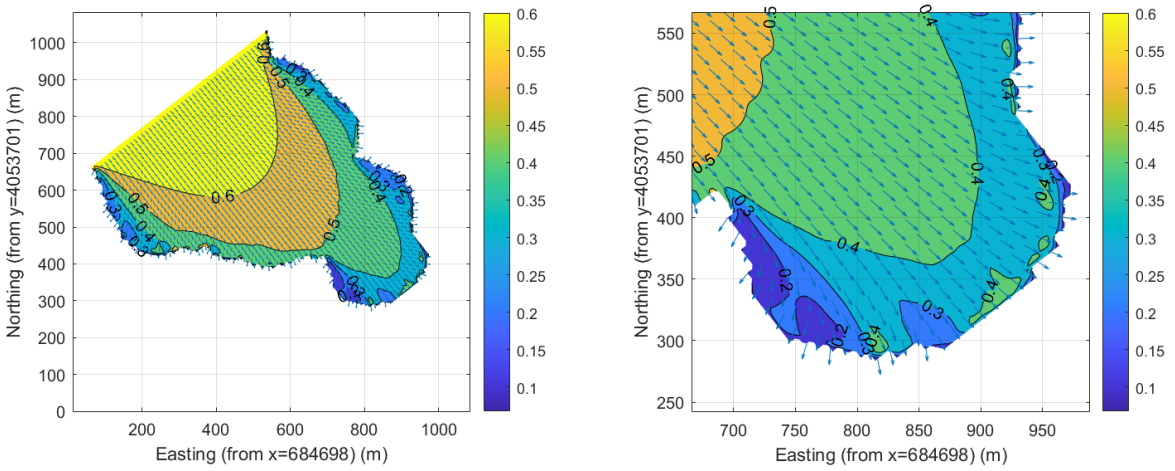

Figure 3.7. SWAN results for significant wave heights in Kalemyel Bay, Wind: 7 m/s NW, Wave BC: $H_s = 0.65$ m, $T = 4.52$ s.

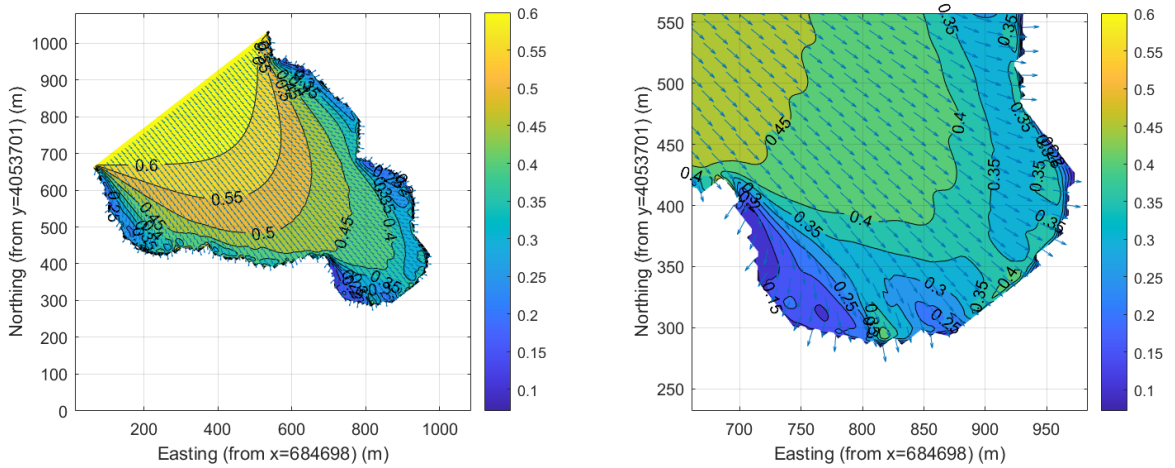

Figure 3.8. SWAN results for significant wave heights in Kalemyel Bay, Wind: 7 m/s WNW, Wave BC: $H_s = 0.6$ m, $T = 4.52$ s.

3.2. Morphology Results

Morphological changes in the beach are analyzed by studying first cross-shore sediment transport. However, the results show that only cross-shore transport is not sufficient to explain the changes in the site. Therefore, longshore sediment transport is added to the model to have a more comprehensive model. For these models, measurements are used as initial profiles and SWAN results are used as wave inputs.

Table 3.1. The first combination of wind and wave order given to XBeach-G.

Wind velocity (m/s)	**Wind direction**	**Yearly occurence**	H_{iA} **(m)**	H_{iB} **(m)**	H_{iC} **(m)**	H_{iD} **(m)**
10	NW	0.32 hour	0.65	0.75	0.75	0.47
10	NNW	0.32 hour	0.60	0.65	0.65	0.65
10	W	0.63 hour	0.55	0.65	0.65	0.65
10	N	0.32 hour	0.55	0.65	0.65	0.60
10	NNE	0.95 hour	0.42	0.45	0.43	0.40
10	WSW	0.32 hour	0.35	0.47	0.43	0.43
7	NW	5.37 hour	0.32	0.40	0.37	0.37
7	WNW	3.16 hour	0.32	0.38	0.38	0.35

XBeach-G simulations are done with an initial profile input up to 6 m depth for cross-sections A1, A2, B, C, and D through the cross-shore direction. Since the sediment motion is observed to be limited up to the 2 or 2.5 m depth, it can be safely assumed that there will not be any sediment transported beyond that depth. Moreover, the existence of the sill at approximately 2.5 m depth contour would prevent the sediments to move beyond that depth. Wave conditions obtained from the SWAN model are implemented in XBeach-G for each section. The wave heights at cross-section A1 and cross-section A2 are considered to be the same because they are close. For the tide input, a sinusoidal tide generator of XBeach-G is used. For the period and signal length, default values of the program for the semidiurnal tide are used, which are 12.42 hours and 89424 seconds respectively. For tide amplitude, both measurements done by BUCEL in two consecutive years and existent values in the literature are considered. BUCEL measurements are based on the values read from a tide gauge in a plexiglass hose approximately each 30 minutes during 2 days in each site survey (see APPENDIX B). The amplitude of the tide is set equal to 0.2 meters since according to BUCEL data and previous research, the tidal range changes between 0.15 to 0.3 meters in the region [2, 34, 35].

Table 3.2. The second combination of wind and wave order given to XBeach-G.

Wind velocity (m/s)	**Wind direction**	**Yearly occurence**	H_{iA} **(m)**	H_{iB} **(m)**	H_{iC} **(m)**	H_{iD} **(m)**
7	WNW	3.16 hour	0.32	0.38	0.38	0.35
7	NW	5.37 hour	0.32	0.40	0.37	0.37
10	WSW	0.32 hour	0.35	0.47	0.43	0.43
10	NNE	0.95 hour	0.42	0.45	0.43	0.40
10	N	0.32 hour	0.55	0.65	0.65	0.60
10	W	0.63 hour	0.55	0.65	0.65	0.65
10	NNW	0.32 hour	0.60	0.65	0.65	0.65
10	NW	0.32 hour	0.65	0.75	0.75	0.47

The wave heights are given to XBeach-G with several combinations of the values obtained by SWAN. In each combination, it is assumed that beyond the simulated time, there is no significant sediment transport. Therefore, the morphology change is only limited to those periods. To assume the profile evolution in 1 year, the model is constructed such that these extreme wind and wave conditions occur immediately one after the other. Hence, the 1 year is squeezed to $\approx$ 12 hours of simulation, with the assumption that the transport in the other periods is negligible.

The combinations are chosen as in Table 3.1, Table 3.2, and Table 3.3. H_i in the table is defined as the incident wave height at 6 m depth, which is used as boundary condition to XBeach-G.

Other inputs to XBeach-G are medium diameter, hydraulic conductivity, wave spectrum type, morphology model type, and angle of repose of the sediment. The sediment used in beach fill was subjected to granulometric analysis by BUCEL. Gravel of medium diameter $D_{50} = 0.0073$ m is used in the nourishment in March 2020. According to Hazen's empirical equation [31], the hydraulic conductivity is found as $k = 0.25$ m/s. JONSWAP spectrum is used for the wave module and the Van Rijn formula is

selected for the morphology calculation. The angle of repose of the sediment of that size is 33^o.

Table 3.3. The third combination of wind and wave order given to XBeach-G.

Wind velocity (m/s)	**Wind direction**	**Yearly occurence**	H_{iA} **(m)**	H_{iB} **(m)**	H_{iC} **(m)**	H_{iD} **(m)**
10	N	0.32 hour	0.55	0.65	0.65	0.60
10	W	0.63 hour	0.55	0.65	0.65	0.65
10	NNW	0.32 hour	0.60	0.65	0.65	0.65
10	NW	0.32 hour	0.65	0.75	0.75	0.47
10	WSW	0.32 hour	0.35	0.47	0.43	0.43
10	NNE	0.95 hour	0.42	0.45	0.43	0.40
7	NW	5.37 hour	0.32	0.40	0.37	0.37
7	WNW	3.16 hour	0.32	0.38	0.38	0.35

Figure 3.9, Figure 3.10, Figure 3.11, and Figure 3.12 show the profiles obtained at the end of the $\approx$ 12 hours of XBeach-G simulation in total for each and compare them to the design post nourishment (6-30 March 2020), and measured post-nourishment profiles (5-7 November 2020). t_1 in the legend of the figures stands for the time counter starting from the nourishment in March 2020. The green line is the output of XBeach-G while the profiles shown with the blue dotted lines are given as the initial profile input.

The wave combinations given in Table 3.1, Table 3.2, and Table 3.3 gave very similar results for each profile (see APPENDIX C). Therefore, the profile change due to different orders of incident wave conditions can be considered an ergodic process. For this reason, only the results of profile evolution subjected to the wave and wind combination order given in Table 3.1 are shown and used for comparisons.

Having a general look over the Figure 3.9, Figure 3.10, Figure 3.11, and Figure 3.12, it can be seen that XBeach-G remains underestimated for the simulated time. The measurements conducted in November 2020 are nearly 7-8 months after the nourishment, while the XBeach-G simulations were run for 1 year to be consistent with the yearly wind occurrence data. Despite this fact, the measured profile is more evolved than the model run for 1 year by XBeach-G. XBeach-G model predicts that the shoreline at cross-section A1 will retreat 3.74 m, cross-section B 3.62 m, cross-section C 4.09 m, and cross-section D 5.16; while the real recession amounts are 4.67 m for cross-section A1, 4.45 m for cross-section B, 4.63 m for cross-section C and 4.93 m for cross-section D, in a shorter period of time. These values are the horizontal difference of the blue dashed line to the green line, and the blue dashed line to the red starred line along the x-axis in the Figure 3.9, Figure 3.10, Figure 3.11, and Figure 3.12, respectively. Moreover, the difference between the measurement and the model expands through deeper parts of the profile.

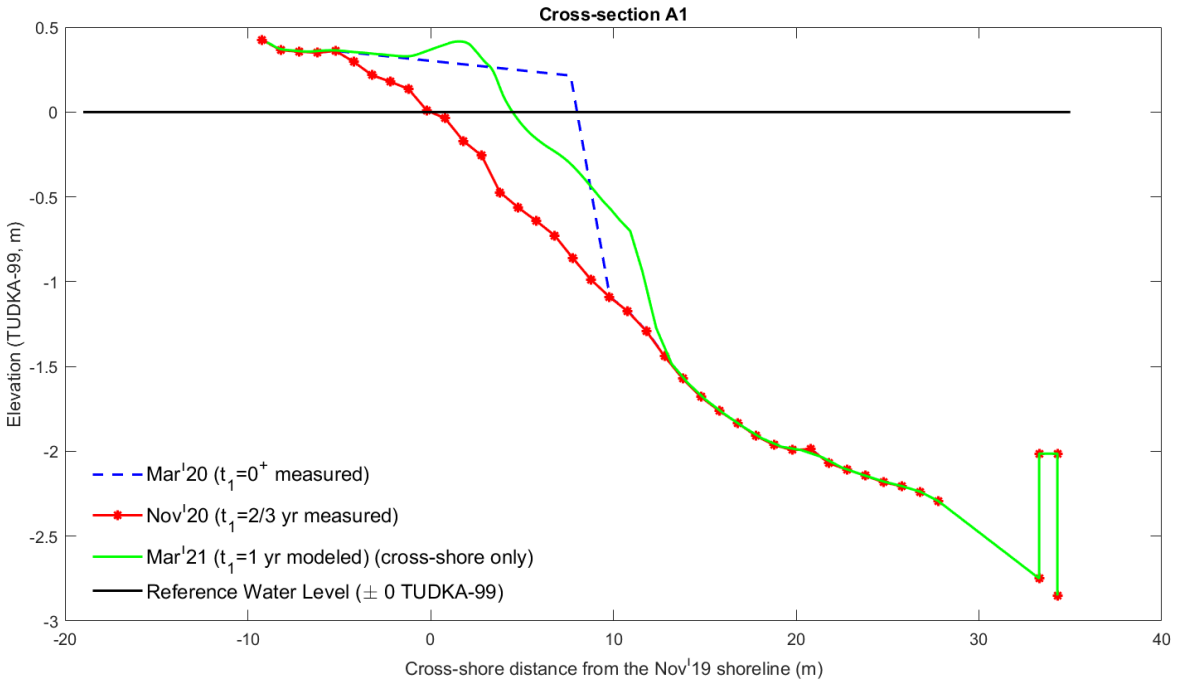

Figure 3.9. Nourishment in March 2020, measurement in November 2020, and XBeach-G results for 1 year after nourishment for cross-section A1.

The difference between the model and the measurements may be related to several reasons. First is that the XBeach-G used the waves simulated for average yearly wind conditions. The wind data taken from [29] was the average wind data of ECMWF between the years 2000 and 2018. However, given the changing climate especially in the last years, different wind conditions may have occurred during Summer 2020 at Fethiye Bay. There may have been storms stronger than the yearly average that generated larger waves. Hence, the profiles might have been subjected to more severe waves after the nourishment.

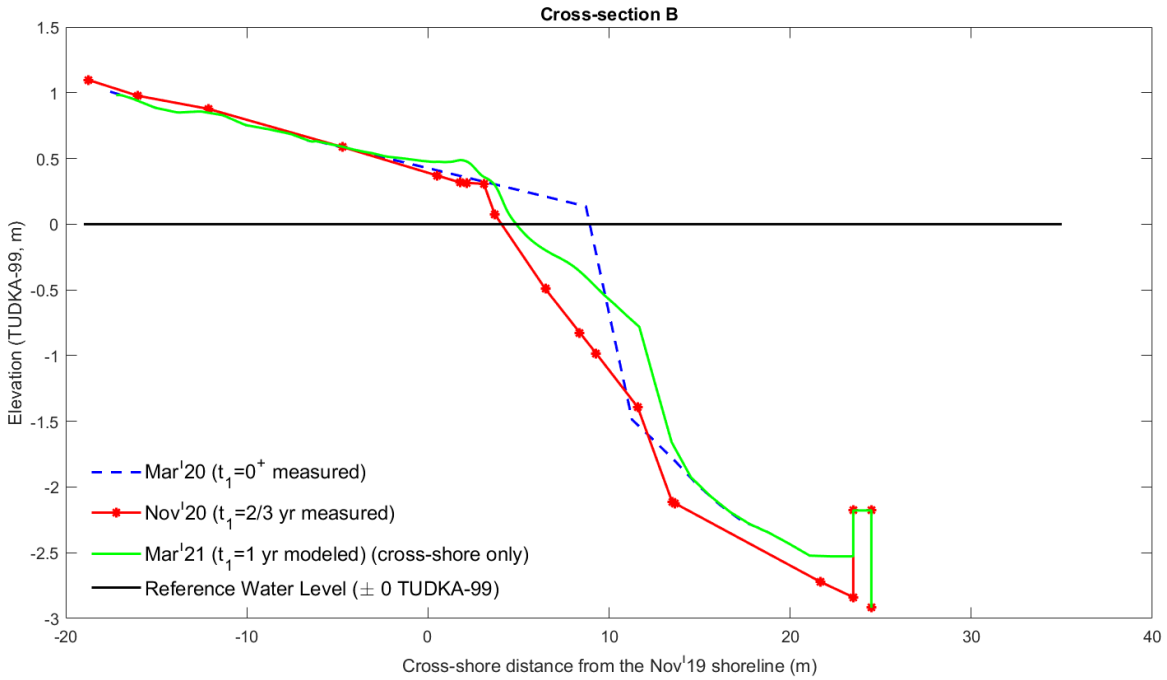

Figure 3.10. Nourishment in March 2020, measurement in November 2020, and XBeach-G results for 1 year after nourishment for cross-section B.

Another possible explanation is the role of longshore transport which is not taken into account by XBeach-G. That is the reason why the longshore model is included in this study as well. A combination of cross-shore and longshore sediment transport models would give better results for such an embayed beach [25].

Figure 3.13 shows the real-scale shoreline in November 2019 and in March 2020 just after the nourishment. The beach is rotated $\approx 31^o$ clockwise for better visualiza-

tion. Even though it is an arc-shaped pocket beach, it has a small curvature compared to its length. Thus, it can be converted to a straight beach with slightly little distortion. In this manner, taking the shoreline in November 2019 as the datum, the perpendicular distance of the shoreline in March 2020 is given as the initial condition for the longshore transport model. The straightened version of the shoreline in November 2019 and the beach fill in March 2020 are shown in Figure 3.14.

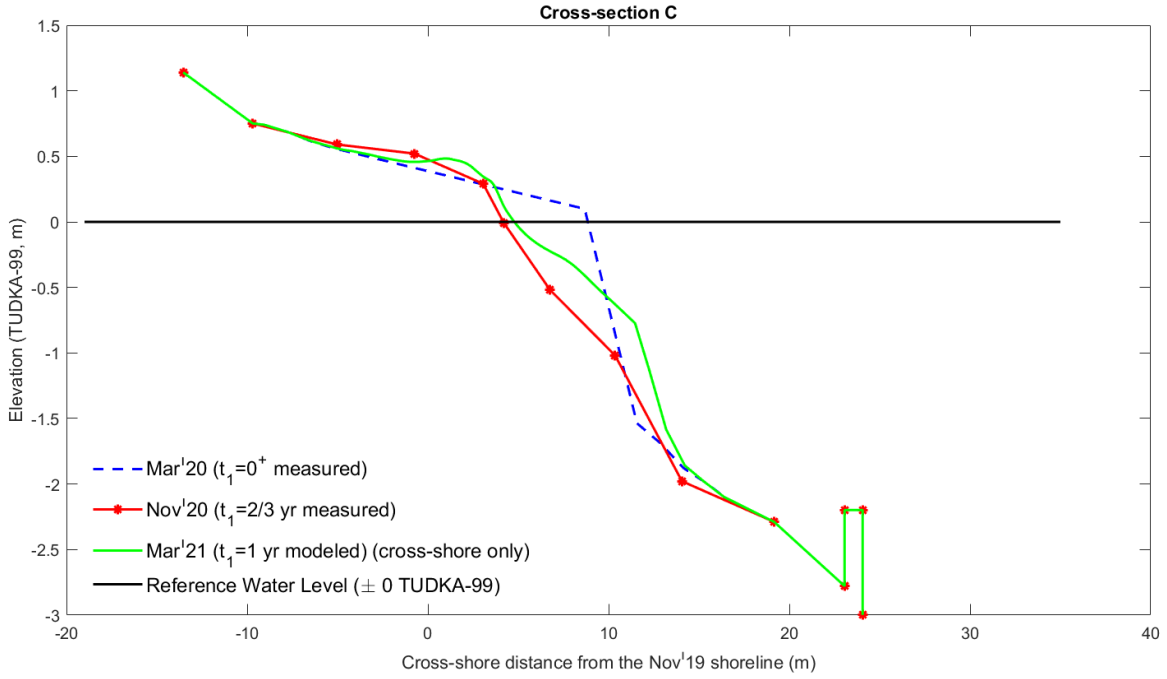

Figure 3.11. Nourishment in March 2020, measurement in November 2020, and XBeach-G results for 1 year after nourishment for cross-section C.

The longshore sediment transport model is also run for 12 hours to be consistent with the cross-shore model. As Equation (2.2) suggests, parameters that affect the longshore diffusivity G are the breaking wave height, depth of closure, berm height, medium sediment diameter, and the porosity of the sediment, and specific gravity of the sediment. The breaking wave height is selected as an average value at the middle of the beach regarding SWAN outputs and decided to be equal to $H_b = 0.7$ m. As indicated before, $D_{50} = 0.0073$ m for the first fill. The depth of closure, which is the depth beyond which there is no sediment motion, is $h_* = 2.5$ m on average regarding XBeach-G results of the 4 cross-sections. So, this value is used in the longshore diffusivity formula. Berm

height can also be read from XBeach-G results, and it is ≈ 0.5 m. For the porosity, the common $p = 0.4$ value is used. The specific gravity of the fill material is $s = 2.5$. The longshore transport coefficient K is 0.77 and the spilling breaker κ is 0.78.

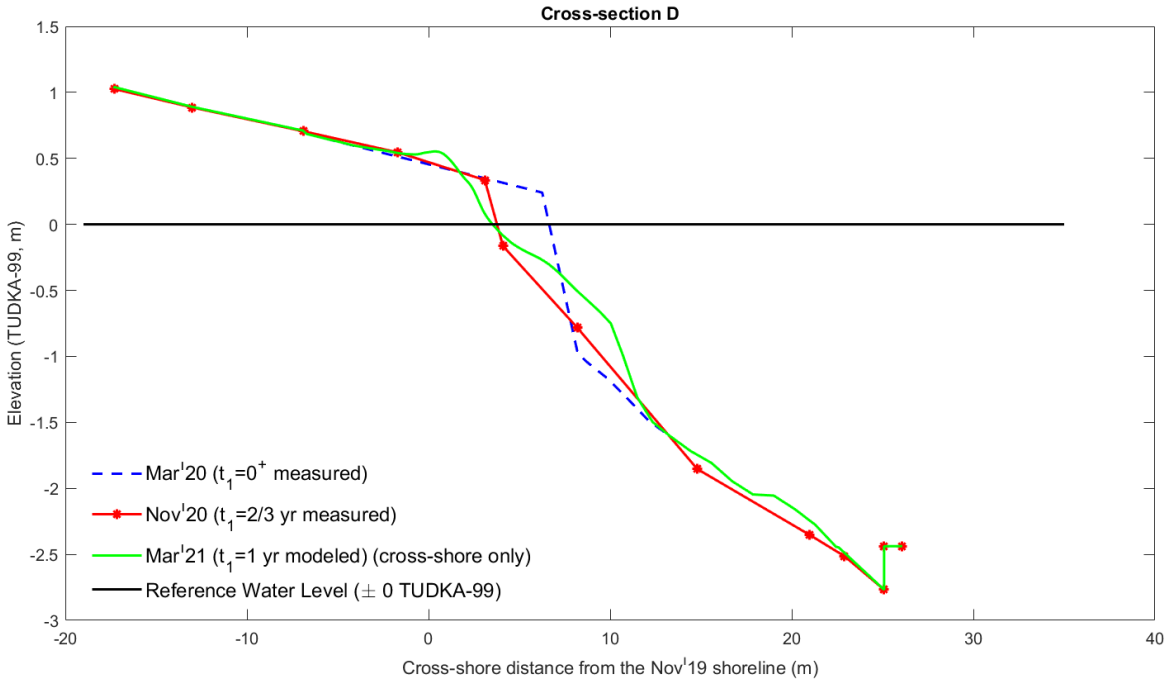

Figure 3.12. Nourishment in March 2020, measurement in November 2020, and XBeach-G results for 1 year after nourishment for cross-section D.

For the numerical model, the space step is not constant since it corresponds to the distances between two consecutive points on the shoreline selected manually. The time step is $dt = 10$ s. Even though it is a relatively high number, the model does not undergo an instability thanks to the implicit finite difference method explained in Section 2.3.2. The result of the longshore diffusivity model is shown in Figure 3.14 with the green line. The straight line at $y = 0$ is the shoreline in November 2019, and the red line is the beach fill amount in March 2020. The longshore model is constructed such as the beach is only subjected to longshore sediment transport. Thereafter, it is superposed with the cross-shore sediment transport model results. The parts of the profiles upper than the depth of closure are moved backward or forwards in the cross-shore direction according to the longshore model results. The shoreline position change in the locations of cross-sections A1, B, C, and D are -3.74 m, -0.26 m, -2.40 m,

and +0.37 m, respectively. These values can be calculated as the horizontal distance of the red starred line to the magenta line at the shoreline in Figure 3.15, Figure 3.16, Figure 3.17, and Figure 3.18. Plus and minus signs here imply the direction along with the normal distance to the shoreline axis. According to these results, the shoreline at cross-sections A1, B, and C is subjected to a recession, while the shoreline at cross-section D is slightly moved seawards. The modeled shoreline has a bell shape and this is due to the nature of diffusion phenomena. This explains the higher amount of recession at cross-section A1. However, there is a beach fill at the cross-section D despite its location near the end. The reason for this is the irregularity in the initial profile, which is the nourishment conducted in March 2020. The thickness of the nourishment is less around cross-section D. So, the sediments are diffused there from the places where the fill is thicker. Cross-sections B and C which are located in the middle of the beach are less affected by the longshore transport than cross-section D. The difference in the shoreline recession amount between cross-sections B and D is also caused by the irregularity in the initial condition. The fill area where the cross-section C is located is larger than the fill around cross-section B. That is why cross-section C lost more of its dry beach.

Shoreline positions of each cross-section from March 2020 up to the simulated time (March 2021) is written in Table 3.4. The values are mainly the normal distance of the shoreline at given dates to the shoreline measured in November 2019.

Comparing the values measured in November 2020 and the result of the simulation that includes both cross-shore and longshore models, there is a drastic difference between the measured and modeled profile for the cross-section A2. This is mostly because of the high longshore sediment transport rate found in the model. In reality, the arc shape of the beach may prevent excessive sediment loss at the ends. However, the only cross-shore model is not sufficient for any of the cross-sections (except for the upper part of section D, but it is inadequate for the lower parts again). This difference may be due to the presence of longshore transport or unconsidered storm conditions specific to Summer 2020. Nonetheless, there are site experiences in favor of the exis-

tence of longshore currents. It can be deduced that including the longshore model is appropriate, however, this particular method is overestimating.

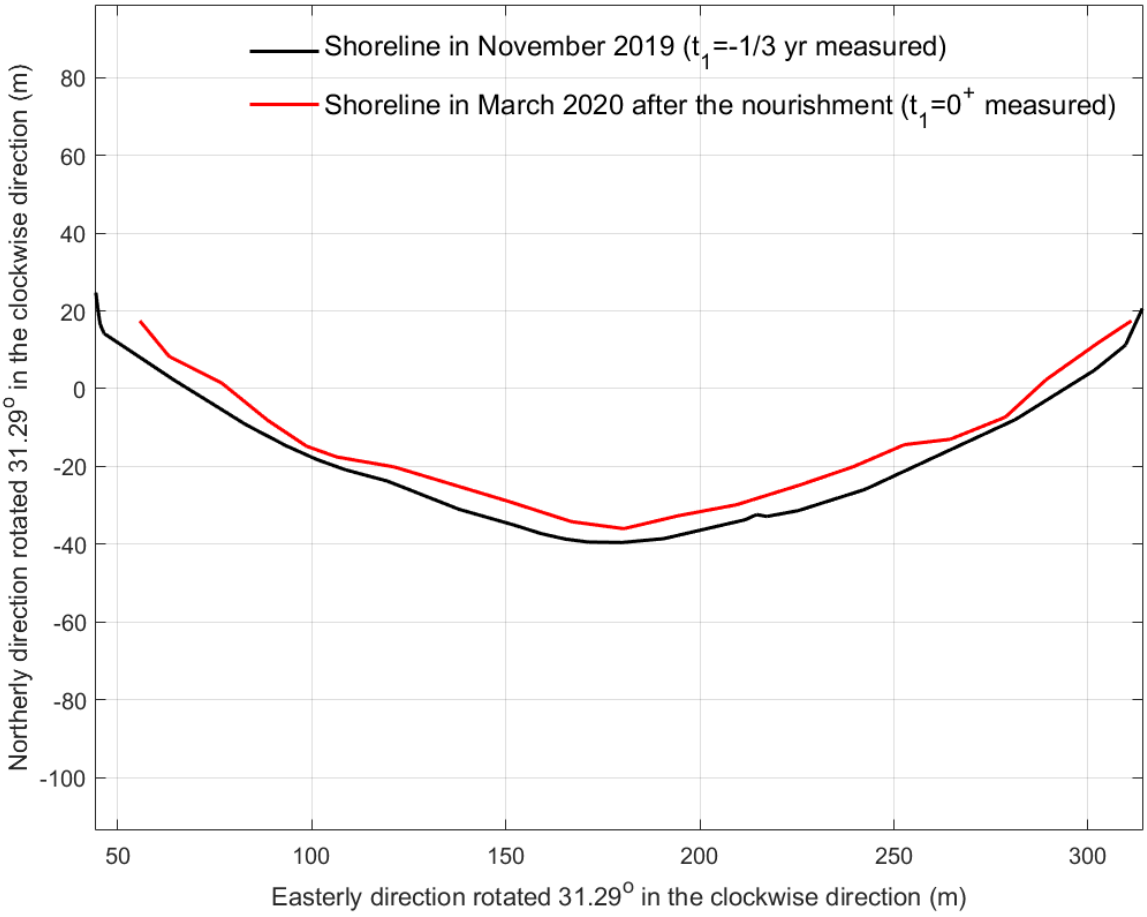

Figure 3.13. Real scaled shoreline in November 2019 and March 2020.

Figure 3.19 shows the distance of the cross-shore only model and the total model to the measurements. The measurements in November 2020 are taken as a reference and the models run for March 2021 are compared to them. For a better visualization, the starred red line is the normalized profile of each section measured in November 2020 shown in Figure 3.15, Figure 3.16, Figure 3.17, and Figure 3.18 with starred red line as well. Green lines stand for the difference between the measurement and cross-shore only model for each profile shown also in Figure 3.15, Figure 3.16, Figure 3.17, and Figure 3.18 with green lines. Magenta lines stand for the difference between the measurement and total model (cross-shore and longshore together) for each profile

shown also in Figure 3.15, Figure 3.16, Figure 3.17, and Figure 3.18 with magenta lines. Bold green and magenta lines are the averages of green and magenta lines standing for each section, respectively. So actually, bold lines represent the average error in the horizontal direction at the shoreline of the predicted profiles from the measurement. Various error values are calculated in the horizontal shoreline position prediction in this work for the cases where only the cross-shore model is considered and where the cross-shore model is superposed with the longshore model. The root mean square is calculated as

$$RMSE = \sqrt{\frac{\sum_{n=1}^{N}(y_{act}(i) - y_{pred}(i))^2}{N}}, \tag{3.1}$$

where n stands for the data points, N is the number of data points, y_{act} is the measured values at these points, and y_{pred} is the predicted values at these points. The root mean square error in the horizontal at the shoreline position in this present work where only the cross-shore transport is considered is 1.71 m. When the longshore transport is added, the root mean square error in the horizontal shoreline position decreases to 0.63 m. Similarly, the mean absolute error in the horizontal shoreline position in both cases are calculated as

$$MAE = \frac{\sum_{n=1}^{N}|y_{act}(i) - y_{pred}(i)|}{n}, \tag{3.2}$$

where n stands for the data points, N is the number of data points, y_{act} is the measured values at these points, and y_{pred} is the predicted values at these points. The mean absolute error where only cross-shore transport is considered is 1.48 m while this value decreases to 0.50 m when the cross-shore and longshore models are superposed. Moreover, normalized root mean square and normalized mean absolute errors are also calculated for the same values. The normalized root mean square is calculated as

$$NRMSE = \frac{RMSE}{mean(y_{act})}, \tag{3.3}$$

where $RMSE$ stands for the root mean square error, and $mean(y_{act})$ is the mean of the actual values. The normalized root mean square error in the horizontal at the shoreline position in this present work where only the cross-shore transport is considered is 0.23

m. When the longshore transport is added, the normalized root mean square error in the horizontal shoreline position decreases to 0.08 m. The normalized mean absolute error is calculated as

$$NMAE = \frac{MAE}{mean(y_{act})}, \tag{3.4}$$

where MAE stands for the mean absolute error, and $mean(y_{act})$ is the mean of the actual values. The normalized mean absolute error where only cross-shore transport is considered is 0.20 m while this value decreases to 0.07 m when the cross-shore and longshore models are superposed. From these results, it can be deduced that the average model results approach the measurement when the longshore transport model is considered.

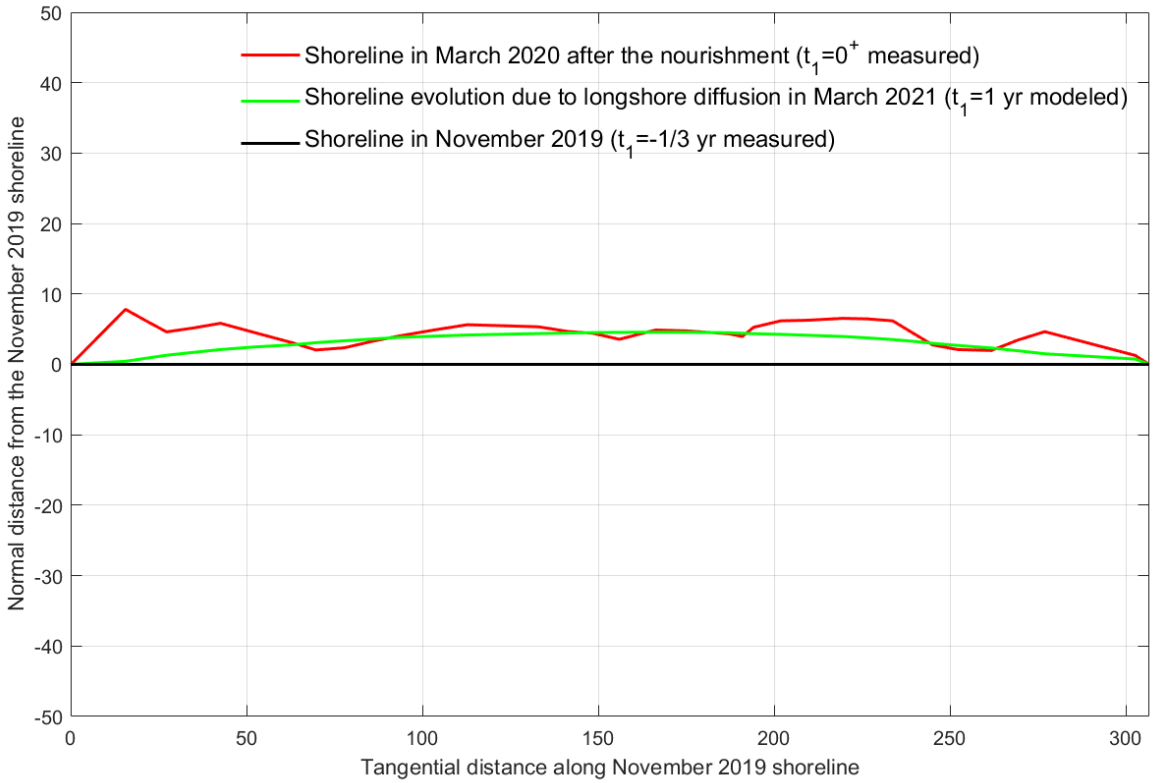

Figure 3.14. Result of 1 year longshore diffusivity with aspect ration 2:1.

Judging from these model results, cross-shore and longshore transport rate ratios can be calculated. According to modeled results which are also shown in Table 3.4,

the ratio of the cross-shore transport to longshore transport at cross-section A1 is 1:1, at cross-section B is 14:1, at cross-section C is 1.7:1, and at the cross-section, D is -14:1. The minus sign is due to deposition prediction of the longshore model at cross-section D. After the dry beach width gain just after the first nourishment which was 8.60 m, the average dry beach width loss due to cross-shore and longshore transport of these four sections are 4.15 m and 1.51 m, respectively. So, the average ratio of the cross-shore transport to longshore transport can be calculated as 2.75:1.

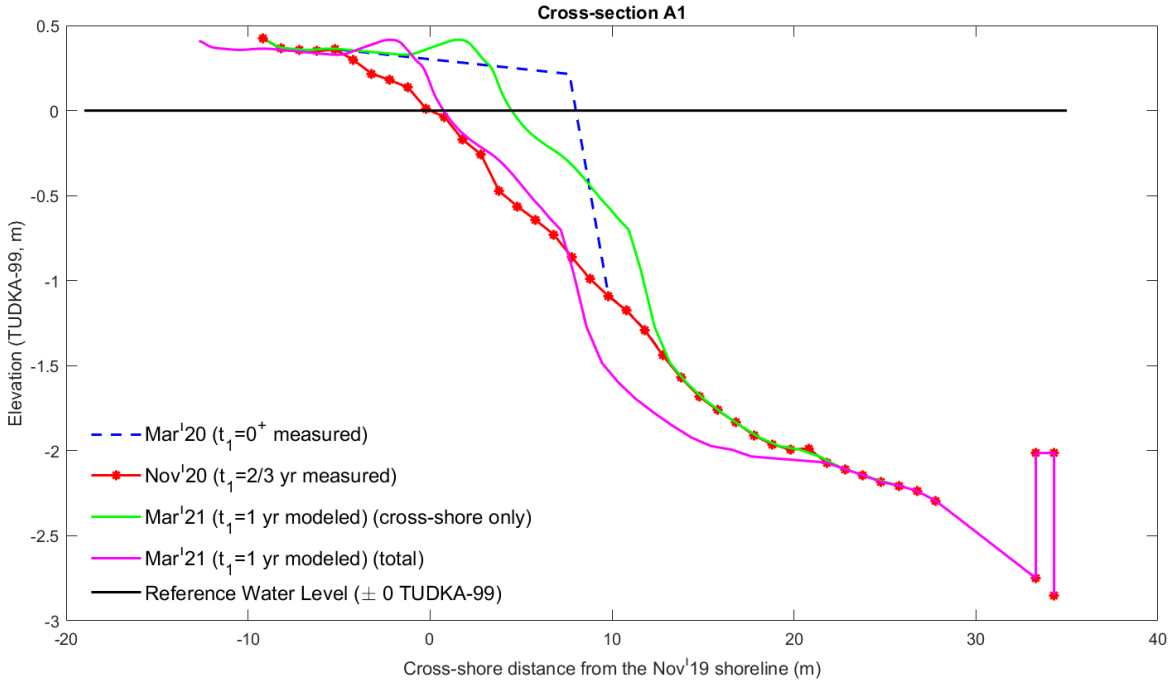

Figure 3.15. Nourishment in March 2020, measurement in November 2019, XBeach-G results and XBeach-G combined with the longshore diffusivity model for 1 year after nourishment for cross-section A1.

For the simulation of the profile evolution after the nourishment in March 2021, most of the numerical inputs are the same as for the previous simulation. Wave conditions are assumed to be consistent with the SWAN outputs, hence with the average data between the years 2000 and 2018 extracted from ECMWF. Tide inputs are also the same as the previous model. The different inputs are indeed the initial profiles, which correspond to the measured nourishment design in March 2021. Also, the medium

diameter of the fill material used in March 2021 is finer than the one of the previous year. $D_{50} = 0.0049$ m is calculated for the sediment sample of that fill. Accordingly, using again the Hazen's formula for the hydraulic conductivity, $k = 0.14$ m/s for this material. All other parameters are the same as the previous year's model.

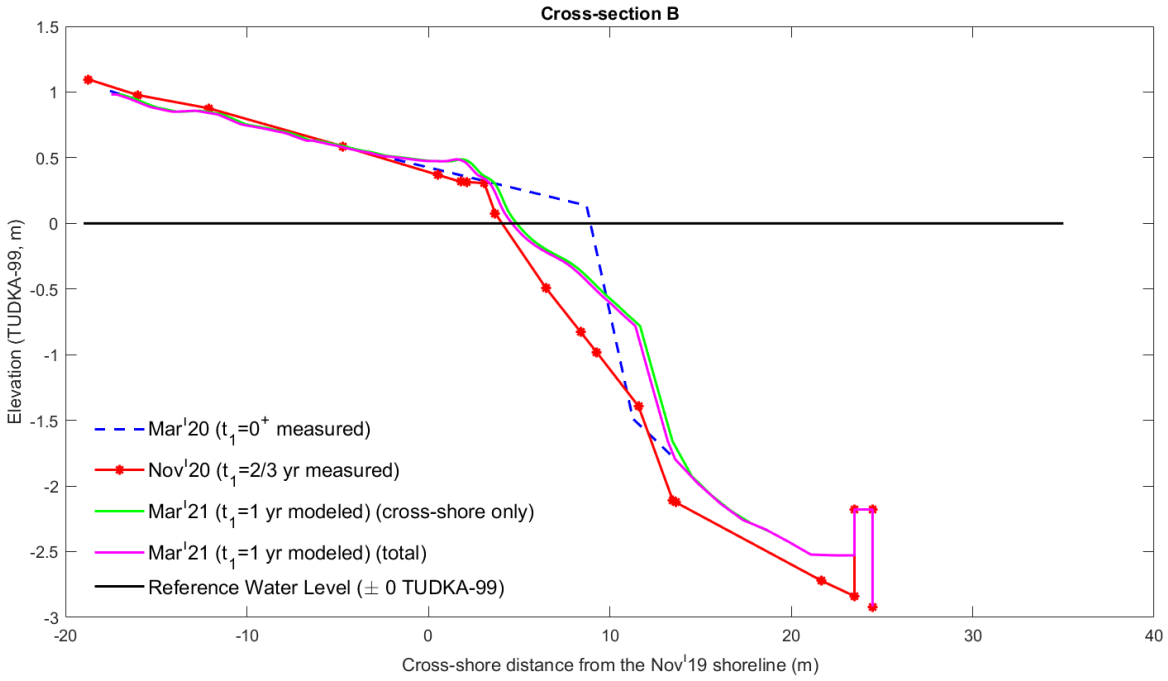

Figure 3.16. Nourishment in March 2020, measurement in November 2019, XBeach-G results and XBeach-G combined with the longshore diffusivity model for 1 year after nourishment for cross-section B.

Figure 3.20, Figure 3.21, Figure 3.22, and Figure 3.23 show the profiles obtained at the end of the $\approx$ 12 hours of XBeach-G simulation in total for each and compare them to the design post nourishment (5-31 March 2021). t_2 in the legend of the figures stands for the time counter starting from the nourishment in March 2021. Accordingly, for the date of measurements in November 2020, both "$t_1 = 2/3$ year" and "$t_2 = -1/3$ year" are used in this study. The green line is the output of XBeach-G while the profiles shown with the blue dotted lines are given as the initial profile input.

As in the simulation for the profile evolution after March 2020, the wave combinations given in Table 3.1, Table 3.2, and Table 3.3 gave likewise similar results for

each profile (see APPENDIX C). Thus, only the results of the first wave conditions are selected for comparison.

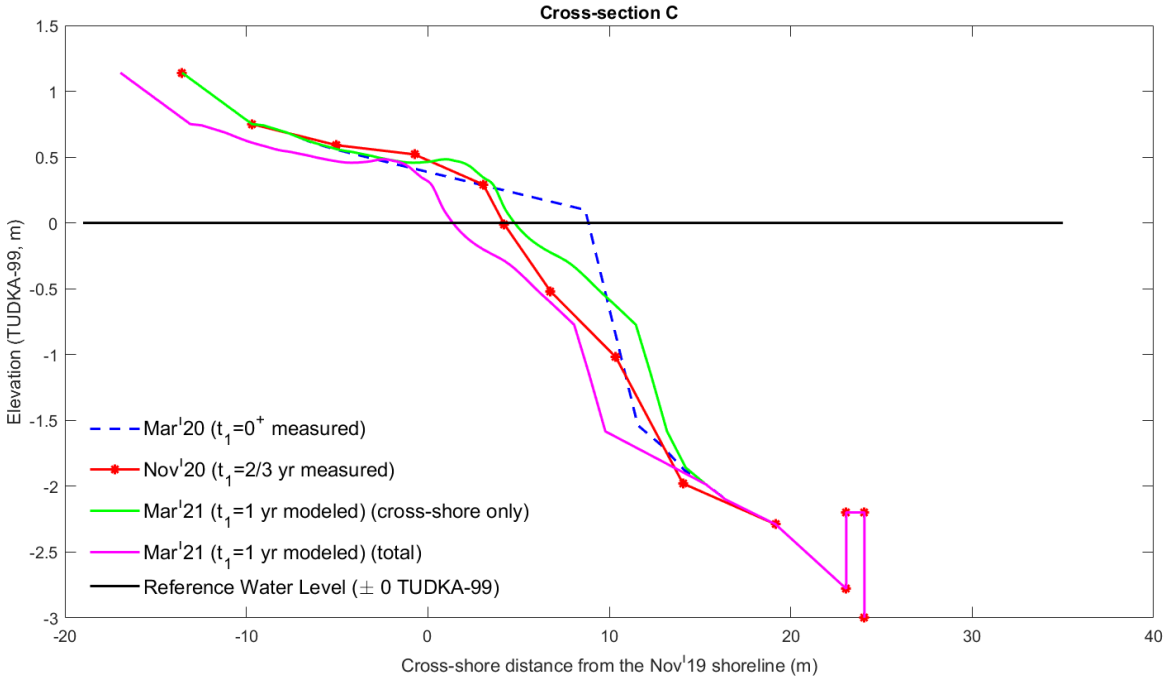

Figure 3.17. Nourishment in March 2020, measurement in November 2019, XBeach-G results and XBeach-G combined with the longshore diffusivity model for 1 year after nourishment for cross-section C.

Looking over the Figure 3.20, Figure 3.21, Figure 3.22, and Figure 3.23, it can be seen that the profile simulated by XBeach-G follows the long term estimation of BUCEL in a relatively accurate manner. Even though there are differences in shoreline position, the general trend of the XBeach-G results is in line with the expected profiles in long term. Given that, it should be noted that the long-term estimations are made for more than 1-year duration after the nourishment. However, only the cross-shore transport model which is run for 1 year has reached the profile estimated for the long term. So, it can be deduced that the long term profile predicted by BUCEL is underestimated.

XBeach-G model predicts that the shoreline at cross-section A2 will retreat 3.92 m, cross-section B 4.74 m, cross-section C 4.56 m, and cross-section D 4.32 m. These

values can be calculated as the horizontal difference between the blue dashed line and green line at the shoreline in Figure 3.20, Figure 3.21, Figure 3.22, and Figure 3.23, respectively. BUCEL estimation for the shoreline recession in the long term is 4.13 m for cross-section A2, 3.47 m for cross-section B, 3.37 m for cross-section C, and 3.64 for cross-section D. As indicated, there is not a significant difference between the XBeach-G model results and BUCEL estimation. However, to simulate the process completely, a longshore sediment transport model should also be added to the cross-shore results.

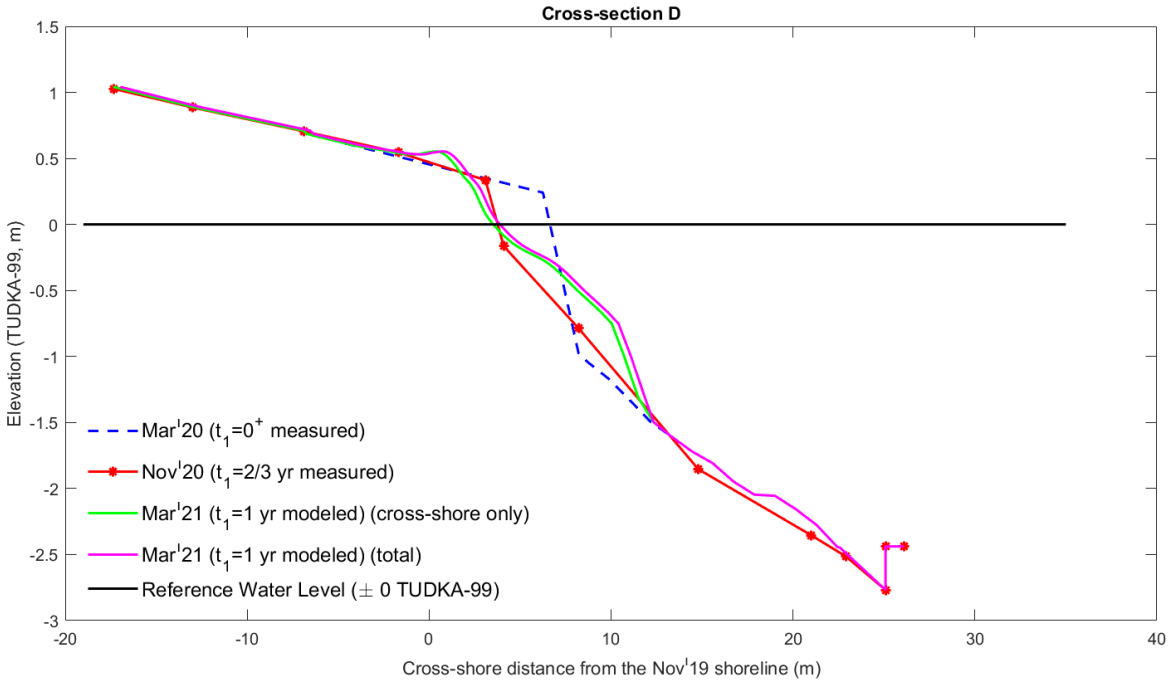

Figure 3.18. Nourishment in March 2020, measurement in November 2019, XBeach-G results and XBeach-G combined with the longshore diffusivity model for 1 year after nourishment for cross-section D.

The processes followed for the longshore sediment transport model are similar to the model run for the profile evolution after the March 2020 nourishment. The real-scale shoreline in November 2020 and March 2021 can be seen in Figure 3.24. Again, the shore is converted to a straight beach in order to be able to use a one-line model of longshore diffusivity. Taking the shoreline in November 2020 as the datum, the perpendicular distance of the shoreline in March 2021 is given as the initial

condition for the longshore transport model. The straightened version of the shoreline in November 2020 and the beach fill in March 2022 are shown in Figure 3.25.

The simulation duration is consistent with the cross-shore model, therefore is 12 hours. Many of the parameters related to the longshore diffusivity are the same as the previous year's model. Only the medium diameter is $D_{50} = 0.0049$ m. The numerical model is constructed in the same manner as the previous year's model.

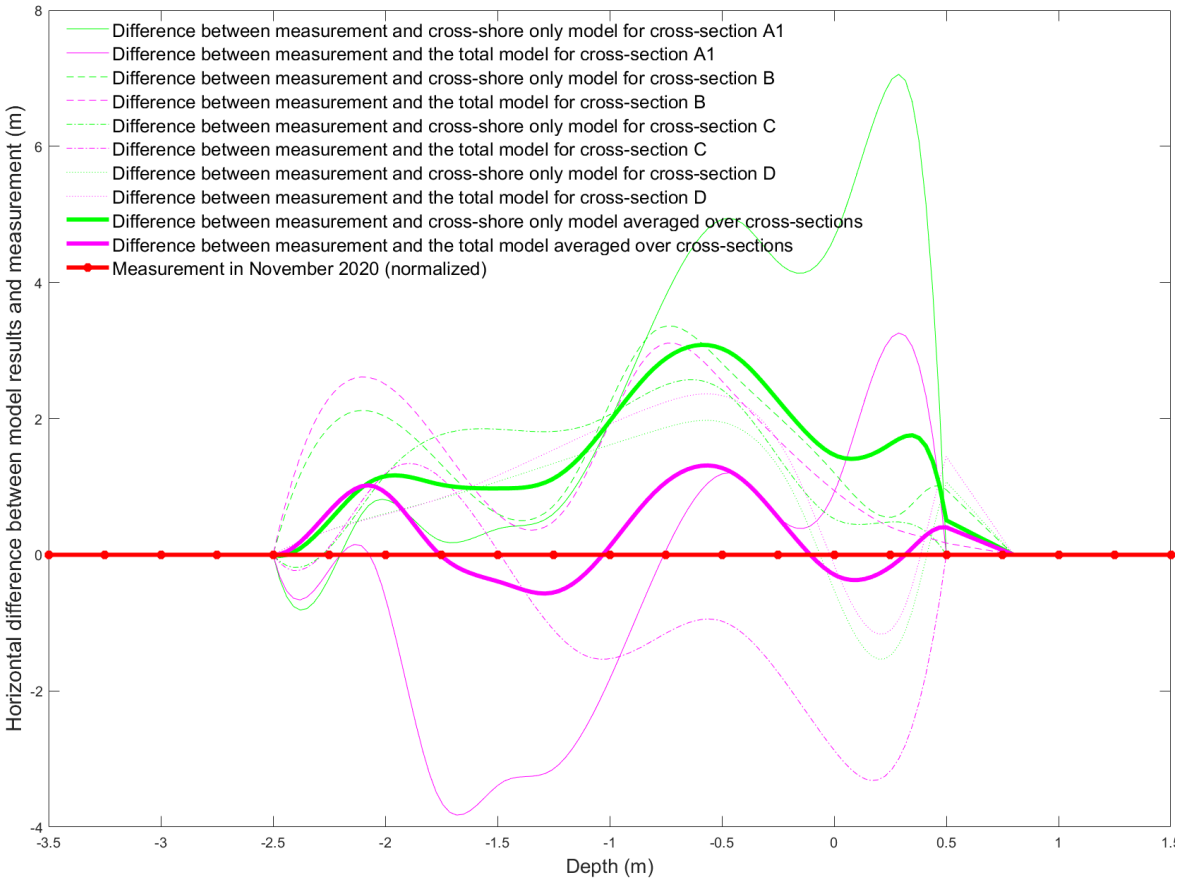

Figure 3.19. Distances of the modeled profiles from the measured profile and their average.

The result of the longshore diffusivity model is shown in Figure 3.25 with the green line. The straight line at $y = 0$ is the shoreline in November 2020, and the red line is the beach fill amount in March 2021. To integrate the results of the longshore model to the cross-shore model results, the parts of the profiles upper than the depth

of closure are moved backward or forwards in the cross-shore direction according to the longshore model results. The shoreline position change due to the longshore sediment transport in the locations of cross-sections A2, B, C, and D are -3.77 m, -0.43 m, -0.22 m, and -2.13 m, respectively. All the cross-sections are subjected to recession. The beach fill in March 2021 is more regularly distributed along the beach compared to the fill in March 2020. Therefore, as expected from the diffusion equation, recessions at the ends are higher than the ones in the middle.

At the cross-sections, A2 and D, where the longshore transport rate is higher, the total modeled profile and BUCEL's long-term estimation do not overlap. This can be deduced from the difference between the red straight and magenta lines in Figure 3.26 and Figure 3.29. XBeach-G model results combined with the longshore diffusivity results predict a more considerable shoreline recession. For the cross-sections B and C, the recession due to longshore transport is calculated to be much smaller. Therefore, the total model predicts a final profile for cross-sections B and C similar to the long-term estimation of BUCEL, which can be observed from the accordance between the red straight and magenta lines in Figure 3.27 and Figure 3.28. According to modeled results shown in Table 3.5, the ratio of the cross-shore transport to longshore transport at cross-section A2 is approximately 1:1, at cross-section B is 11:1, at cross-section C is 20:1, and at cross-section, D is 2:1. After the dry beach width gain just after the second nourishment which was 5.90 m, the average dry beach width loss due to cross-shore and longshore transport of these four sections are 3.67 m and 1.64 m, respectively. So, the average ratio of the cross-shore transport to longshore transport can be calculated as 2.23:1. The dominance of the cross-shore transport in the middle of the beach can be observed from these ratios.

Table 3.4. Cross-shore distances in meters from November 2019 shoreline from March 2020 up to March 2021.

Shoreline position	**Cross-section A1**	**Cross-section B**	**Cross-section C**	**Cross-section D**
Mar' 20 ($t_1 = 0^+$ measured)	8.18	8.51	8.83	8.70
Nov' 20 ($t_1 = 2/3$ yr measured)	3.51	4.06	4.20	3.77
Mar' 21 ($t_1 = 1$ yr modeled) (cross-shore only)	4.44	4.89	4.74	3.54
Mar' 21 ($t_1 = 1$ yr modeled) (longshore only)	-3.74	-0.26	-2.40	+0.37
Mar' 21 ($t_1 = 1$ yr modeled) (total)	0.70	4.63	2.34	3.91

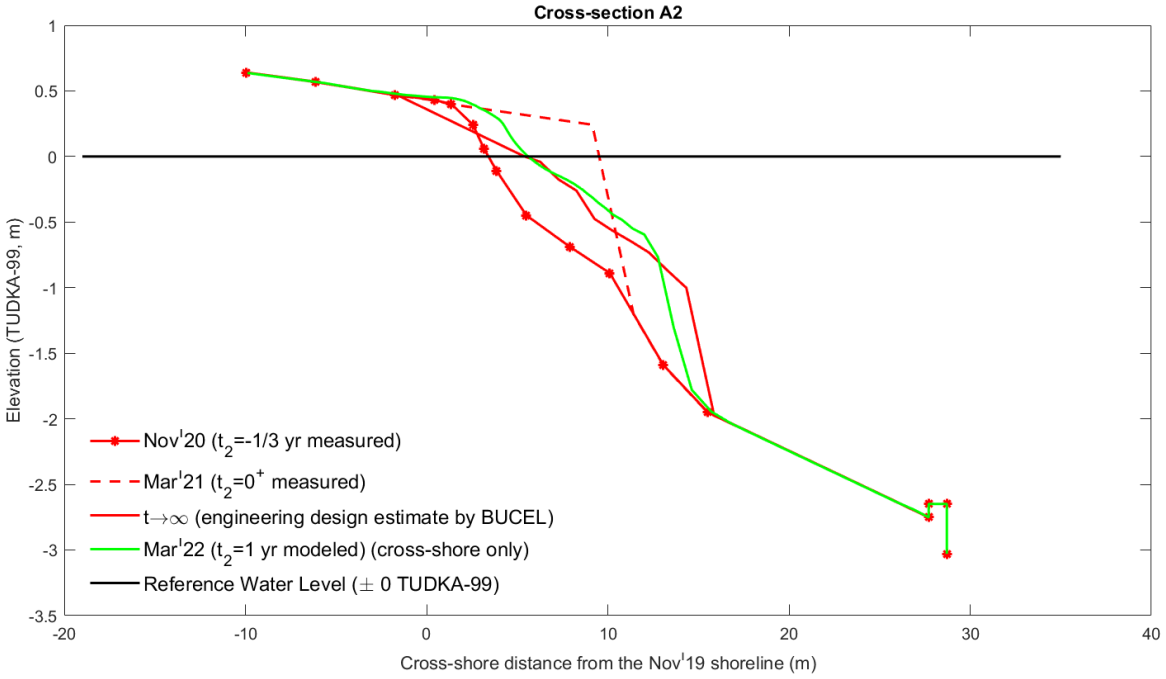

Figure 3.20. Nourishment at March 2021, measurement in November 2021, and XBeach-G results for 1 year after nourishment for cross-section A2.

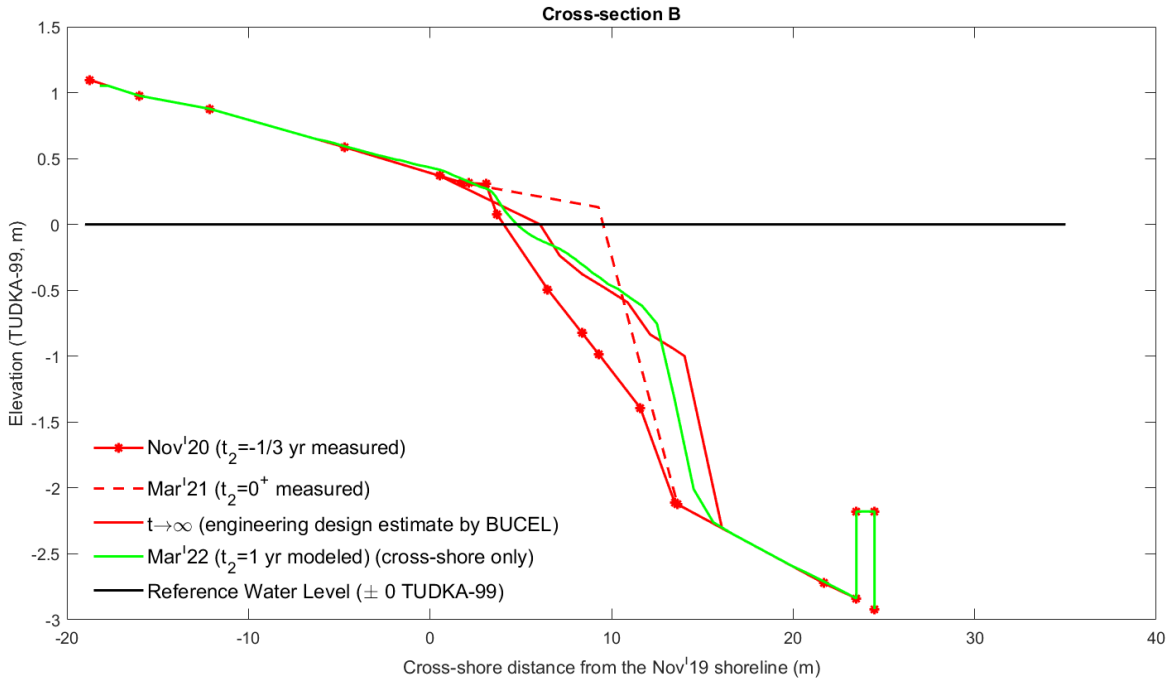

Figure 3.21. Nourishment in March 2021, measurement in November 2021, and XBeach-G results for 1 year after nourishment for cross-section B.

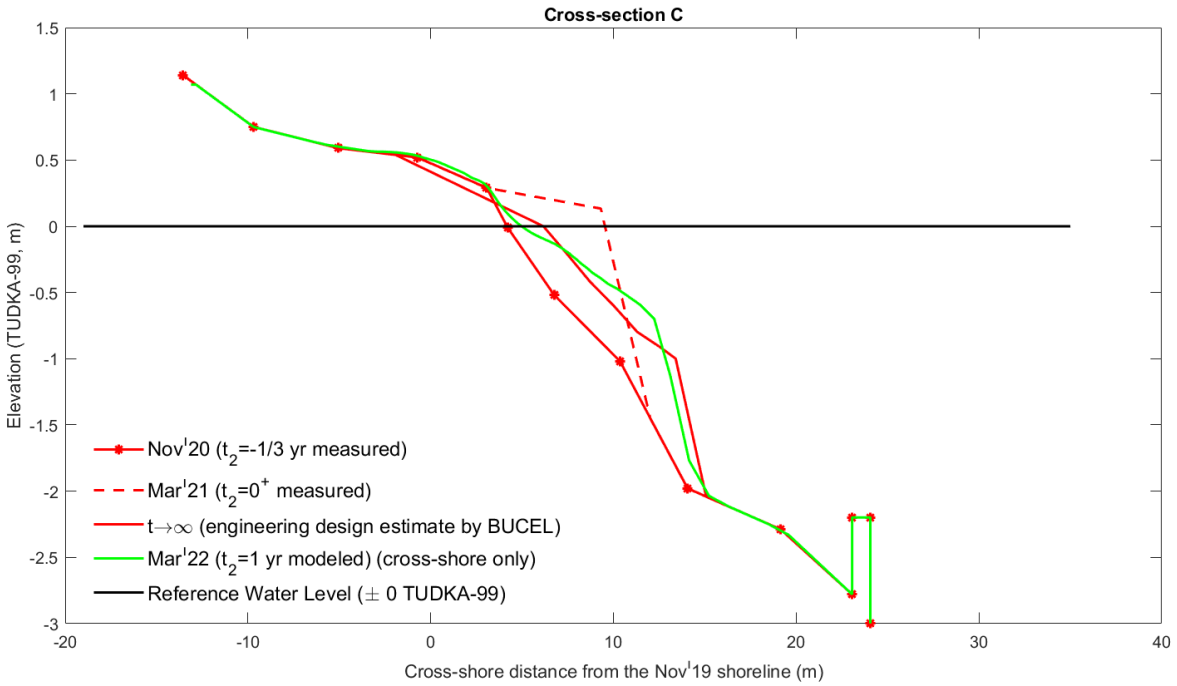

Figure 3.22. Nourishment in March 2021, measurement in November 2021, and XBeach-G results for 1 year after nourishment for cross-section C.

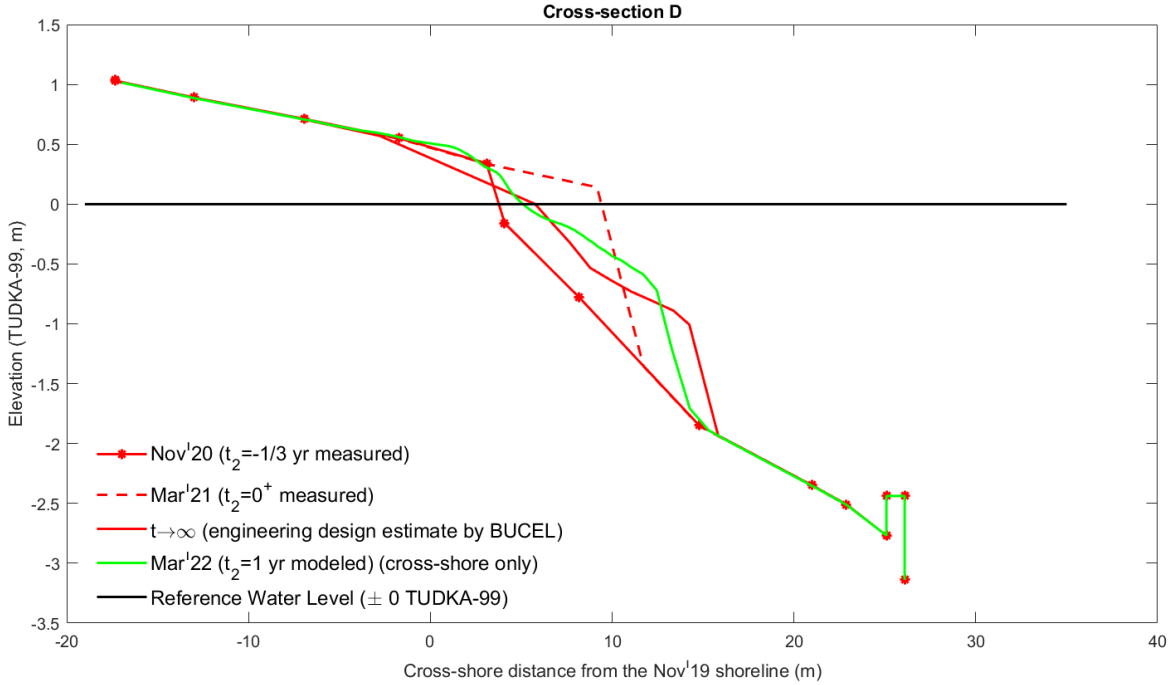

Figure 3.23. Nourishment in March 2021, measurement in November 2021, and XBeach-G results for 1 year after nourishment for cross-section D.

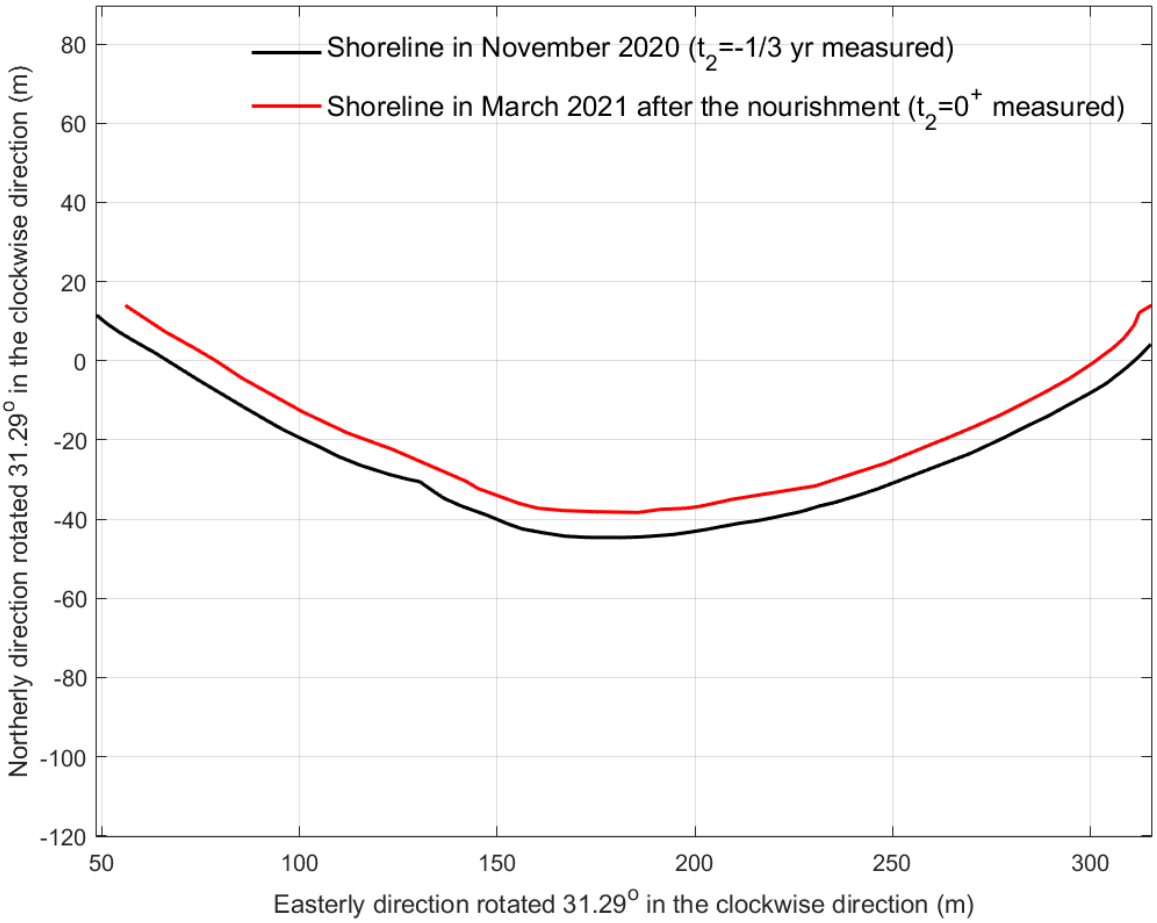

Figure 3.24. Real scaled shoreline in November 2020 and March 2021.

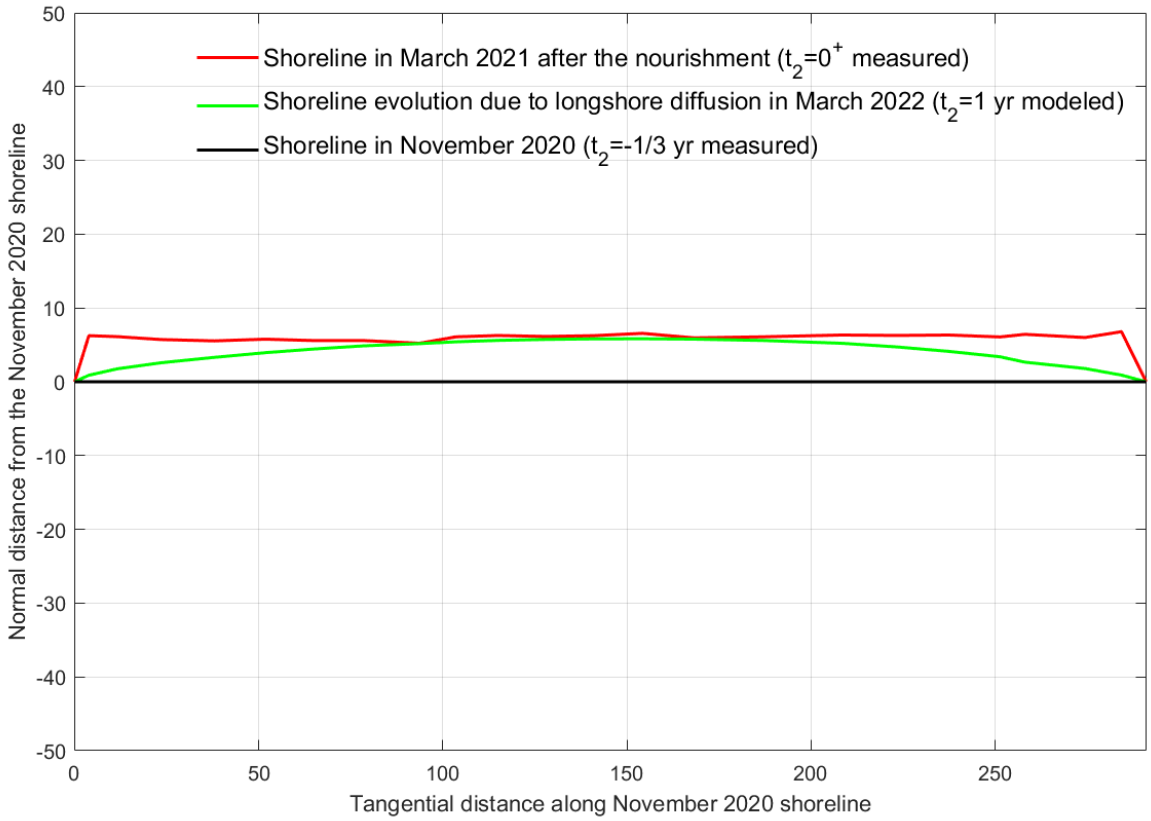

Figure 3.25. Result of 1 year longshore diffusivity with aspect ration 2:1.

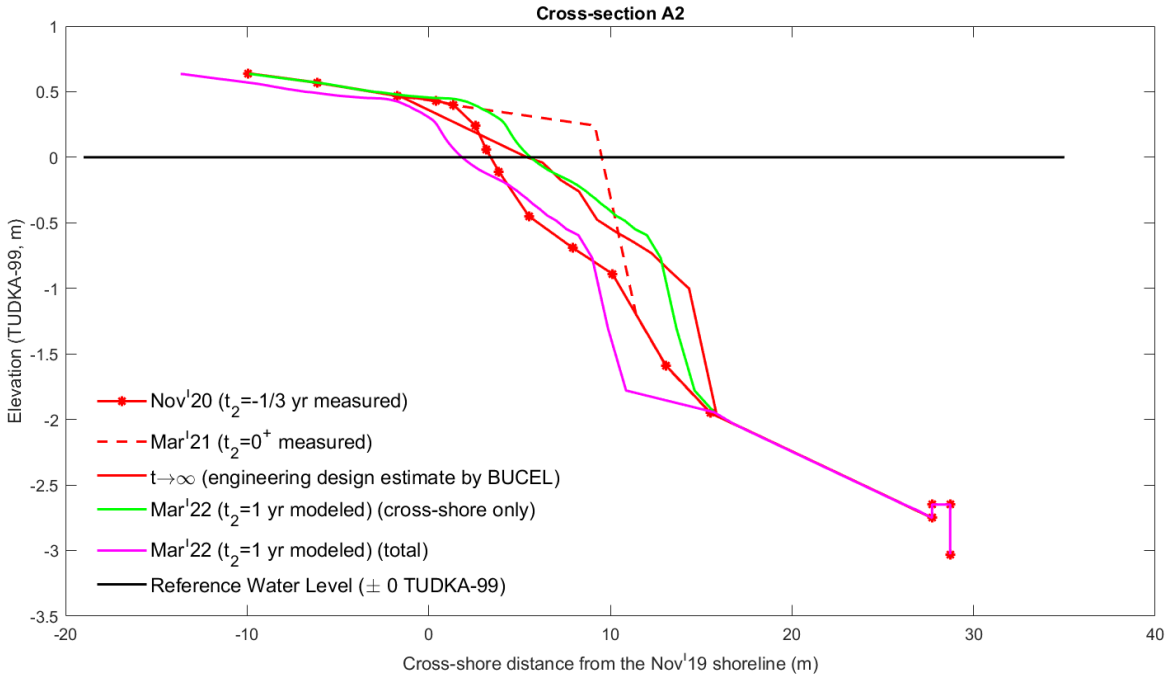

Figure 3.26. Nourishment in March 2021, measurement in November 2020, long term estimation of BUCEL, XBeach-G results and XBeach-G combined with the longshore diffusivity model for 1 year after nourishment for cross-section A2.

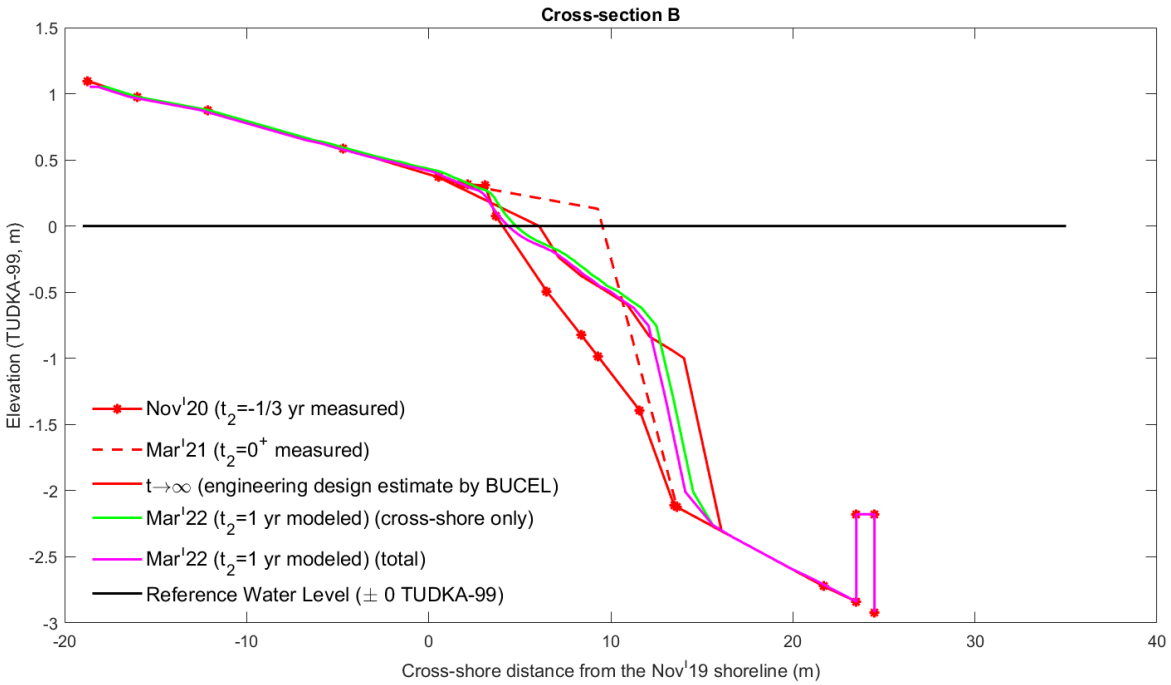

Figure 3.27. Nourishment in March 2021, measurement in November 2020, long term estimation of BUCEL, XBeach-G results and XBeach-G combined with the longshore diffusivity model for 1 year after nourishment for cross-section B.

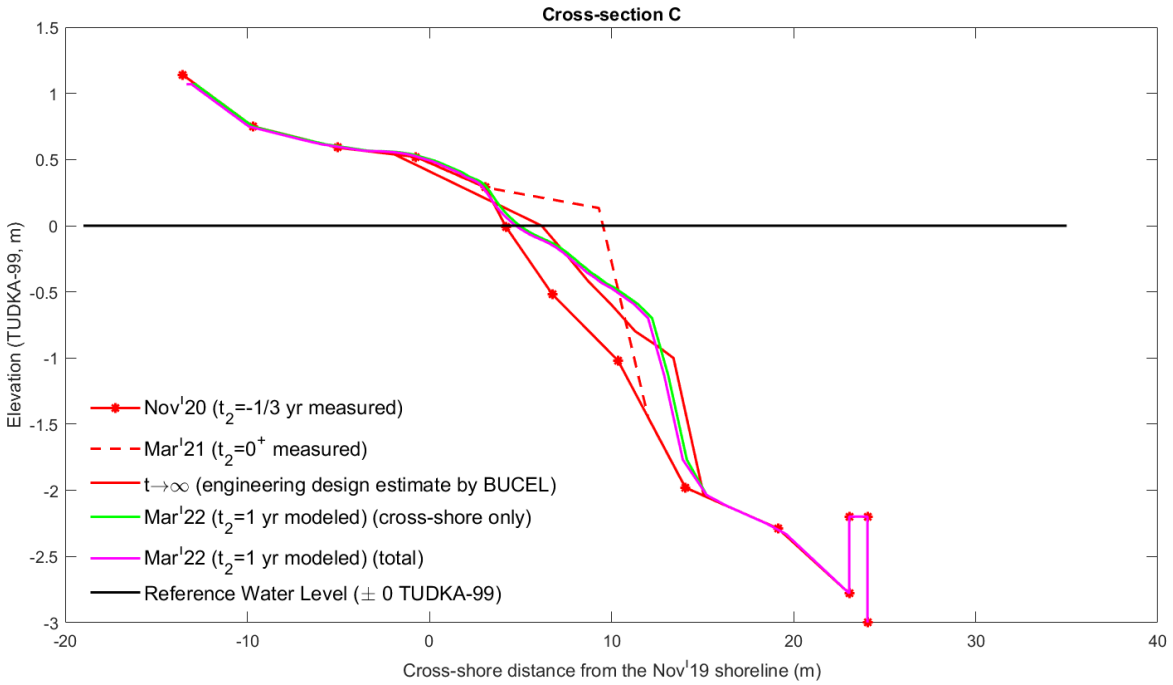

Figure 3.28. Nourishment in March 2021, measurement in November 2020, long term estimation of BUCEL, XBeach-G results and XBeach-G combined with the longshore diffusivity model for 1 year after nourishment for cross-section C.

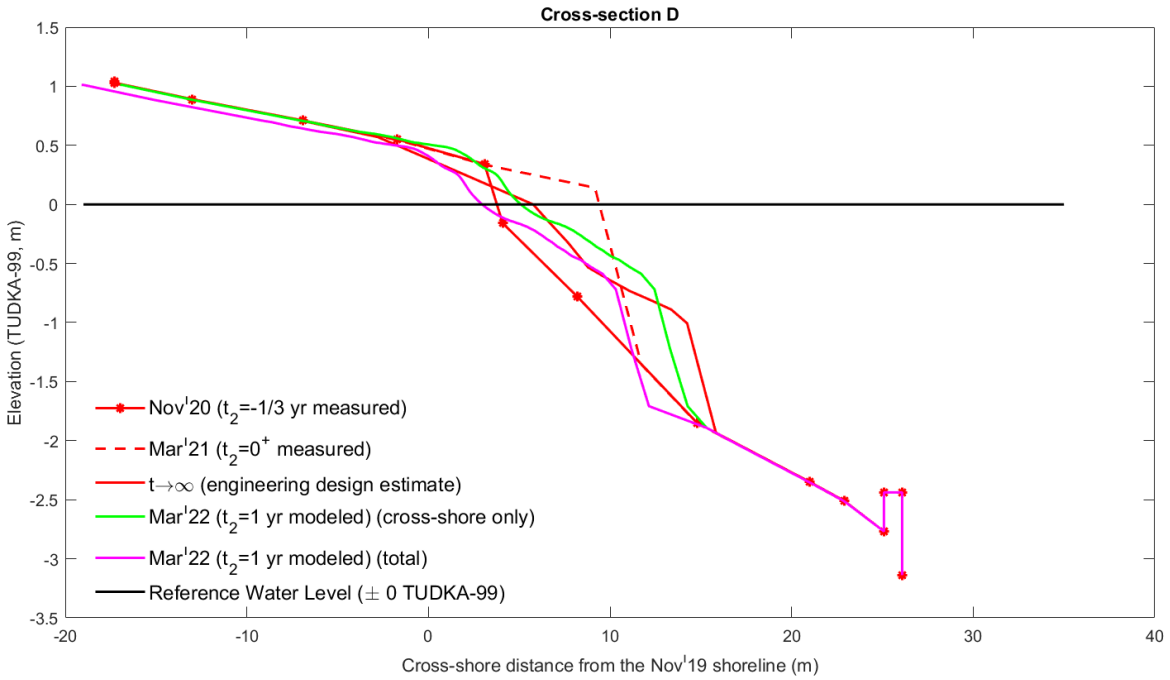

Figure 3.29. Nourishment in March 2021, measurement in November 2020, long term estimation of BUCEL, XBeach-G results and XBeach-G combined with the longshore diffusivity model for 1 year after nourishment for cross-section D.

Table 3.5. Cross-shore distances in meters from November 2019 shoreline from March 2020 up to March 2021.

Shoreline position	**Cross-section A2**	**Cross-section B**	**Cross-section C**	**Cross-section D**
Mar' 21 ($t_2 = 0^+$ measured)	9.53	9.53	9.54	9.41
$t_2 \to \infty$ (equilibriated)	5.4	6.06	6.17	5.77
Mar' 22 ($t_2 = 1$ yr modeled) (cross-shore only)	5.61	4.79	4.98	5.09
Mar' 22 ($t_2 = 1$ yr modeled) (longshore only)	-3.77	-0.43	-0.22	-2.13
Mar' 22 ($t_2 = 1$ yr modeled) (total)	1.84	4.36	4.76	2.96

4. CONCLUSION AND RECOMMENDATIONS

Coastal sediment erosion can be prevented by sustainable and soft methods such as beach nourishment. Positive beach enhancement gained by this method has favorable effects on social and economic activities. Modeling the morphologic evolution of beach nourishment in time provides to see its sustainability. Therefore, the post-nourishment morphodynamics of a semi-protected embayed gravel beach at Kalemyel Bay is studied in this project. The beach was nourished two consecutive years, in March 2020 and March 2021. In addition to its protected location, there is a sill approximately 2.5 m deep which also prevents sediment motion further from that depth. The model to predict the long-term evolution of the beach morphology has been constructed in light of data collection and analysis of BUCEL. The analysis was conducted mainly on four cross-sections each year, at different locations on the beach.

Waves have the most important impact on the sediment transport phenomena. The main generator of the waves is wind. Thus, a fine grid mesh (a bathymetry resolution of 7.5 m $\times$ 9 m and a computational grid resolution of 3 m $\times$ 3 m) wave model is constructed for the Kalemyel Bay by use of SWAN software. The bathymetry map was taken from Navionics (2022). Wind data presented in the work of [29] which is taken from ECMWF from the year 2000 to 2018 is used. For the wave boundary conditions, coarse grid wave climate analysis of BUCEL [2] is used. Wave outputs at the entrance of Kalemyel Bay of their model are used as input for the model of the present study. Stationary runs for each wind-wave condition are done so that the detailed wave conditions reaching the beach for different wind and wave scenarios are obtained. Those wave conditions are used as inputs for the morphologic models.

Because of the time limitations of the morphologic models, only 8 storm conditions are modeled, both in wave and morphologic simulations. Cross-shore and longshore sediment transports are modeled separately in order to better calibrate and have a better understanding of each of these phenomena separately. To model the morpho-

logic change due to cross-shore sediment transport, XBeach-G software is used. The storm conditions are modeled such that they occur immediately one after the other. Three different orders of the storm conditions are modeled. It is observed that the order of different wave conditions does not change the final shape of the profiles. Thence, the rest of the analysis and the discussion are based on the first ordering of the wave conditions (Table 3.1), which allows us to assume this process as nearly linear. The cross-shore model is combined with the longshore diffusivity model, which is mainly the one-line model of Pelnard-Considere [33]. Given that the longshore diffusivity is a linear equation and the cross-shore transport phenomenon is assumed to be nearly linear, the shoreline recession values obtained for each cross-section are superposed to the result of the cross-shore transport model.

There are simulations for the profiles after the nourishment of both March 2020 and March 2021. BUCEL also conducted a measurement in November 2020, which can be compared with the first model results. The measurements are approximately 8 months after nourishment, while the models are run for 1 year. Despite this fact, the measured shoreline recession is higher than the modeled recession due to cross-shore transport. When the cross-shore model is combined with the longshore model, the shoreline recession is found to be too high at the cross-section at the west side of the beach with 7.48 m in total. This means that a big portion of the dry beach gain immediately after the nourishment is lost at the end of 1 year. Longshore transport model results have a great effect on this number. The cross-shore model predicts only 3.74 m of recession only. While the measurements after 8 months show that there had been a recession of 4.67 m. Both from the measurement and from the site experiences, the existence of longshore currents and hence longshore sediment transport can be validated. However, it can be said that the results obtained from the diffusivity model are overestimating the change in the profile due to longshore transport. One main reason that this result at the west end of the beach is so exaggerated is that the diffusion equation causes the largest changes near the edges. Yet, the change in the cross-section on the east side is much smaller, moreover, it is in the seawards direction. The reason for this is the irregularity in the nourishment application. The fill thickness

around that cross-section is less than places around. So, the diffusion equation suggests that sediments are going to move where they are less in the first place. If the run was longer, there would be an erosion there too. The other two profiles that remain in the middle of the beach are subject to smaller longshore sediment transport. The dominance of the cross-shore sediment transport over the longshore transport for these two profiles are 14:1 and 1.7:1. Regarding the whole beach, the average of the ratio of the beach loss due to cross-shore transport to longshore transport is 2.75:1 after the first nourishment.

The model of the profiles after the nourishment in March 2021 is compared with the long-term estimations of BUCEL. XBeach-G results of that year are mostly in line with the estimation. When those results are superposed with the longshore diffusivity model, again higher recession values are found at the ends of the beach due to the nature of diffusion phenomena. The fill thickness in March 2021 is more regular than the one in March 2020. Therefore, the model predicts erosion on the east side as well. The ratio of the cross-shore sediment transport to the longshore transport at the end cross-sections are 1:1 and 2:1. While at the cross-section in the middle these values are 11:1 and 20:1. Regarding the whole beach, the average of the ratio of the beach loss due to cross-shore transport to longshore transport is 2.23:1 after the second nourishment, which imply the dominance of the cross-shore transport.

From the results of especially the first year's simulations, the importance of a regular beach fill distribution becomes evident for the longshore diffusivity model. Regarding the bell shape of the final profile, the initial fill can also be adjusted so that the thickness of the fill at the middle parts can be more than the ends. Because the material in the middle is going to diffuse through the sides in the long term anyway. This application can provide a more economic nourishment design.

Another reason for the inconvenience between the measured profile in November 2020 and the modeled profile for March 2021 might be extreme wind conditions that occurred during Summer 2020 that are not considered in the model because the simu-

lations are according to yearly average wind conditions. Therefore, for a more accurate model, wind data of the specific year that is to be modeled can be used.

A remedy to XBeach-G results could be running longer simulations with other wave conditions which are assumed to have negligible effects on the morphology. However, if the simulations for the real 8 months could be run with this model, the results might approach the measurements.

An important factor in the longshore results is the nature of the diffusion equation. In this study, longshore diffusivity in cartesian coordinates is used with the assumption that the curvature of the beach is small compared to its length and that it can tolerate the distortion caused by straightening the beach and depth contours. Nevertheless, the longshore results suggest that the model with these assumptions does not work very accurately at the domain ends. So, the diffusion equation could be adapted to polar coordinates to have more accurate results, especially at the near-end points.

REFERENCES

1. Grottoli, E., D. Bertoni, A. Pozzebon and P. Ciavola, "Influence of Particle Shape on Pebble Transport in a Mixed Sand and Gravel Beach During Low Energy Conditions: Implications for Nourishment", *Ocean & Coastal Management*, Vol. 169, pp. 171–181, 2019.

2. Otay, E. N., M. Aslani, O. D. Tanrıkulu, B. Bıçak and O. Akagün, *Hillside Beach Club Kıyı Araştırmaları Raporu*, 2020.

3. Sammut, S., R. Gauci, A. Drago, A. Gauci and J. Azzopardi, "Pocket Beach Sediment: A Field Investigation of the Geodynamic Processes of Coarse-Clastic Beaches on the Maltese Islands (Central Mediterranean)", *Marine Geology*, Vol. 387, pp. 58–73, 2017.

4. Bagnold, R. A., *Mechanics of Marine Sedimentation*, Vol. 3, The Sea: Ideas and Observations, M. N. Hill ed, Interscience, 1963.

5. Bailard, J. A., "An Energetics Total Load Sediment Transport Model for a Plane Sloping Beach", *Journal of Geophysical Research: Oceans*, Vol. 86 (C11), pp. 10938–10954, 1981.

6. Bailard, J. A. and D. L. Inman, "An Energetics Bedload Model for a Plane Sloping Beach: Local Transport", *Journal of Geophysical Research: Oceans*, Vol. 86 (C3), pp. 2035–2043, 1981.

7. Ishikawa, T., T. Uda, S. Miyahara, M. Serizawa, M. Fukuda and Y. Hara, "Recovery of Sandy Beach by Gravel Nourishment - Example of Ninomiya Coast in Kanagawa Prefecture, Japan", *Coastal Engineering Proceedings*, Vol. 1 (34):6.

8. Barati, R., S. A. A. S. Neyshabouri and G. Ahmadi, "Issues in Eulerian-Lagrangian Modeling of Sediment Transport nder Saltation Regime", *International Journal of*

Sediment Research, Vol. 33 (4), pp. 441–461, 2018.

9. Bohorquez, P. and C. Ancey, "Particle Diffusion in Non-Equilibrium Bedload Transport Simulations", *Applied Mathematical Modelling*, Vol. 40 (17-18), pp. 7474–7492, 2016.

10. Pedrozo-Acuña, A., D. J. Simmonds, A. K. Otta and A. J. Chadwick, "On the Cross-shore Profile Change of Gravel Beaches", *Coastal Engineering*, Vol. 53 (4), pp. 335–347, 2006.

11. Pedrozo-Acuña, A., D. J. Simmonds, A. J. Chadwick and R. Silva, "A Numerical–Empirical Approach for Evaluating Morphodynamic Processes on Gravel and Mixed Sand–Gravel Beaches", *Marine Geology*, Vol. 241 (1-4), pp. 1–18, 2007.

12. Oh, J. E., Y. S. Chang, W. M. Jeong, K. H. Kim and K. H. Ryu, "Estimation of Longshore Sediment Transport Using Video Monitoring Shoreline Data", *Journal of Marine Science and Engineering*, Vol. 8 (8):572, 2020.

13. Harley, M. D., U. Andriolo, C. Armaroli and P. Ciavola, "Shoreline Rotation and Response to Nourishment of a Gravel Embayed Beach Using a Low-Cost Video Monitoring Technique: San Michele-Sassi Neri, Central Italy", *Journal of Coastal Conservation*, Vol. 18, pp. 551–563, 2014.

14. Stark, N. and A. E. Hay, "Pebble and Cobble Transport on a Steep, Mega-tidal, Mixed Sand and Gravel Beach", *Marine Geology*, Vol. 382, pp. 210–223, 2016.

15. Bertoni, D., E. Grottoli, P. Ciavola, G. Sarti, G. Benelli and A. Pozzebon, "On the Displacement of Marked Pebbles on Two Coarse-Clastic Beaches During Short Fair-Weather Periods (Marina di Pisa and Portonovo, Italy)", *Geo Marine Letters*, Vol. 33, pp. 463–476, 2013.

16. Grottoli, E., D. Bertoni, P. Ciavola and A. Pozzebon, "The Role of Particle Shape on Pebble Transport in a Mixed Sand and Gravel Beach (Portonovo, Italy)",

Coastal and Maritime Mediterranean Conference, Ferrara, Italy, 2015.

17. Bertoni, D., P. Ciavola, E. Grottoli and G. Sarti, "Transport of Marked Pebbles in Short Periods of Time on a Coarse Clastic Beach (Marina di Pisa, Italy)", EGU2012-10044, EGU General Assembly 2012.

18. Miller, I. M. and J. Warrick, "Measuring Sediment Transport and Bed Disturbance with Tracers on a Mixed Beach", *Marine Geology*, Vol. 299-302, pp. 1–17, 2012.

19. Bergillos, R. J. and G. M. M. Ortega-Sànchez, "Morpho-sedimentary Dynamics of a Micro-tidal Mixed Sand and Gravel Beach, Playa Granada, Southern Spain", *Marine Geology*, Vol. 379, pp. 28–38, 2016.

20. Poate, T., G. Masselink, M. Davidson, R. McCall, P. Russell and I. Turner, "High Frequency in-situ Field Measurements of Morphological Response on a Fine Gravel Beach During Energetic Wave Conditions", *Marine Geology*, Vol. 342, pp. 1–13, 2013.

21. Austin, M. J., G. Masselink, P. E. R. I. L. Turner and C. E. Blenkinsopp, "Alongshore Fluid Motions in the Swash Zone of a Sandy and Gravel Beach", *Coastal Engineering*, Vol. 58 (8), pp. 690–705, 2011.

22. Masselink, G., P. Russell, C. Blenkinsopp and I. Turner, "Swash Zone Sediment Transport, Step Dynamics and Morphological Response on a Gravel Beach", *Marine Geology*, Vol. 274 (1-4), pp. 50–68, 2010.

23. Elshinnawy, A. I. and M. Gonzalez, "Dynamic Equilibrium Planform of Embayed Beaches: Part 2. Design Procedure and Engineering Application", *Coastal Engineering*, Vol. 135, pp. 123–137, 2018.

24. Roelvink, D., A. Reniers, A. van Dongeren, J. T. de Vries, R. McCall and J. Lescinski, "Modelling Storm Impacts on Beaches, Dunes and Barrier Islands", *Coastal Engineering*, Vol. 56 (11-12), pp. 1133–1152, 2009.

25. Bergillos, R. J., G. Masselink and M. Ortega-Sànchez, "Coupling Cross-shore and Longshore Sediment Transport to Model Storm Response Along a Mixed Sand-Gravel Coast Varying Wave Directions", *Coastal Engineering*, Vol. 129, pp. 93–104, 2017.

26. Lopez, I., L. Aragones, Y. Villicampa and F. J. Navarro-Gonzàlez, "Gravel Beaches Nourishment: Modelling the Equilibrium Beach Profile", *Science of Total Environment*, Vol. 619-620, pp. 772–783, 2018.

27. Cohen, O. and E. J. Anthony, "Gravel Beach Erosion and Nourishment in Nice, French, Riviera", *Mediterrannee*, Vol. 108, pp. 99–103, 2007.

28. Pagan, J. I., M. López, I. Lopez, A. J. Tenza-Abril and L. Aragones, "Study of the Evolution of Gravel Beaches Nourished with Sand", *Science of the Total Environment*, Vol. 626, pp. 87–95, 2018.

29. Genc, A. N., N. Vural and L. Balas, "Modeling Transport of Microplastics in Enclosed Coastal Water: A Case Study in the Fethiye Inner Bay", *Marine Pollution Bulletin*, Vol. 150, p. 110747, 2020.

30. McCall, R. T., G. Masselink, T. G. Poate, J. A. Roelvink, L. P. Almeida, M. Davidson and P. E. Russell, "Modelling Storm Hydrodynamics on Gravel Beaches with XBeach-G", *Coastal Engineering*, Vol. 91, pp. 231–250, 2014.

31. Hazen, A., "Some Physical Properties of Sands and Gravels, with Special Reference to Their Use in Filtration", *24th Annual Report, Massachusetts State Board of Health Annual Report*, pp. 539–556, 1892.

32. Turki, I., R. Medina, M. Gonzalez and G. Coco, "Natural Variability of Shoreline Position: Observations at Three Pocket Beaches", *Marine Geology*, Vol. 338, pp. 76–89, 2013.

33. Pelnard-Considère, R., "Essaie de Thie de l'Union des Formes de Rivage en Plages

de Sable et de Galet", *Journeé de l'Hydraulique*, Vol. 4-1, pp. 289–298, 1957.

34. Otay, E. N., M. Aslani, S. Farazande, İ.Bilgün and O. Akagün, *Hillside Beach Club Kıyı İzleme ve Geliştirme Raporu*, 2020.

35. Balas, L. and A. Küçükosmanoğlu, "3-D Numerical Modelling of Transport Processes in Bay of Fethiye, Turkey", *Journal of Coastal Research*, pp. 1529–1532, 2006.

APPENDIX A: XBEACH-G OUTPUTS SAMPLE

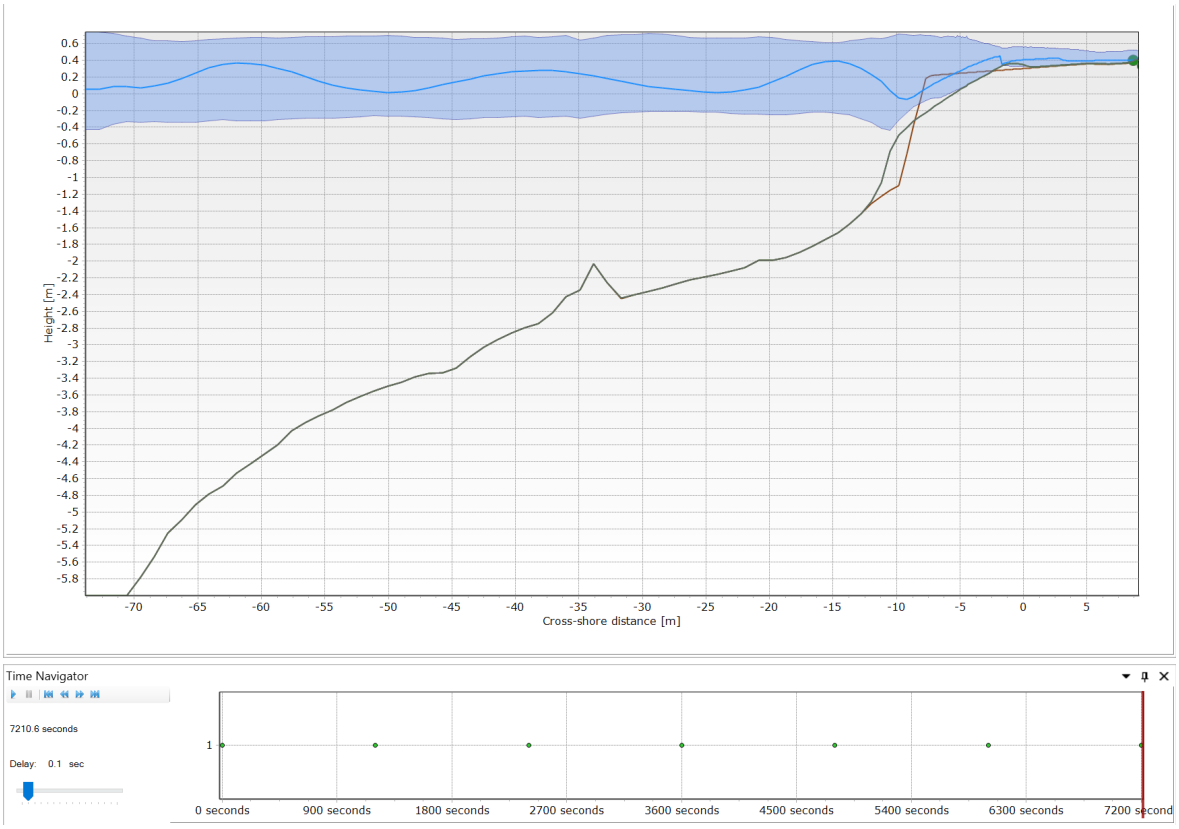

Figure A.1. XBeach-G result for the first 2 hours of the simulation of the profile after the Mar'20 nourishment for cross-section A1.

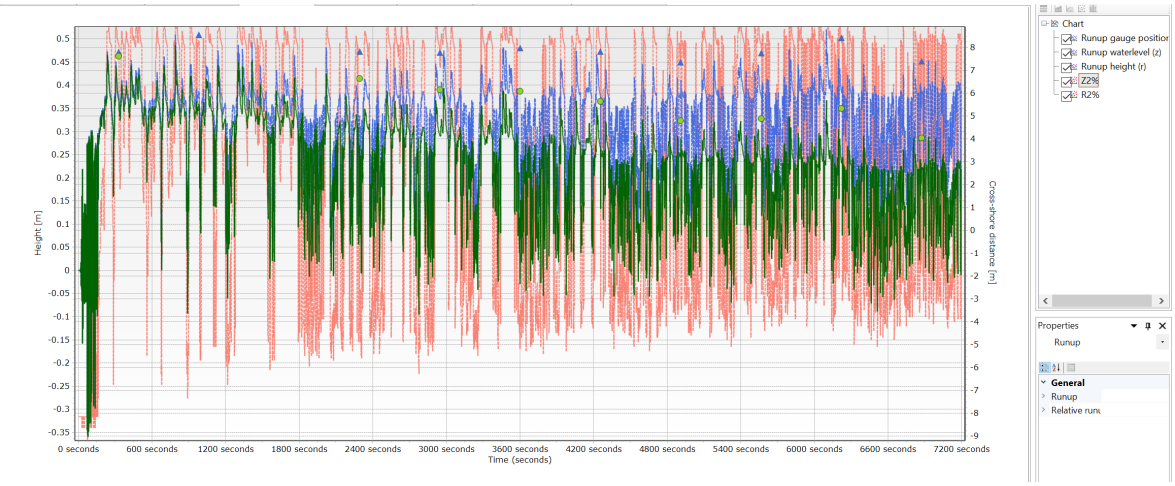

Figure A.2. XBeach-G result pf the runup for the first 2 hours of the simulation after the Mar'20 nourishment for cross-section A1.

APPENDIX B: WATER LEVEL MEASUREMENTS BY BUCEL

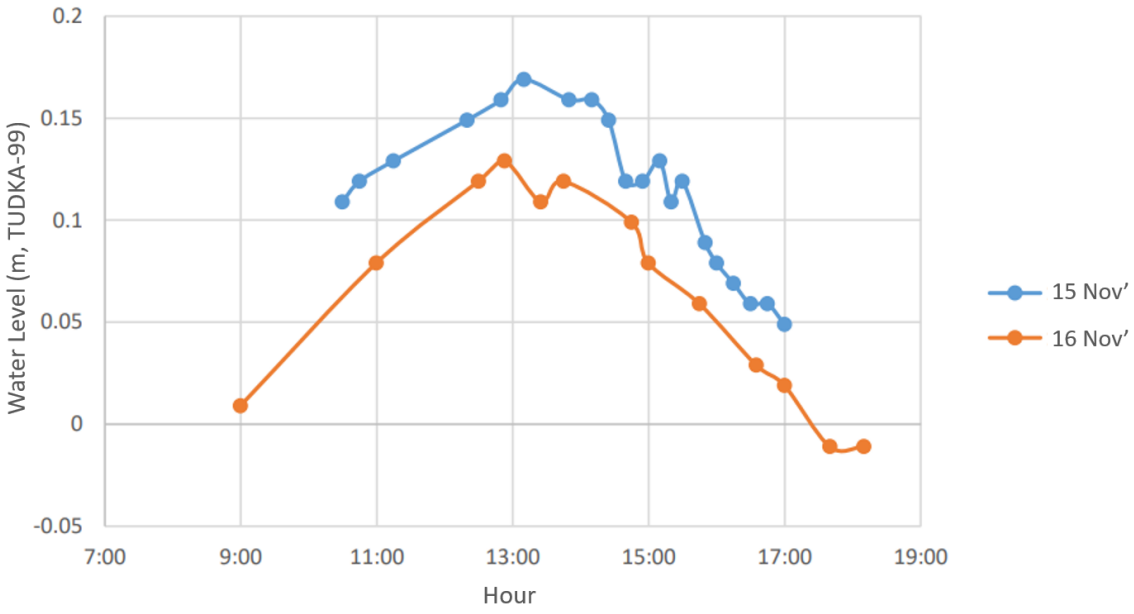

Figure B.1. 15-16 November 2019 water level measurements [2].

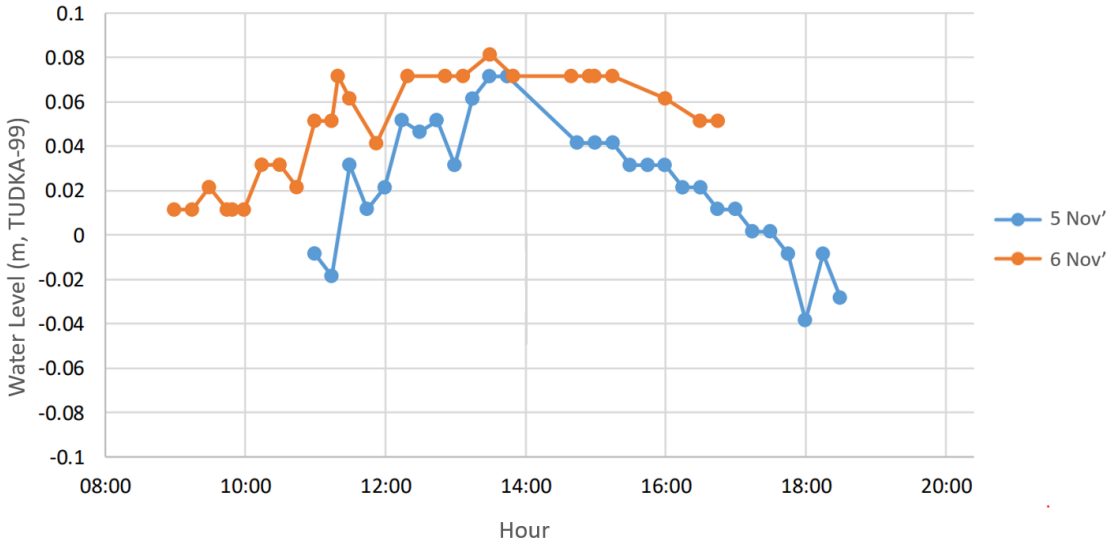

Figure B.2. 5-6 November 2020 water level measurements [34].

APPENDIX C: XBEACH-G RESULTS FOR DIFFERENT WAVE COMBINATIONS (SUPERPOSED)

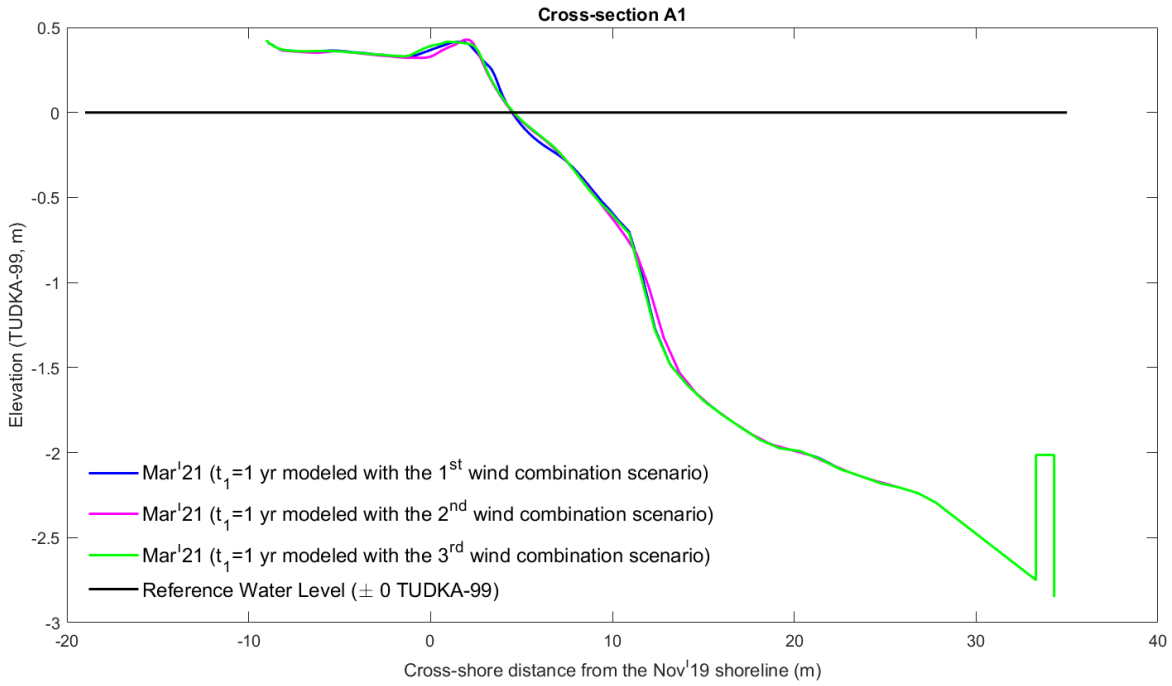

Figure C.1. XBeach-G results of three different wind combination scenarios for 1 year after the nourishment in March 2020 for the cross-section A1.

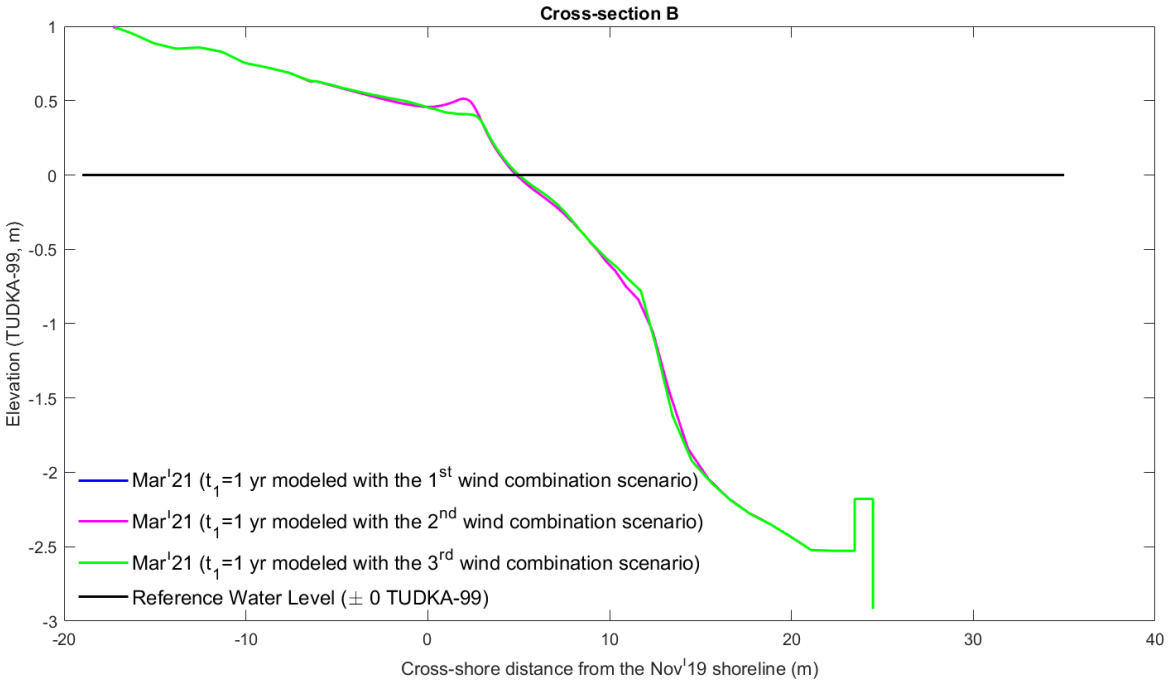

Figure C.2. XBeach-G results of three different wind combination scenarios for 1 year after the nourishment in March 2020 for the cross-section B.

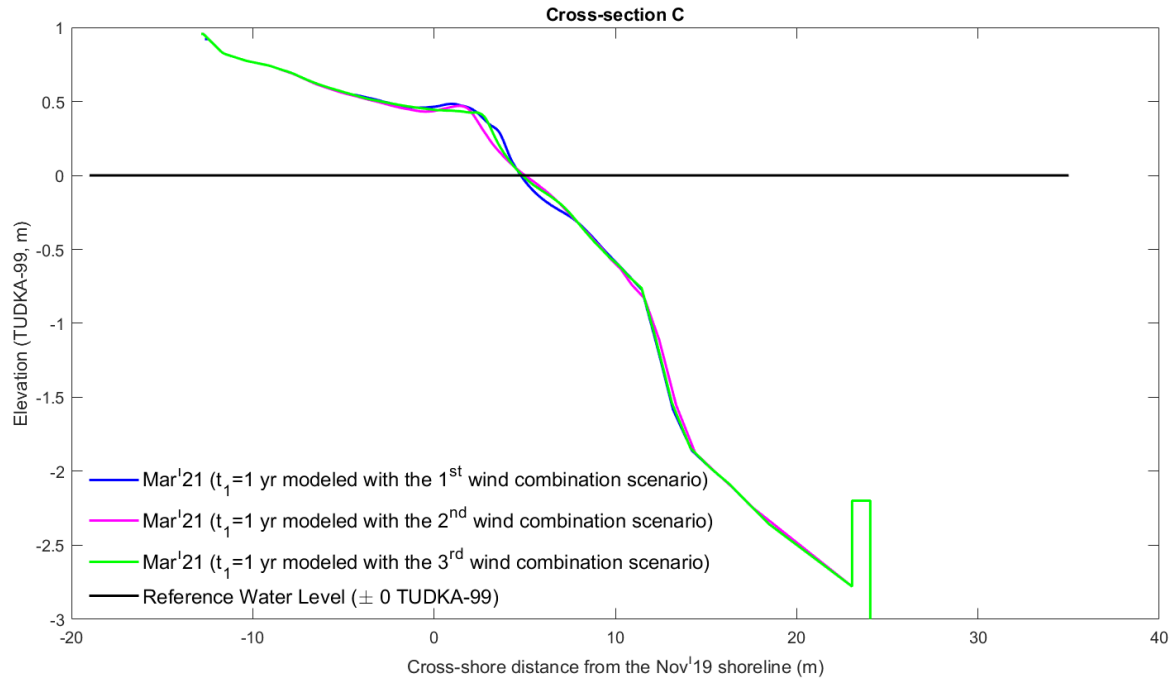

Figure C.3. XBeach-G results of three different wind combination scenarios for 1 year after the nourishment in March 2020 for the cross-section C.

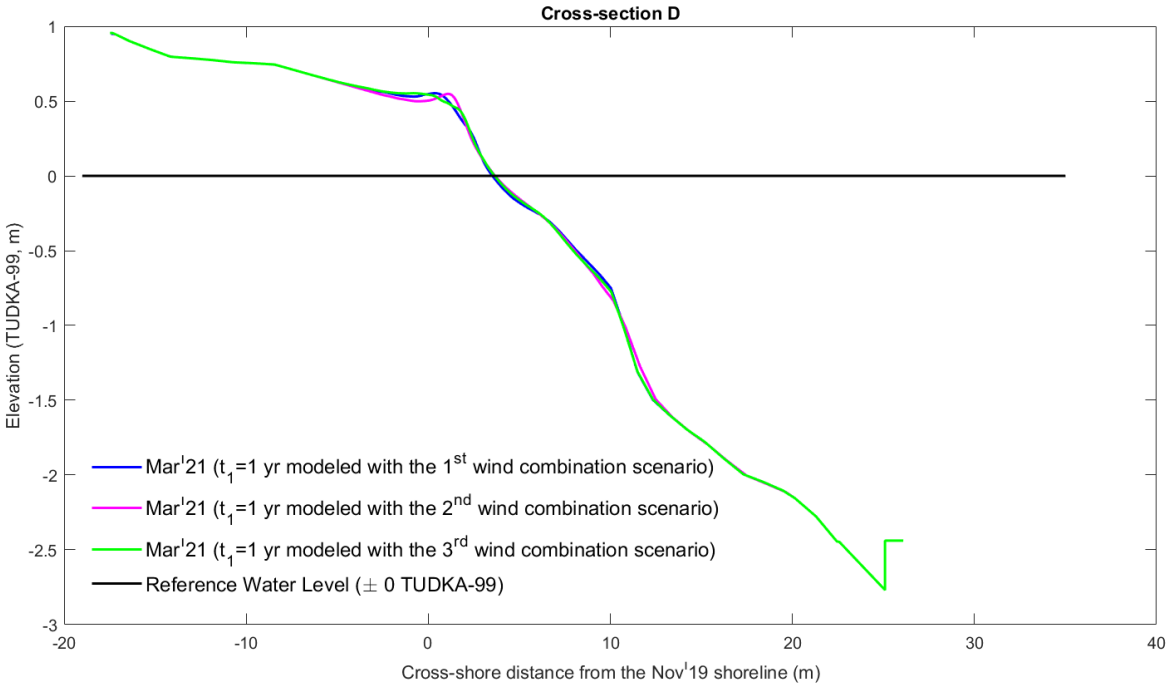

Figure C.4. XBeach-G results of three different wind combination scenarios for 1 year after the nourishment in March 2020 for the cross-section D.

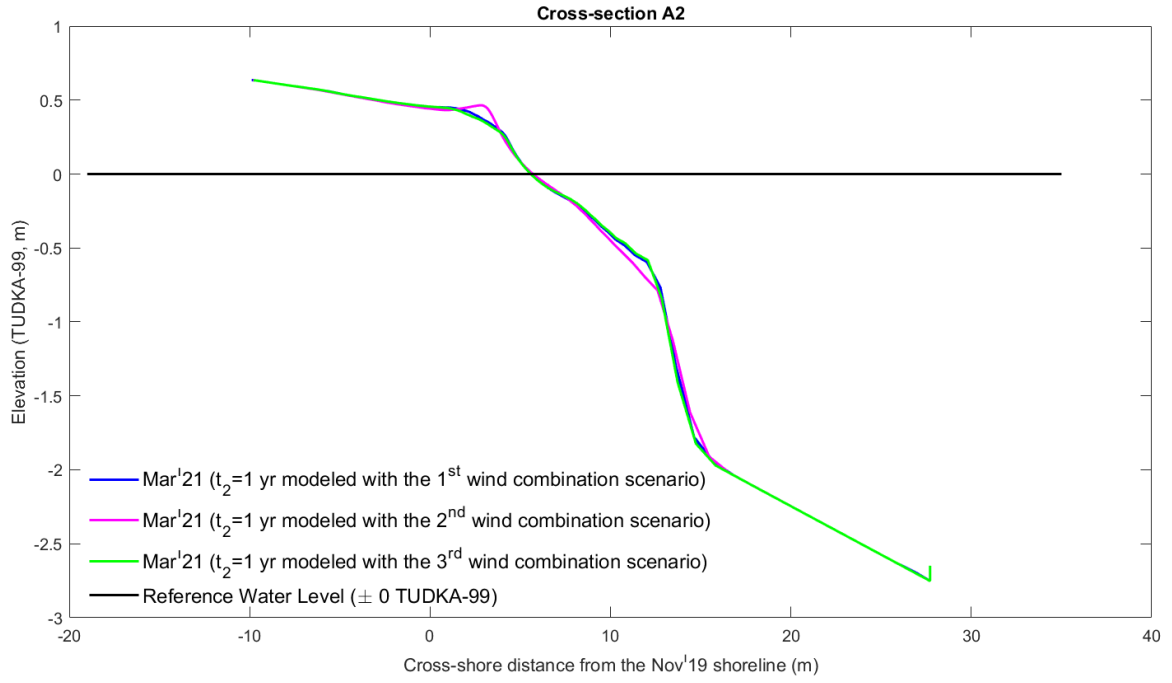

Figure C.5. XBeach-G results of three different wind combination scenarios for 1 year after the nourishment in March 2021 for the cross-section A2.

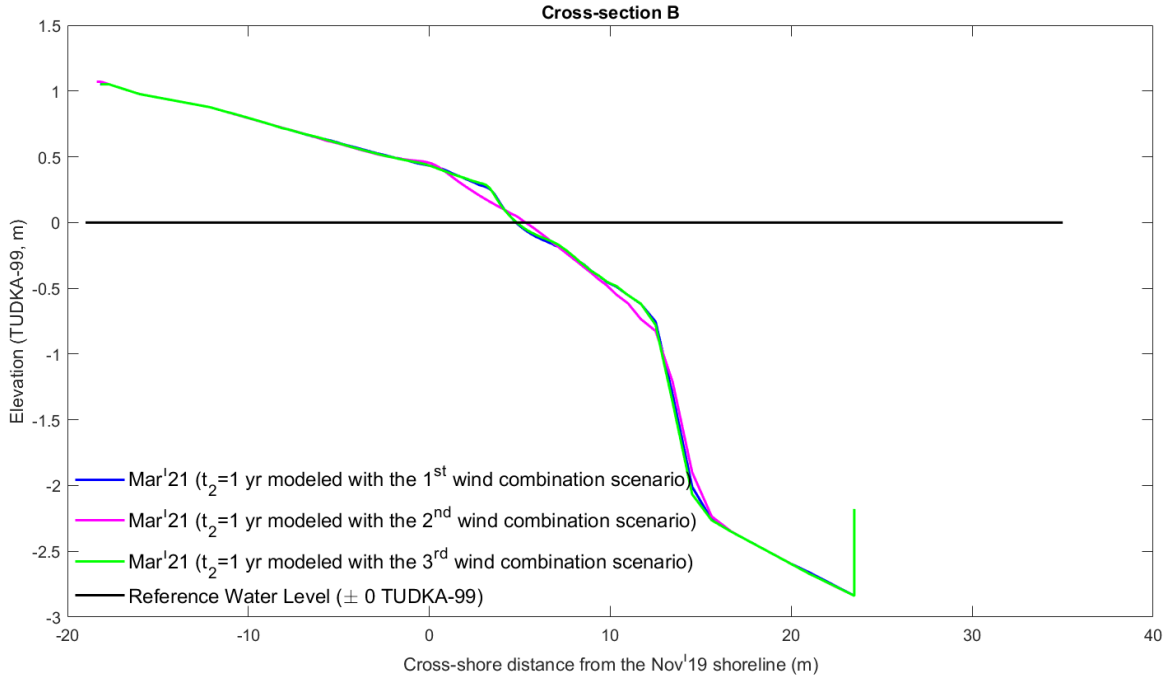

Figure C.6. XBeach-G results of three different wind combination scenarios for 1 year after the nourishment in March 2021 for the cross-section B.

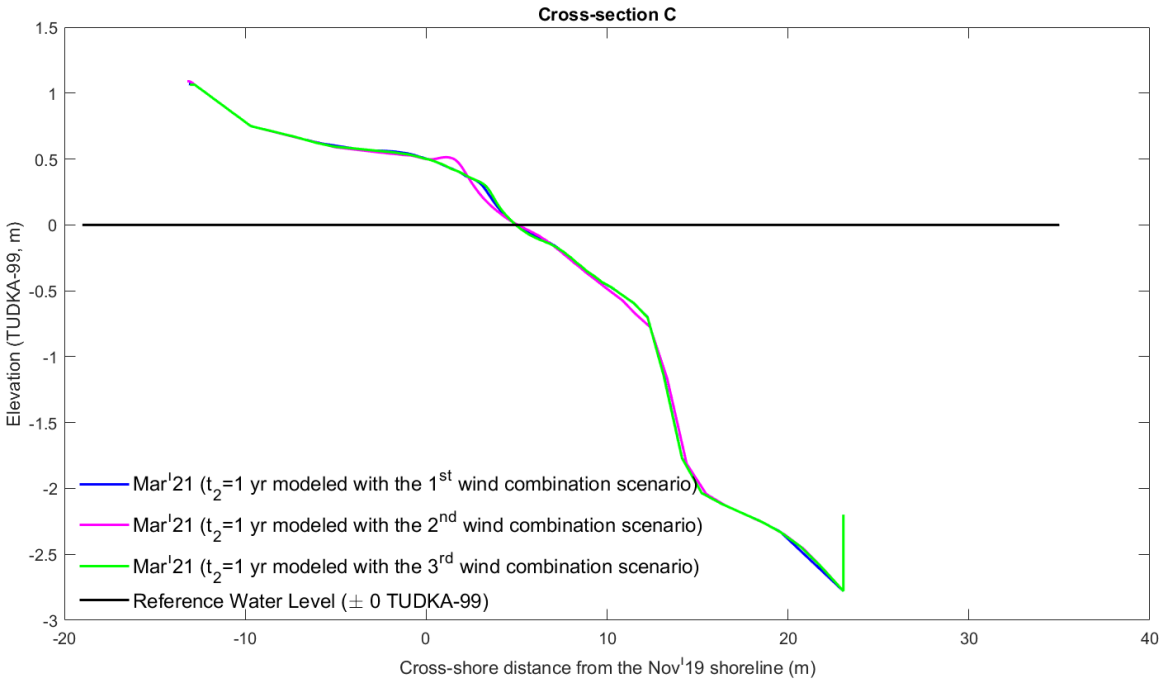

Figure C.7. XBeach-G results of three different wind combination scenarios for 1 year after the nourishment in March 2021 for the cross-section C.

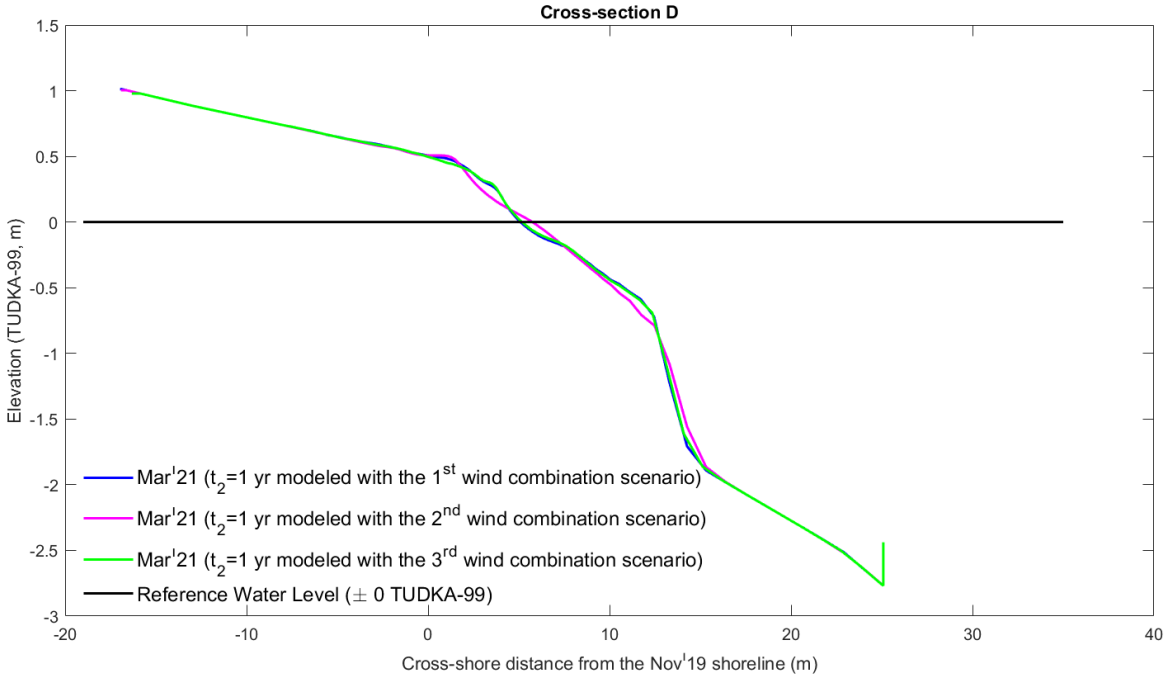

Figure C.8. XBeach-G results of three different wind combination scenarios for 1 year after the nourishment in March 2021 for the cross-section D.